RapidArc – Inverse Planning, Dose Calculation and Clinical Application

A thesis
submitted in partial fulfilment
of the requirements for the Master's Degree
in Medical Physics

by

David Jolly

Department of Physics and Astronomy
University of Canterbury
Christchurch, New Zealand

2009-2011

Supervisor: Dr. Juergen Meyer

"*To make an apple pie from scratch, one must first create the universe*" – Carl Sagan

Abstract

Volumetric modulated arc therapy delivers highly conformal radiotherapy treatments to cancer patients in a continuous arc whilst dynamically varying the multi-leaf collimator (MLC) position, dose rate and rotational angular velocity. The present master's thesis seeks to develop a better understanding of delivering treatment in this manner, ranging from progressive resolution inverse optimisation, class solutions, clinical application and the ability of dose calculation algorithms to model such a complex modality.

A progressive resolution based class solution for inverse planning has been developed, outlining contouring, field set-up and optimisation. This class solution was then applied to 10 prostate patients and subjected to an inter-comparative planning study with static gantry intensity-modulated radiotherapy. The results of this justification study showed the presented class solution produces plans that are generally and directly comparable with previously published data. Following this result, the class solution was applied to a previously uninvestigated clinical site (treatment of prostate bed following radical prostatectomy) in an effort to solve persistent clinical problems involving target volumes and dose escalation. The results of this secondary study provisionally showed the feasibility of treating prostate beds with rotational intensity-modulated techniques whilst maintaining the integrity of the target volumes and escalating the delivered dose.

The potential for improving the accuracy of the dose calculation analytic anisotropic algorithm for volumetric modulated plans was also investigated, through configuration of two independent algorithms containing beam data taken with either the linac jaws or MLCs defining the field. The two algorithms were inter-compared in virtual water phantoms and against physical verification measurements. The configuration process has shown to be sensitive to depth dose data but not beam profiles. Furthermore, the two algorithms show no significant difference and therefore it is recommended that beam be taken with the jaws defining the field.

Acknowledgments

First and foremost I would like to express my gratitude toward my academic supervisor Dr. Juergen Meyer. He is always responsive and willing to give feedback, while his dedication to visit the hospital from afar is also appreciated. His direct and indirect contributions have been pivotal to the completion and quality of this work.

I would like to extend the sentiment of gratitude to my clinical supervisor Dineli Alahakone. Dineli's clinical knowledge and inverse planning experience has been invaluable both throughout the writing of this thesis and my development as a medical physicist.

Without clinical input from Dr. John Violet, this thesis would not have gotten to the point it is today, and for this I am very grateful. His time spent contouring PTVs, discussing clinical issues and the literature he has provided is much appreciated.

Many other staff members in the Wellington Blood and Cancer Centre have contributed throughout the process of writing this thesis, principally the medical physics group. Whether it be for educational, organisational or editorial reasons, I would like to extend my thanks to each and every medical physicist (past and present) that I have worked with in the past two years. To name just a few, Lynne Greig, Blair Steer, Dr. Anthony Venning and Karsten Peick. I would also like to thank the radiation therapists for whom I worked along side during the clinical development of RapidArc. Thanks are also appropriate for Dr. Dalice Sim (Victoria university of Wellington) for her discussions on statistical analysis.

Lastly, I would like to thank my friends and family for their moral support throughout the past two years.

Contents

List of Figures

direction in which the profile was taken. (b) Brain profile subtraction

List of Tables

Nomenclature

a	Organ specific dose volume parameter
β	Beamlet
CI_{95}	The conformity index of the 95% isodose line
$D_{5\%}$	The dose to 5% of a specified volume
$D_{95\%}$	The dose to 95% of a specified volume
D_{95}	Dose to 95% of the target
D_i	The dose to each individual voxel within an investigated structure
D_{max} (1)	The maximum dose to a specified volume
D_{max} (2)	Depth of dose maximum
D_{mean}	The mean dose to a specified volume
$D_\beta(x,y,z)$	Dose contribution from each beamlet
HI	Homogeneity index
$I_\beta(z,\rho)$	Energy deposition function
$K(x,y,z,\rho)$	Scatter kernal
N	Number of voxels within an investigated structure
V_{95}	Percentage of target receiving 95% of the prescribed dose
V_{91}	Percentage of target receiving 91% of the prescribed dose
V_{PTV2}	Volume of the target structure PTV2
Φ_β	Beamlet fluence

Glossary

1D	One-dimensional
2D	Two-dimensional
3D	Three-dimensional
3DCRT	3D conformal radiotherapy
AAA	Analytic anisotropic algorithm
WBCC	Wellington Blood and Cancer Centre
CBCT	Cone beam CT
cc	Cubic centimetres
CCW	Counter-clock wise
CW	Clock wise
CHHiP	Conventional or Hypofractionated High Dose Intensity-Modulated Radiotherapy for Prostate Cancer
CI	Conformity index
CIRS	Computerized Imaging Reference Systems Inc.
CT	Computed tomography
CTV	Clinical target volume
DTA	Distance to agreement
DCF	Distribution calculation framework
DVH	Dose volume histogram
DVO	Dose-volume optimiser
EDW	Enhanced dynamic wedge
EORTC	European Organisation for Research and Treatment of Cancer

EPI	Electronic portal imaging
et. al.	*et alibi*
EUD	Equivalent uniform dose
FH	Femoral head
FWHM	Full width at half maximum
GHz	Giga-Hertz
Gy	Gray (J/kg)
GTV	Gross tumour volume
HI	Homogeneity index
HU	Hounsfield unit
ICRU	International Commission on Radiation Units and Measurements
IGRT	Image guided radiotherapy
IMAT	Intensity-modulated arc therapy
IMRT	Intensity-modulated radiotherapy
kV	kilovoltage
Linac (s)	Lineal accelerator (s)
MV	Megavoltage
MU (s)	Monitor unit (s)
MC	Monte Carlo
MLC	Multi-leaf collimator
n	Number
NS	Not significant
NTO	Normal tissue objective
OAR	Organ at risk
OF	Output factor

P (1)	Priority
P (2)	Prescribed dose
PBC	Pencil beam convolution
PDD	Percentage depth dose
PTV	Planning target volume
PRO	Progressive resolution optimizer
PSA	Prostate specific antigen
RA	RapidArc
ROI	Region of interest
SV	Seminal vesicles
SIB	Simultaneous integrated boost
SAD	Source-to-axis distance
SSD	Source-to-skin distance
SWOG	Southwest Oncology Group
TCP	Tumor control probability
TT	Treatment time
TPS	Treatment planning system
VMAT	Volumetric modulated arc therapy

Chapter 1 – Introduction

1.1 Introduction to Radiotherapy

Since the initial discovery of the x-ray by Wilhelm Röntgen over a century ago the applications of radiation have been wide, with arguably many of the most important in medical diagnostics and therapy. Major clinical and technological advancements have driven the field from a simple tool used to image the bones of one's wife, to the successful therapy of deep malignant tumours with large – and dynamic – linear accelerators (linacs).

Following this initial discovery, progress within the field was swift, with the term 'radioactivity' coined by Madame Curie the year following. Her subsequent work, including the isolation of radium in 1898, was integral to this development. It was noticed early on, that exposure of radiation to superficial cancers caused them to regress, with anecdotal historical evidence suggesting that the first cancers were 'cured' with radiation just four years [7] following Röntgen's initial discovery in 1895. Many of these early treatments would later prove to be palliative in nature due to normal tissue complications and the high rate or recurrence, as a result of the crude delivery techniques [8]. Following these initial disappointing results it was realised that higher energy radiations were required to adequately treat deeper disease, and by 1913 Coolidge had developed an x-ray tube with peak energy of 140 kV, and by 1922 this was further increased to 200 kV. The basis for modern radiotherapy fractionation can be traced back to as early as 1911 [8]. Claudius Regaud first demonstrated the benefit of fractionated treatment schemes with a series of experiments applied clinically to head and neck cancers, followed by cancer of the cervix [9], with improved treatment outcomes with multiple smaller daily fractions to the same treatment site.

Higher energy radiotherapy was not realised until the implementation of the first megavoltage teletherapy machine in 1937 [1], coinciding with the move from

palliative to true curative treatments, as clinical knowledge grew and treatment became more reproducible and systematic [10]. This machine treated patients at St Bartholomew's Hospital in London, up to an energy of 1 MV using dual 9.25 m long, 500 kV x-ray generators [1]. The mid 1930s also saw the conceptual development of an electron accelerator using resonant microwave cavities, but was not clinically practical due to the low power levels of the then current microwave generators [1]. This impracticality was overcome due technological developments as a result of military radar research, related to World War II. Based on this design, the first medical linac (Figure 1.1) was installed for clinical use, treating the first patient on September the 7th 1953, at Hammersmith Hospital in London [1]. Other noteworthy developments in this early period included the installation of the first three linacs in Australia (1956-57), one soon after in New Zealand and the first Varian isocentric linac (6 MV) installed at the University of California, Los Angeles, Medical Centre in 1962.

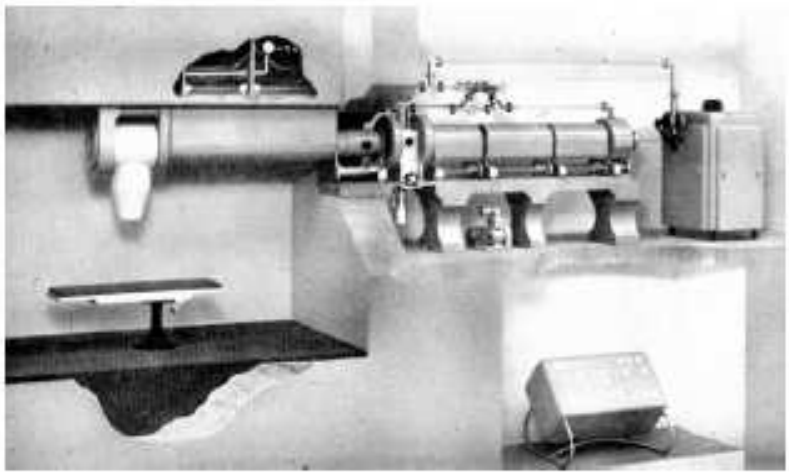

Figure 1.1: Scale model of the first linac installed in Hammersmith Hospital, 1952. Reproduced from [1].

The next major development in radiotherapy came with the invention of the computed tomography (CT) scanner by Sir Godfrey Hounsfield. First proposed in 1968, and acquiring the first clinical image on October 1st 1971 at Atkinson Morley's Hospital, London (Figure 1.2), aiding in the diagnosis of a frontal lobe tumor that was later excised [2]. Conceptually, the CT scanner took digital radiographs using an x-ray generator-detector system at all angles around an object, and digitally reconstructed a three-dimensional (3D) dataset from the combined attenuation values. The 1970s also saw further refinements in linac design, to a point where modern linacs can easily trace their lineage. Technological advancements including improved vacuum pumps, bending magnets and wave guides meant that linacs were relatively stable, compact, reliable, fully isocentric, and capable of producing both photons and electrons [1].

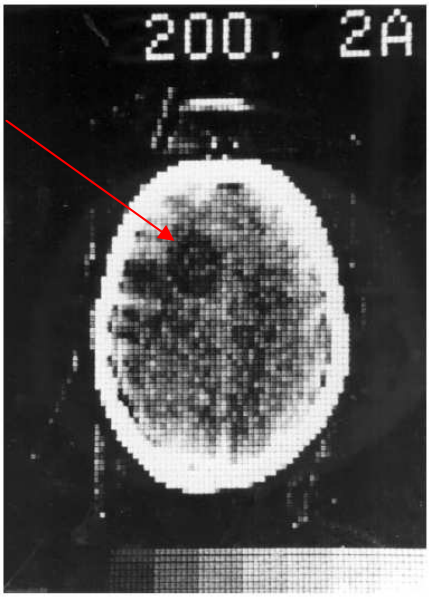

Figure 1.2: The first clinical CT scan, performed at Atkinson Morley's Hospital on October 1st 1971. Red arrow indicating left frontal lobe tumor. Reproduced from [2].

Clinical knowledge continued to grow in parallel with the above technological advancements. This fact in conjunction with advancements in other clinical methods for cancer treatment (surgery and chemotherapy), resulted in survival analysis for all cancer sites showing a significant increase in five year survival; from 39% in the 1960s to 50% by the end of the 1970s [8]. Although this increase was promising, with a number as low as 50%, it was obvious that further advancements were still required.

Modern radiotherapy is yet to experience a revolution in the technology it uses to deliver therapeutic doses of radiation, with the basic concepts of design and structure - formed in the 1970s - still underlying the construction of modern linacs [8]. However, as with any technology dependent technique, further refinement of the major components, coupled with the continual improvements in computing power (correctly predicted by Moore's law [11]) have improved to a standard of performance that is essential for the delivery of modern conformal techniques [8].

Until the introduction of CT imaging, treatment planning was done in a purely two-dimensional (2D) manner. Radiation fields were placed with the aid of bony anatomy visualised on plane radiographs and were often simple rectangular shapes. The technology of CT imaging had since progressed to a point where 3D data sets of patient anatomy could be imaged and reconstructed in a matter of minutes, with a high level of resolution and contrast, and therefore could be used for not only diagnostic imaging but therapeutic treatment planning. Radiation fields could now be shaped to fit anatomical specific targets, resulting in what is now called 3D conformal radiotherapy (3DCRT).The advantage of this technique came with more conformal dose distributions, allowing higher doses to the tumor, with lower doses to normal tissues, improving clinical outcomes. Further developments in linac functionality included mounted imaging devises and multi-leaf collimators (MLCs), pioneering the way for image guided radiotherapy (IGRT) and intensity-modulated radiotherapy (IMRT) respectively.

1.2 Intensity-modulated Radiotherapy

IMRT is considered (by some [12, 13]) as the most important development in radiotherapy treatment planning and delivery since the above mentioned integration of CT imaging [4]. The seminal IMRT paper was published in 1988 by Anders Brahme et. al. [3], suggesting that even more conformal dose distributions could be achieved through modulating the intensity not only between separate fields but within each field itself (Figure 1.3). This allows the intensity of radiation passing through sensitive normal structures to be reduced, and the intensity through target volumes increased [4]. Thus, allowing higher doses to be given to target structures with similar or reduced doses to normal tissue, and therefore, theoretically improve clinical outcomes. The implementation of this theoretical work was dependent on development of beam modifiers (MLCs) and the methods used to calculate the non-intuitive beam apertures, through inverse planning techniques. No concise, universal definition of IMRT exists but many have been suggested, for example [4]:

"IMRT is a radiation treatment technique with multiple beams in which at least some of the beams are intensity-modulated and intentionally deliver a non-uniform intensity to the target. The desired dose distribution in the target is achieved after superimposing such beams from different directions. The additional degrees of freedom are utilized to achieve a better target dose conformality and/or better sparing of critical structures"

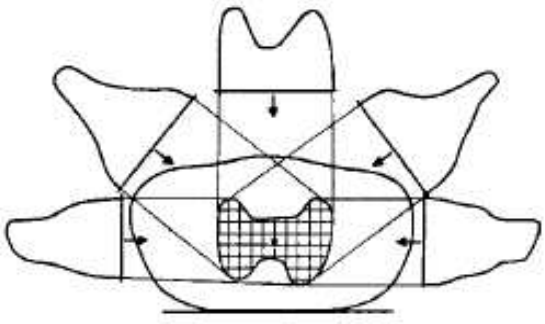

Figure 1.3: Original IMRT illustration from Brahme [3] indicating five intensity modulated beams and their corresponding intensity profiles. The hatched area indicated the target volume. The intensity profiles show a reduction in areas where the path covers mainly normal tissue and an increase when the path is mainly target.

The development of inverse planning algorithms has several major milestones. The concept of defining upper and lower structural constraints was first introduced in 1988 [14], but Steve Webb was the first to realise that inverse planning for IMRT was an optimisation (minimising an objective or cost function) problem due to the fact that there was no exact solution [15]. This is a result of the physical constraints of radiation and the fact that it is impossible to produce negative dose intensities. Therefore, no set of modulated beams can deposit a prescription dose to the target and no dose to the surrounding normal tissues. Since there is no exact solution, the optimal solution will be the one that comes as close as possible to this unachievable solution, or in mathematical terms, the sum of the squared deviations between the delivered and prescription dose, which is to be minimised [4]. Many of the modern inverse planning algorithms are based on subsequent work by Bortfeld, published in 1990 [16]. Bortfeld realised that the above problem with a quadratic objective function does not have local minimums, and therefore fast gradient decent methods can be used to find the optimal solution [4], greatly reducing optimisation times.

Much of this early optimisation work was purely theoretical, with no knowledge of how the optimised, modulated beams would be physically produced. The use of various beam modifiers, such as metal compensators, were envisioned but this was impractical due the specificity of each patient, field and field segment [4]. This was overcome as MLCs (Figure 1.4) became commercially available in the early 1990s. Consisting of multiple individually driven tungsten leaves, MLCs were originally designed for beam shaping in 3DCRT, but would soon become invaluable in the delivery of IMRT treatments.

Figure 1.4: Multi-leaf collimator (MLC) with tungsten leaves producing a complex shape. MLCs that move dynamically throughout treatment are an essential component of IMRT treatment delivery. Reproduced from [4].

The first publication outlining a feasible method for delivering arbitrary intensity profiles using an MLC that moved dynamically, in a unidirectional sweep throughout treatment, was published in 1992 [17]. Here, relatively large dynamic apertures are used with the field open to areas of high intensity for a larger fraction of time than areas of low intensity, hence producing a profile with varying modulation. This model was subsequently improved to include the finite acceleration and velocity of individual leaves, leaf transmission and penumbra affects, to form the basis for modern sliding window IMRT delivery [4]. A separate delivery method was developed independently and simultaneously [4], whereby each intensity profile is built up using a succession of discrete field segments each delivering a fraction of the total field fluence. This work was the basis for the modern step-and-shoot IMRT. Each intensity-modulated delivery technique has advantages and disadvantages, but the driving force for step-and-shoot being the fact that MLC movements are made while the beam is off and therefore the probability for an error in treatment may be reduced [4].

The use of medical imaging for patient position verification in radiotherapy has a long history, with the first reports of pre-treatment electronic portal imaging (EPI) dating back to 1958 [18]. Further advancements of these techniques have made imaging a useful tool in routine clinical patient set-up. The advent of IMRT has taken these tools from the useful to the essential. Modern linacs (Figure 1.5) now incorporate MV (EPIs) and on board kV imaging systems (including cone beam CT), to detect systematic or random set-up error, and guide field set up and patient positing in radiotherapy. The sharp dose gradients produced by intensity modulation increases the risk for a geographical miss. Therefore, imaging becomes essential for patient verification to ensure that the target is receiving the desired dose and normal tissues are not being over dosed [19]. IGRT also has the potential to reduce the target volume size and therefore further reduce the volume of normal tissue irradiated.

Figure 1.5: IGRT and RapidArc capable Varian Trilogy iX. IGRT capabilities include MV (EPI) detector and kV source and detector. Reproduced from Varian Medical Systems, Inc., Palo Alto, CA, USA.

The first IMRT verification measurements were taken in 1994 by Bortfeld [20]. This verification was done for a prostate step-and-shoot IMRT plan with 225 segments, in an anthropomorphic pelvis phantom stacked with film. The delivery of this treatment took over three hours (mainly due to a cumbersome MLC) but produced surprisingly good agreement between planned and delivered dose. Following further work, the first clinical patient treated with inverse planned, MLC delivered IMRT was at the Memorial Sloan Kettering Cancer Centre, New York, in 1996 [21]. This treatment was done as an extension of the centers long standing dose escalation prostate study and conservatively gave a 9 Gy sliding window IMRT boost, on top of the previously treated 72 Gy 3DCRT plan. Early comparative planning study data presented the related dose volume histogram (DVH), showing a reduced rectal dose for the composite IMRT plan, compared with the standard 3D plan [21]. In concurrent development was an independent method of delivering intensity-modulated radiation, whereby fields are delivered through a rotational fan-beam in a similar fashion to a CT scanner, coined Tomotherapy by the seminal paper in 1993 [22]. The first clinical Tomotherapy treatment was in August of 2002 at the University of Wisconsin [23].

Further development in modern oncology (across all disciplines) has continued the trend to improve the prognosis for all cancers [8]. As illustrated in figure 1.6, deaths directly attributed to cancer are significantly below what was extrapolated in 1990, in the United States [5]. The overall death rate for men decreasing by 19.2% and 11.4% for women, between 1990 and 2005. Despite this, in 2004 cancer was still the leading cause of death worldwide, being attributed to 13% of all deaths [24], and in 2009 cancer caused more deaths in developed countries than heart disease in the under 85 year old age bracket [5]. These world wide statistics are reflected in local regions, with cancer ranked as the second leading cause of death in New Zealand [25] and Australia [26, 27]. In conjunction with this, cancer incidence is predicted to continue to rise [24, 27]. As a result, further development in the field is required, both clinically and technologically, with the goal of improving therapeutic ratios and curing more people.

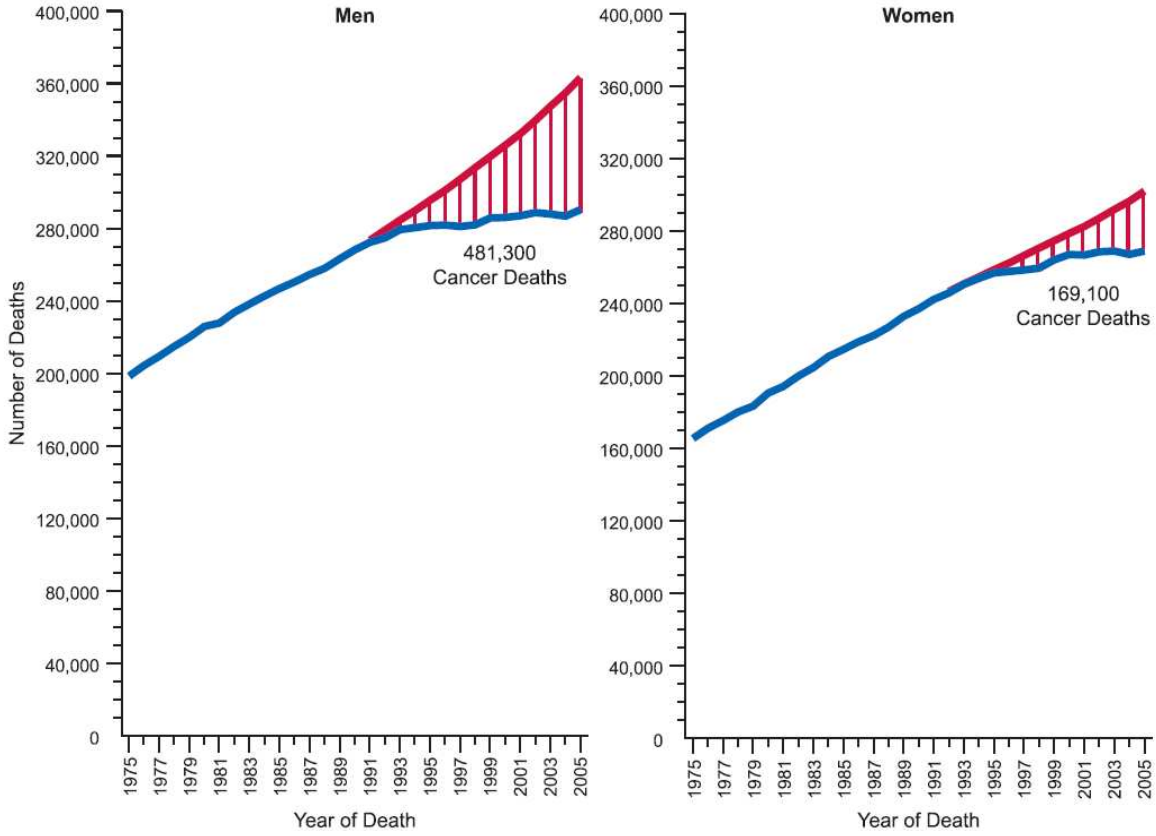

Figure 1.6: Total number of avoided cancer deaths in the United States. The blue line represents the total number of reported cancer deaths per year. The red line represents the expected number of deaths if mortality rates had not improved from 1990 through to 2005. Reproduced from [5].

1.3 Volumetric-modulated Arc Therapy

The two major disadvantages of IMRT when compared with conventional 3DCRT include an increase in both the time and monitor units required for treatment. These two disadvantages result in decreased productivity, increased costs, and potentially an increased risk of secondary cancers due scatter and leakage radiation [28, 29]. An attempt to address both of these issues comes in the form of rotational based IMRT or volumetric-modulated arc therapy (VMAT). The seminal paper for this technique was published in 2008 by Karl Otto [6] but work on rotational IMRT dates back to the inception of more traditional intensity modulated techniques. Namely, the early development of intensity-modulated arc therapy (IMAT) was published by Cedric Yu in 1995 [30]. This method proposed a sliding window type IMRT, delivered over several continuous arcs.

Further IMAT based developments have since been made [31] but wide spread clinical implementation has been sparse due to several limiting factors. Firstly, in order for the treatment to be delivered throughout constant gantry rotation, the changes in MLC leaf position must be restricted between consecutive gantry positions. This has been overcome through the use of several superimposed arcs [30, 32, 33] but this increases treatment time to the point where it is comparable with conventional IMRT. Secondly, inverse optimisation of the dynamic treatment is simulated through a coarse sampling of gantry angles and beam apertures, often resulting in unacceptable dosimetric differences between the planned and delivered treatment [6, 33].

The recent work by Otto [6] builds on the original concepts outlined by Yu [30] but introduced two further dynamic variables on top of the dynamic gantry and MLCs, namely dose rate and gantry angular velocity [6]. This initial work also outlines the mathematical grounding for an efficient inverse planning algorithm used to produce this complex plan and treatment delivery [6], and overcome the above limitations of IMAT. This algorithm is based on the previously published concept of direct aperture optimisation [32], rather than more conventional inverse optimisation of beam fluence, followed by MLC sequencing. This aperture based algorithm varies the MLC

position and monitor unit (MU) weight then evaluates the change based on a quadratic cost function and the dose-volume constraints that define it [6].

The revolutionary step that VMAT takes is the method used to sample the continuous dynamic arc by a finite set of static fields, or control points. Initially, a relatively coarse sample of the full arc is taken (Figure 1.7(a)) with a control point at the start and end of the arc, and evenly spaced points between. After a certain number of iterations (MLC and/or MU weight changes) further control points are added (Figure 1.7(b)-(c)) between each existing point. The MLC positions and MU weights for these new points are interpolated and calculated from neighboring points respectively [6]. This process is repeated (Figure 1.7(d)) until the finite sample gives an accurate representation of the dynamic arc [6]. Sampling the arc in this fashion allows the optimiser to converge towards an optimal solution in a practical time frame, whilst still giving a dosimtrically accurate representation of the full dynamic arc.

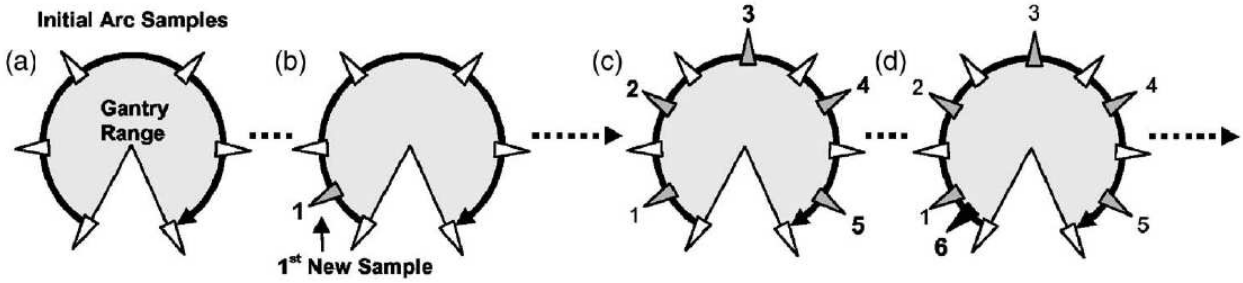

Figure 1.7: Illustration of VMAT progressive control point sampling. (a) Shows the initial coarse distribution of static control points, (b) the introduction of the first interpolated point, (c) the full sample in the second progressive level and (d) the addition of further points. Reproduced from [6].

Since this initial publication, there has been three clinical implementations of VMAT, each with subtle differences in both optimisation and delivery; RapidArc™ (Varian Medical Systems, Inc., Palo Alto, CA, USA), Elekta VMAT™ (Elekta, Inc., Stockholm, Sweden) and Phillips SmartArc™ (Phillips, Inc., Andover, MA, USA). At the time of writing volumetric-modulated are still in the early stages of development, with the RapidArc (RA) system seeing the largest uptake in both the clinic and literature [34]. The first planning study comparing 3DCRT, conventional IMRT and VMAT was published later in the same calendar year [35], comparing prostate delivery for 3DCRT, IMRT and VMAT. VMAT plans were calculated using a predecessor algorithm that would eventually become Varian's RA, and were optimised using both constant and variable dose rates throughout gantry rotation. The results of this paper show that the VMAT plans had comparable conformity, homogeneity, and organ sparing to conventional IMRT. A further improvement in organ sparing with variable dose rate VMAT was also observed. As expected, both intensity modulated techniques had greatly improved organ sparing when compared with 3DCRT. One of the techniques driving advantages was also upheld with an average reduction in MUs of 40%, when compared with static gantry IMRT. Although treatment times were not directly addressed, a reduction in treatment time can be inferred as a consequence of the large reduction in MUs.

Subsequent planning studies have extended this *proof of principal* to other treatment sites, including; prostate with seminal vesicles (SV) and pelvic nodes [36-38], head and neck [39, 40], malignant gliomas [41, 42], anal canal [43], breast [44], cervix [45], multiple brain metastases [46, 47] and peadiatric cancers [48]. To generalise these studies, the results have shown that VMAT produces comparable or even slightly improved dose distributions, with a significant reduction in both MUs and treatment time over a wide range of clinical sites [34]. The above studies are all based around RA optimisation and delivery, but similar results have been published for both Elekta VMAT [49] and Phillips SmartArc [50]. The theoretical advantages of volumetric-modulated techniques are the subject of ongoing debate within the literature [51-53].

1.4 Motivation and Outline of Work

Arc-based radiotherapy is a complex technique that has been made possible due to recent developments in both linac hardware and optimisation algorithms. Although the technique is still in its infancy, the proposed advantages are already well established. The reduction in treatment time gives immediate advantages within the clinic, increasing patient throughput or allowing more time for image guided or adaptive treatments. The long term follow up of a large cohort of patients is required to determine if the reduction in MUs does in fact result in less secondary cancers. Volumetric-modulated based techniques still have a long way to grow until maturity is reached, with much still unknown about the inner workings and user consequence of the progressive optimiser, accuracy of the associated dose calculation algorithms, and areas of unexplored clinical application. The present work attempts to address the following questions:

- How does the PRO differ from static gantry inverse planning and what is the result for the end user?
- Can planning class solutions improve and standardise the planning process?
- To produce the optimum plan, are user interactions required throughout optimisation?
- What further clinical issues can be solved with conformal RA techniques?
- When calculation dose from volumetric modulated deliveries, can the accuracy of the analytic anisotropic algorithm be improved by applying more appropriate configuration beam data?

Chapter 2 – RapidArc Planning Strategy

2.1 Introduction

Living up to it's namesake, interest in and the clinical uptake of rotational forms of IMRT has been rapid since the seminal publication by Otto [6]. This uptake has come on the back of a variety of planning related studies [35-39, 41-44, 46-48, 54-59] comparing 3DCRT, static gantry IMRT, rotational IMRT and sometimes Tomotherapy or proton therapy [37, 38, 48, 55], for various clinical sites (including prostate [35-38]). The increasing maturity of the technique is such that it has even been described in review [34] along with several institutions publishing experience and data from their first 12 months of clinical treatments [60, 61]. In general, these studies have shown rotational IMRT to be at least comparable with static gantry IMRT (both IMRT techniques make improvements over standard 3DCRT) while many show an improved level of conformity, sparing of critical structures, and a slightly reduced level of homogeneity in the target volume. These studies have justified this rapid clinical adoption by providing evidence in favour for the major selling points of rotational techniques, by reducing both treatment time (TT) and monitor units (MUs) significantly, when compared with other intensity modulated techniques.

Although the clinical advantages of rotational techniques seem to be establishing themselves, a systematic process providing a turnkey solution for the inverse planning process is yet to be established. As a result, there is a strong correlation between the experience of the planner and the resulting plan quality. Therefore, reproducing this planning study data in the clinic can be a non-trivial undertaking. Rotational IMRT planning is performed through inverse planning techniques in a similar vein to that of static gantry IMRT but is further complicated due to the increased number of dynamic variables involved during delivery. Varian's solution (based on [6]) to this further complexity is the introduction of a new resolution based optimisation algorithm to aid in the inverse planning process. The aim of this current work is to provide a robust strategy or class solution [62], which streamlines the planning process, produces

clinically acceptable plans in the majority of cases and is generally and directly consistent with previously published planning study data.

An IMRT class solution has been previously defined by Mott et. al.[62] as:

"…as a set of IMRT planning parameters (beam arrangements, dose limits and penalties) that can be applied to every patient"

In the same fashion, this strategy will concentrate on RapidArc (RA) plans produced using the complementary planning software and the progressive resolution optimiser (PRO) for intermediate and high risk prostate patients, with a simultaneous integrated boost (SIB). The strategy will outline a systematic and streamlined workflow diagram and will cover; initial contouring and field set up, recommended starting objectives and required user interactions to be made throughout optimisation. This will be followed by a comparative planning study with standard static gantry IMRT, but will not be used as a justification for rotational techniques in general - as previously published - but instead for the methods used to produce the RA plans themselves. The results of this study will then be compared with to previously published data.

2.2 Methods

Prostate cancer is the most frequently diagnosed cancer in men globally [24] and in local regions [25-27]. The following strategy is intended for the use of planning SIB RA plans for patients with intermediate and high risk prostate carcinoma with at least one phase including the SVs. This empirical strategy has been devised through extensive planning experience and modifications made to the many planning parameters involved across a range of patients, both adopting time proven static gantry IMRT inverse planning techniques and devising new RA specific techniques. In the following, the application of this strategy, which is divided into pre-optimisation, optimisation and post-optimisation is described in general terms (2.2.1 and figure 2.3) before it is applied to a specific prostate planning protocol (2.2.2), namely the Conventional or Hypofractionated High Dose Intensity-Modulated Radiotherapy for Prostate Cancer (CHHiP) trial protocol [63]. All planning was done in the Eclipse treatment planning system (TPS), version 8.5.

2.2.1 Planning Strategy

2.2.1.1 Pre-optimisation

Contouring

The first step of the planning process is the contouring. In addition to standard contours, such as the body, planning target volumes (PTV) and organs at risk (OAR), further structures are created to aid in the inverse planning process. This approach is in analogy to the use of complementary contours used for IMRT planning to improve spatial targeting of dose and is an essential step for this RA based planning strategy. Henceforth, these additional contours are referred to as virtual contours, but others may refer to them as auxiliary contours. These structures are produced through a combination of automated cropping tools built into the Eclipse TPS. Examples are shown in Figure 2.1. In general, a virtual contour is created for any areas of overlap between PTV and OAR (Fig. 2.2a) and, if multiple dose levels exist within the target (e.g. prostate and seminal vesicles + margin → PTV1, prostate + margin → PTV2 and prostate → PTV3) (Fig. 2.2b). The virtual OAR structures allow for improved sparing

of the associated OAR while not giving conflicting optimisation inputs. The PTV rings are necessary due to the fact that all PTVs occupy the same physical space and therefore non-conflicting objectives can be applied to each individually to reduce hot areas and improve homogeneity in the more superficial PTV areas.

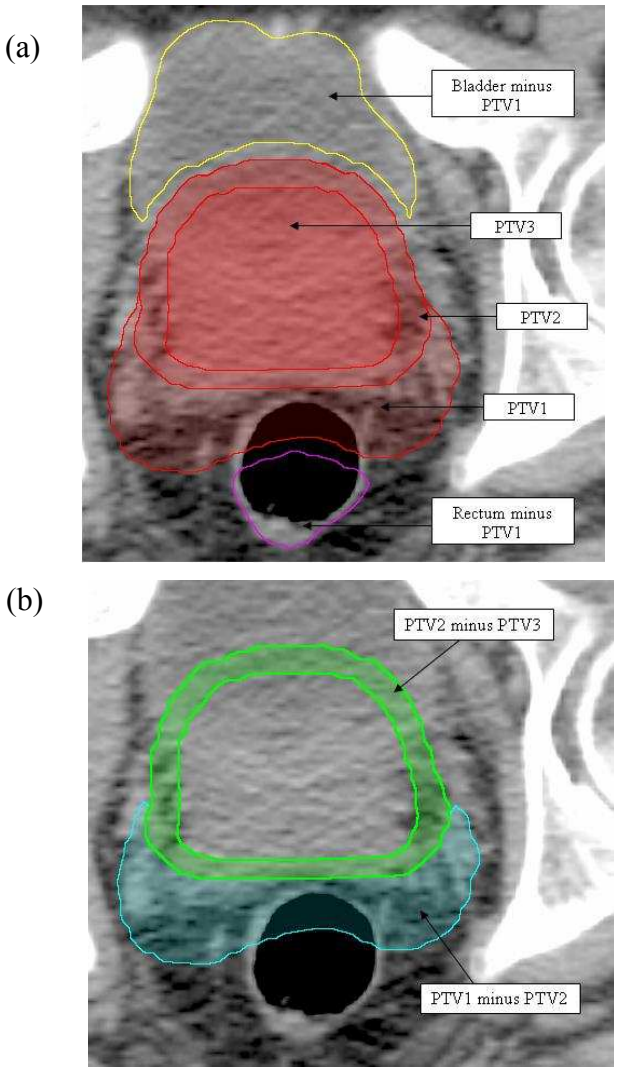

Figure 2.1: Virtual contours, as indicated by arrows. Image showing all three PTVs and two virtual structures (a). The two virtual structures represent the OAR (bladder and rectum) minus the largest volume PTV, plus an extra margin of 3mm. Illustration of two virtual PTV structures (PTV1 minus PTV2 (cyan) and PTV2 minus PTV3 (green)) (b).

Field set up

Once all the contours have been created a single arc field is set with a collimator rotation of 45° [64]. All RA plans require some degree of collimator rotation as to reduce the cumulative effects of tongue and groove leakage throughout gantry rotation, and to allow spatial modulation in the transverse plane. A collimator angle of 45° has been chosen as it gives the maximum level of modulation in the transverse plane and has been shown by other authors to be the optimal angle for prostate simulated geometries [64]. The jaws are set to be open to the largest PTV throughout the entirety of the gantry rotation, with an extra margin of approximately 10 mm. Although not employed here, the above two parameters may then be automatically optimised in Eclipse version 8.6 and above. The arc is set to run from 179° through to 181° in a counter clock-wise (CCW) direction or from 181° through to 179° in a clock-wise (CW) direction and the energy of the irradiating beam is 6MV. Although the target volume is deep, the fact that radiation is entering the patient from all angles, a beam energy of 6MV is adequate to produce acceptable dose coverage, without the increased neutron dose that will result from higher energy beams [65]. Other energies such as 10MV are not currently available in the Wellington Blood and Cancer Centre (WBCC) for planning or delivery, and are therefore not considered. The above field set up allows the optimisation algorithm the largest range of parameters, so that the chance of the best plan being produced is maximised.

Progressive resolution optimiser

RA optimisation and calculation in the Eclipse TPS utilises two identical algorithms to that of standard IMRT: the dose-volume optimiser (DVO) and anisotropic analytical algorithm (AAA). In brief, the DVO is an algorithm used to sample the dose distribution throughout optimisation. Points within investigated structures are sampled in a quasi-random nature and the dose calculated using the relatively fast multi-resolution dose calculation (MRDC) algorithm [66, 67]. The calculated dose is not stored but is used to calculate the current DVH and evaluate dose objectives. The AAA is the full dose calculation algorithm implemented post-optimisation, improving on accuracy when compared with the MRDC, at the cost of computational resource [66, 67]. The AAA is the topic of study in chapter 4.

The new - and unique - algorithm introduced specifically for RA is the progressive resolution optimiser (PRO) [6], as introduced in 1.3. Throughout optimisation the PRO makes iterative changes to the dynamic delivery variables (MLC, dose rate and gantry angular velocity) iteratively, in an effort to find the global minimum of the following objective function [6, 67]:

$$F_{obj}(j) = \xi_j \cdot w_j \sum_{i=1}^{N} (d_i - p)^2 \quad (1)$$

Where j is the current iteration, d_i is the dose at the i^{th} point within a structure, p is the prescribed dose, w_j is the multiplicative priority, and ξ_j is set to 1 if the objective is violated and zero if it is met [6, 67]. The global minimum (optimum solution) to this equation is found when the derivative is set to zero. The state of this function is assessed at the end of each iteration (based on the dose calculated by the MRDC), before further aperture based changes are applied. A real time graphical representation of this function is presented throughout optimisation, the gradient of which can indicate when user interactions are required (as referred to in 2.2.1.2).

These iterations are separated into five independent resolution levels, as introduced in figure 1.7. The first resolution level represents the full arc by 10 control points (essentially static fields). This number of control points is then doubled plus one for each successive resolution level, with the final arc being represented by up to 177 control points (Fig. 2.2 (a)-(e)). As each new control point is added, the dynamic variables are interpolated and calculated based on the two neighbouring and already existing points. The nature of this process means that the lower resolution levels are flexible to optimisation objective change but give a poor representation of the full arc, while the higher levels are less flexible but give a much more accurate representation of the full dynamic arc. What the introduction of this new algorithm means from a planning perspective will be outlined in the planning strategy below.

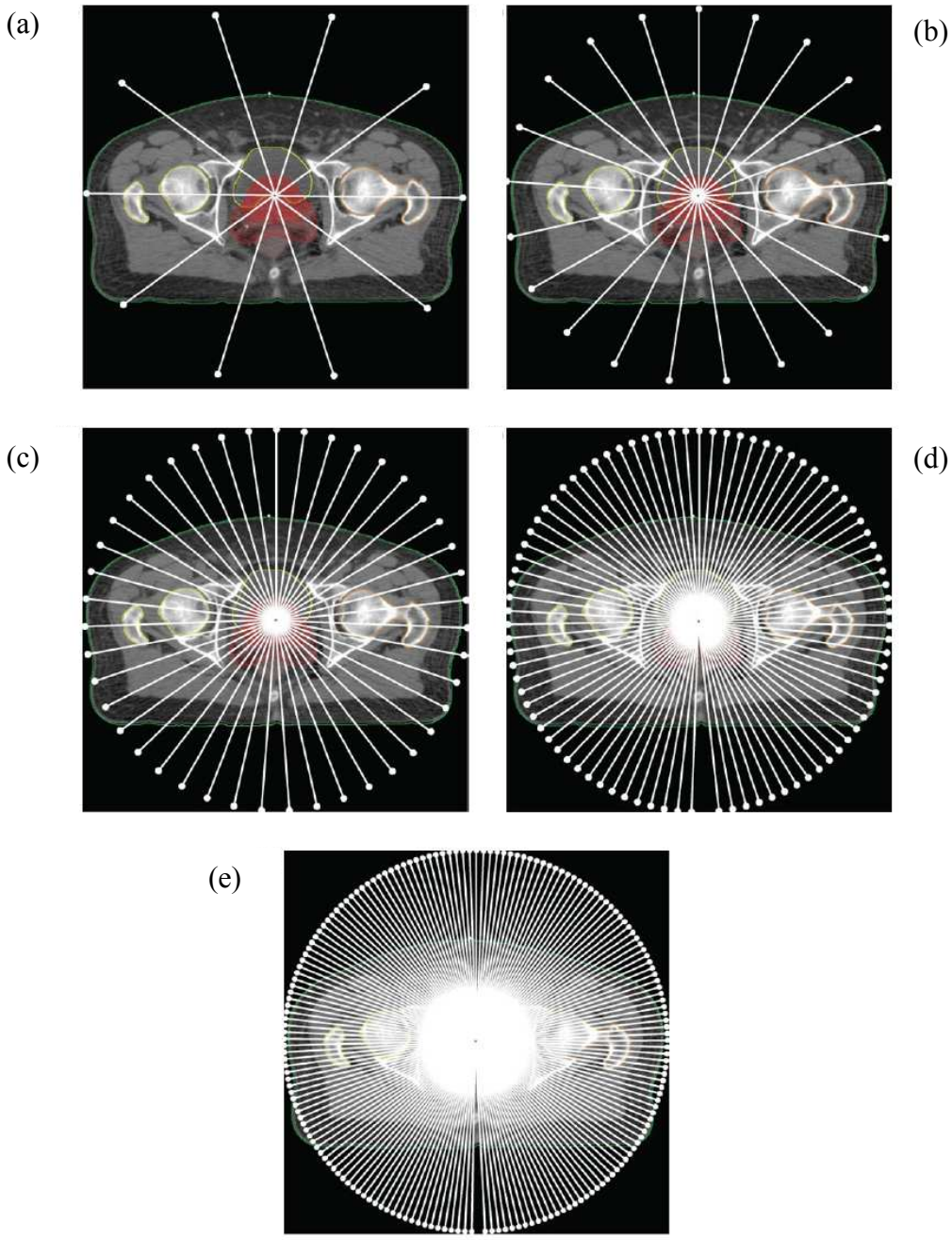

Figure 2.2: Figures (a) through (e) give a graphical representation of optimisation resolution levels 1 through 5, respectively. Each level illustrates the control point distribution in relation the patient data set.

Pre-optimisation dose objectives

The inverse planning process is aided through the definition of optimisation planning objectives. These can be either upper or lower objectives that define the input data for optimisation penalty functions. Each objective corresponds to a point in the dose-volume data space. Upper objectives give a maximum limit to the corresponding

DVH whilst lower objectives give a minimum. Each objective has an assigned priority related to the penalty function input, acting in a multiplicative fashion. The normal tissue objective (NTO) is a set of input parameters that defines how dose falls off outside a defined PTV, and can be used to reduce hot spots in normal tissue and produce a sharp dose fall off outside target volumes. This function is mathematically defined as follows [68]:

$$f(r) = f_0 e^{-k(r-r_{Start})} + f_\infty (1 - e^{-k(r-r_{start})}), r \geq r_{start} \quad (2)$$
$$f(r) = f_0, r < r_{start},$$

where r = distance from the target border, r_{start} = starting fall-off point, f_0 = start dose (%), f_∞ = end dose (%) and k = fall off. An empirical set of these parameters, maximising organ sparing when only the NTO is applied throughout optimisation, is as follows; r_{start} = 0.2 cm, f_0 = 103%, f_∞ = 60%, k = 0.13, with a priority (P) of 150.

The number of MUs required to deliver the sum of any given control point combination is directly related to the size of the corresponding MLC apertures. Furthermore, small MLC apertures may be associated with dosimetric errors between AAA calculated and deliverable dose (see chapter 4). Therefore, it is important that the maximum number of MUs is constrained throughout optimisation, as to uphold the advantages of RA in general and improve dosimetric accuracy, by increasing the average beam aperture size. The strength of this objective should be high (100) but may vary depending on clinical site (an example is given in the planning comparison).

The planning strategy utilises a set of dose objectives that are set prior to the initiation of optimisation. A set of three objectives are assigned for each PTV, one lower and two upper objectives. The lower objective corresponds to 100% of the PTV volume and approximately 98% of the prescribed dose and the first upper objective, 0% volume and 105% of the largest prescribed PTV dose. Each of these objectives initially has a low priority (P = 50). The third objective is an upper objective with identical values to the above lower objective, except that it has a priority of zero. As alluded to earlier, the NTO needs a defined starting local, r_{start}. This position is the

PTV upper objective with the lowest corresponding dose. This third objective, henceforth referred to as the 'butterfly objective' (due to the fact that an upper and lower objective set at the same dose-volume point resembles a butterfly) is this starting point for the NTO. The priority of zero ensures that it has no effect on the penalty function output. In general, experience has shown that plans employing the NTO without a butterfly objective have a reduced level of PTV homogeneity, conformity and a higher maximum point dose, when compared to those that do include a butterfly objective.

An upper objective for each OAR is defined so as to push any relative hot spots away from any OAR-PTV overlap areas. These objectives are set at the dose-volume point corresponding to 0% of the structure volume and 98% of the prescribed dose, with P = 100. An upper objective for each of the virtual PTVs created to exclude overlap with other PTVs is also assigned. These objectives should have a volume of 0% and a dose half way between the two PTV prescribed doses and have a priority of P = 150.

At this point, it is useful to add a variety of 'ghost' objectives. These objectives will be solely used as a visual aid for the planner and will have a priority of zero, and therefore not directly contribute to the optimisation. They may directly correspond to the planning protocol OAR dose constraints (as below) or any other user defined DVH points of interest. Once confidence in the above strategy is established, a planning protocol can be set within Eclipse to further automate and streamline the planning approach.

2.2.1.2 Optimisation

As previously stated, the lower optimisation resolution levels are sensitive to change but give a coarse representation of the final arc, where the reverse is true for the higher levels. As a consequence, it is important that appropriate MLC apertures are defined early in the optimisation process, as control points added further through the optimisation process will be interpolated from these initial apertures. This is achieved through reserving lower levels (1-3) for sparing of critical structures while PTV coverage is concentrated on during the later stages (4-5). This is reflected through the relative priorities of the corresponding structures. Once optimisation has been initialised, it is first allowed to stabilise to what is achievable through the initial

starting objectives and the NTO. Following this, OAR sparing is improved upon through the addition of several upper objectives added to the associated virtual OAR structures. Further objectives are not added directly to the OAR structures themselves as to eliminate conflicts of objectives in areas of overlap. In saying this, improved sparing of the virtual OAR will have an associated sparing of the OAR itself, due to the spatial link shared by the two structures. Highly critical structures (e.g. rectum) have assigned priorities of P = 125 while other less critical structures (e.g. bladder) have a lower priority of P = 50. These objectives are initially placed just below the corresponding DVH but are refined over the first three resolution levels to improve OAR sparing well within any user defined (ghost) constraints, using the gradient of the objective function values as a guide (pull DVH further when the corresponding DVH is less that -0.5). It is expected that PTV coverage throughout these resolution levels will be relatively poor, with sometimes sharp sigmoidal shapes, hot volumes and even larger cold volumes, but will show improvements throughout. In saying this, it is important that the PTVs' DVHs at least cross through the upper and lower objective threshold. If this is not the case then there may be an issue with the defined objectives (including a conflict with dose prescription) or jaw positions.

Once the optimisation reaches level four, the priority of the PTV objectives are increased to P = 200 (excluding the butterfly constraint that should be frozen at zero). In general, all other objectives and their associated priorities are frozen from this point, through to the completion of the optimisation process. Throughout the final two resolution levels the ability of the optimiser to meet the PTV objectives will improve. This will be at the cost of reduced OAR sparing but will be of minimal effect. If the virtual OARs' DVHs move significantly from the objectives as they were at the end of level three, then they can be relaxed slightly as to give the optimiser a higher concentration on PTV coverage. Any PTV lower objective should be strictly met towards the end of level five. The priorities of the PTV objectives are increased in iterations of 50 (up to P = 400), at points when the gradient of the PTV objective functions drops below -0.5. Increasing the priorities in this fashion often results in an objective function that resembles an increasing sawtooth function. The collective PTV upper objectives do not need to be strictly met but should not be far off achieving the 105% dose-volume point. It is not of high importance that any virtual PTV structures be strictly met and may be hidden from resolution level one. The optimisation is only

allowed to come to completion if the total objective function gradient is close to zero and the above guidelines are met. If this is not the case, the optimisation must be paused and PTV priorities increased further, until the above requirements are met.

2.2.1.3 Post-optimisation

Following optimisation, dose calculation is done using the optimised MU value and the AAA dose calculation algorithm with a dose grid size of 2.5 mm. The dose distribution is then evaluated and the DVHs examined for the plans ability to meet any dose constraints. If target volume coverage does not meet ICRU 83 criteria, there may be a need to re-normalise the whole plan by adjusting the plan normalisation value, usually by no more than 1-2%.

2.2.2 Planning Study

The following comparative planning study serves a two-fold purpose. Firstly, it provides a practical example of the above SIB RA planning strategy, implementing the CHHiP protocol. It secondly serves as an inter-comparison of the produced RA plans to static gantry IMRT plans, as a justification for the methodology used to create the RA plans. The study compares RA and IMRT plans produced for 10 randomly selected high and intermediate risk (as defined by the CHHiP protocol; clinical stages: T1b/c, T2a/b/c or T3a, and with PSA + ((Gleason score - 6)*10)>15), previously treated patients with prostate carcinoma at the WBCC. The comparison with 3DCRT has been omitted due to the results of previously published studies [35-38] and the difficulty of comparing SIB and sequential boost plans.

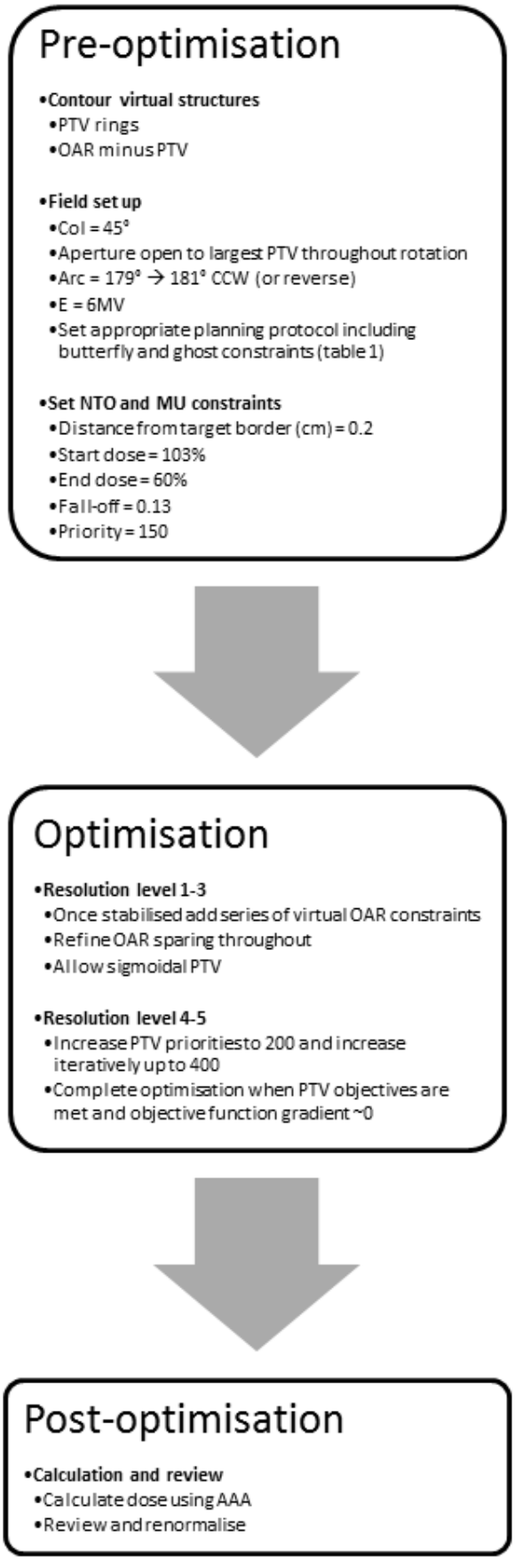

Figure 2.3: Summary of planning strategy, represented as a work flow diagram.

2.2.2.1 Planning Method

All RA and IMRT plans were produced to comply with the control arm of the CHHiP protocol, and optimised using Eclipse V8.5, on a single PC housing a quad core 2.5GHz processor. For both types of plans, dose calculation was done with the aid of the distribution calculation framework (DCF), whereby the computational workload was shared by eight networked PCs that were identical to that used for optimisation. The CHHiP protocol comes from a current prostate hypofractionation trial out of the United Kingdom [63]. The control arm of this trial gives up to 74 Gy to three separate PTVs using a SIB in 2 Gy daily fractions.

All RA plans used in the study were planned as per the above strategy. Comparative sliding window IMRT plans consisted of five separate fields of gantry angles 0°, 45°, 100°, 260° and 315°. These beam angles are in line with the local protocol that consistently produces plans of comparable quality to published class solutions [69]. The energy of these fields was 6MV and an identical NTO as above, was employed. A high priority was initially given to the target structures and once PTV coverage was sufficient, virtual organ objectives (P = 125) were added to spare the associated OAR as much as possible, without compromising the PTV coverage. See table 2.1 for a summary of IMRT starting objectives and priorities.

As per the CHHiP protocol, the gross tumour volume (GTV) is defined as the prostate only, the clinical target volume (CTV) 1 as the prostate and seminal vesicles with a 5 mm margin, CTV2 as the prostate plus a 5 mm margin and CTV3 as the prostate only. All PTVs (1-3) add an extra 5 mm to the corresponding CTV, except that for PTV2 and PTV3 the margin in the posterior region (towards the rectum) is reduced to nil. PTVs one through three have prescribed 2 Gy equivalent doses of 54, 70 and 74 Gy respectively. See table 2.2 for a summary of contouring and prescribed doses.

Structure	Objective	Volume (%)	Dose (Gy)	Priority	Type
PTV1	Upper	0	77.0	250	PTV Upper
	Lower	100	59.2	300	PTV Lower
PTV2	Upper	0	77.0	200	PTV Upper
	Lower	100	71.0	300	PTV Lower
PTV3	Upper	0	77.0	200	PTV Upper
	Lower	100	74.0	300	PTV Lower
Rectum	Upper	0	73.0	100	OAR
Bladder	Upper	0	73.0	100	OAR

Table 2.1: IMRT starting objectives. Butterfly and ghost objectives omitted.

Structure	Structure grown from	Margin in all directions/posterior (mm)	Prescribed dose (Gy)	2 Gy equivalent	Minimum isodose coverage (%)
PTV1	Prostate + SV	10/10	59.2	54	76
PTV2	Prostate	10/5	71	70	91
PTV3	Prostate	5/0	74	74	95

Table 2.2: Summary of CHHiP trial contouring and dose prescription. SV = seminal vesicles

Normal tissues structures include the rectum, bladder, femoral heads (FHs) and the body (all defined as solid structures). The rectum is contoured from the anus superiorly through to the recto-sigmoid junction. The bladder is contoured in full from base to dome (any randomly selected patient deemed to have insufficient bladder filling (<140cc) was rejected from the study (n = 1)). All CHHiP dose constraints are replicated as ghost constraints in table 2.3.

Structure	Objective	Volume (%)	Dose (Gy)	Priority	Type
PTV1	Upper	100	57.7	0	Butterfly
	Upper	0	77.0	50	PTV upper
	Lower	100	57.7	50	PTV lower
PTV2	Upper	100	69.2	0	Butterfly
	Upper	0	77.0	50	PTV upper
	Lower	100	69.2	50	PTV lower
PTV3	Upper	100	73.0	0	Butterfly
	Upper	0	77.0	50	PTV upper
	Lower	100	73.0	50	PTV lower
Rectum	Upper	0	73.0	100	OAR
	Upper	80	30.0	0	Ghost
	Upper	70	40.0	0	Ghost
	Upper	60	50.0	0	Ghost
	Upper	50	60.0	0	Ghost
	Upper	30	65.0	0	Ghost
	Upper	15	70.0	0	Ghost
	Upper	3	74.0	0	Ghost
Bladder	Upper	0	73.0	100	OAR
	Upper	50	50.0	0	Ghost
	Upper	25	60.0	0	Ghost
	Upper	5	74.0	0	Ghost
FH	Upper	50	50.0	0	Ghost

Table 2.3: RapidArc starting objectives. Butterfly and ghost objectives included.

2.2.2.2 Evaluation Tools

All statistical analysis was done using a one sided paired t test with values deemed to be statistically different if $p \leq 0.05$. Estimated RA treatment times were calculated by dividing the arc length (358°) by the average gantry rotation rate, taken from the

Eclipse TPS output. Estimated IMRT treatment times were calculated through the sum of multiple factors; the time to deliver the beam (total MU/dose rate), the time to rotate through the range of field angles while travelling at 360°/min and an extra factor that accounts for the amount of time for mode up, data transfer of the MLC delivery files, error in the estimated rotation time and the operator deliver time. This method was devised by Oliver et. al. [55] and the time allocated for the above mentioned extra factor, equals 19.1 ± 2.2 seconds, per field. The quality of PTV3 coverage was evaluated through the statistical comparison of the V_{95}, $D_{95,}$ CI, HI, D_{max} and D_{mean}, where V_{95} is calculated as the percentage of PTV3 receiving 95% of the target dose (or 70.3 Gy), the D_{95} is defined as the dose to 95% of PTV3 and the modified conformity index (CI_{95}) defined as follows [70]:

$$CI_{95} = \frac{V_{91}}{V_{PTV2}} \tag{3}$$

where V_{91} is the 91% isodose volume (equivalent to 95% of the prescribed dose to PTV2) and V_{PTV2} is the volume of PTV2. The conformity index gives an indication as to how conformal the minimum (95% as per ICRU) prescribed dose is to PTV2. CI_{95} values closer to 1 indicate a higher level of conformity with any values outside the range of 0.9-1.5 deemed clinically unacceptable [70]. Due to the PTV geometries and dose gradients involved, the CI_{95} of PTV2 is the only index that gives an accurate indication of the overall conformity of the plan. The homogeneity index (HI) is defined as follows:

$$HI = 100 * \left[1 - \left(\frac{D_{5\%} - D_{95\%}}{D_{mean}} \right) \right], \tag{4}$$

where $D_{5\%}$ is the dose to 5% of PTV3, $D_{95\%}$ is the dose to 95% of PTV3 and D_{mean} is the mean PTV3 dose. HI values closer to 100% indicate more homogeneous dose coverage within the target volume. The ability of the two treatment modalities to spare critical structures was assessed through dosimetric end points that correspond to the CHHiP protocol dose constraints, maximum and mean dose along with OAR equivalent uniform doses (EUD). The EUD is defined as the uniform dose that will produce the equivalent radiobiological effect as the organ specific non-uniform dose distribution. This value is mathematically defined as [71]:

$$EUD = \left(\frac{1}{N} \sum_i D_i^a \right)^{\frac{1}{a}}, \quad (5)$$

where N is the number of voxels within the investigated structure, D_i represents the dose to each individual voxel within the structure and a is an organ (or tumour, see chapter 4) specific dose volume parameter (a = 8.3 for rectum and a = 2 for bladder [35]).

RA spreads low doses of radiation to larger areas of normal tissue and correlations between the induction of secondary malignancies and the volume of peripheral normal tissue receiving low doses of radiation have been reported [72]. Although this is not the concentration of the paper, volume of tissue receiving low doses (> 2 and 5 Gy) of radiation are also reported.

2.2.3 User Interaction

To further scrutinise the hypothesis that applying IMRT like class solutions to the RA planning process does not produce optimal plans and that user interaction is required (as presented above), all 10 patients were retrospectively re-planned with a single planning template set at the start of optimisation and the PRO allowed to run without user interaction. This template contained identical objectives to those found in table 2.2, except that all PTV priorities were increased to 300. A set of five upper objectives were also added to the virtual organs at risk that correlate to the average values achieved in the previous RA plans, with a priority of 125. As a measure of the differences in the two sets of plans, the PTV D_{mean}, D_{max}, HI and CI_{95}, along with all rectal dose-volume points were then compared.

2.3 Results

Justification for the outlined planning strategy is provided by the results of the comparative planning study as presented. The 10 patient mean PTV3 (Fig. 2.4 (c), rectum, bladder and left femoral head volumes were 94 ± 57 (standard deviation), 48 ± 11, 300 ± 120 and 182 ± 31 cm^3 respectively. A summary of plan and target coverage parameters is found in table 2.4 and mean target and OAR DVHs in figures 2.4 and 2.5 respectively. Representative dose distributions can be found in figure 2.6 and example control point beams eye view (BEV) in figure 2.7. Consistent with previously published data and the driving force for rotational techniques, the MU and TT is significantly reduced for RA compared with static gantry IMRT. The V_{95}, D_{95} and D_{mean} all show no significant difference. The conformity of the RA plans is improved on average over IMRT although the maximum dose and homogeneity is slightly worse. Detailed analysis of PTV1 (Fig. 2.4 (a)) and PTV2 (Fig. 2.4 (b)) is not considered here but all 10 RA and IMRT plans comply with the CHHiP protocol requirements.

	RA		**IMRT**		**Significance**
	Average	**Std dev**	**Average**	**Std dev**	
MU	541.0	21.1	805.7	81.9	RA<IMRT
TT (s)	65.0	0.1	243.2	11.6	RA<IMRT
V_{95} (%)	99.8	0.3	99.9	0.3	NS
D_{95} (Gy)	71.6	0.3	71.7	0.4	NS
CI_{95}	1.08	0.08	1.17	0.08	RA<IMRT
HI (%)	95.8	0.2	96.3	0.6	RA<IMRT
D_{max} (Gy)	76.4	0.6	75.6	0.5	RA<IMRT
D_{mean} (Gy)	73.0	0.4	73.2	0.3	NS

Table 2.4: Summary of planning study PTV3 analysis.
Std dev = absolute standard deviation, NS = not significant

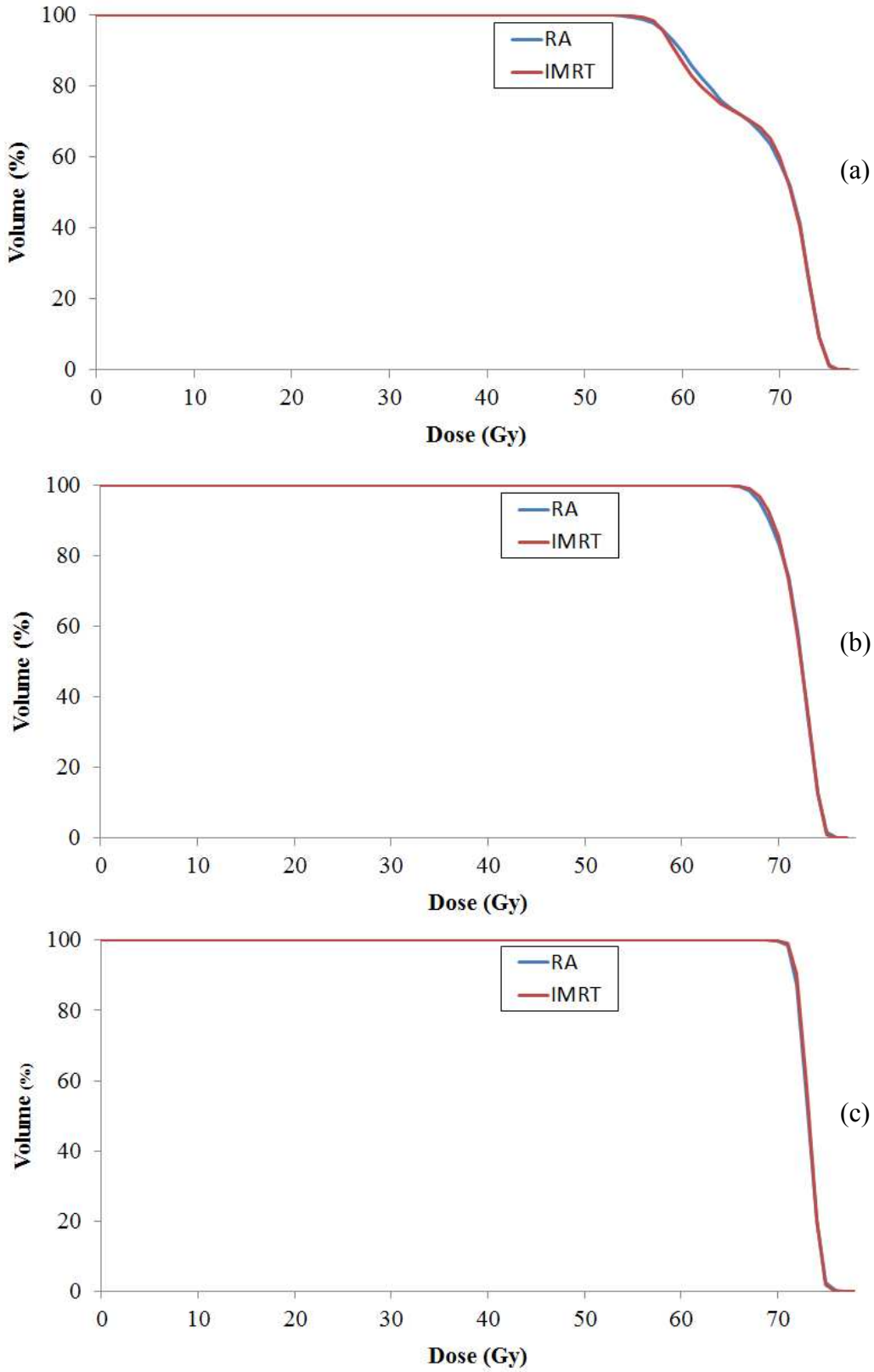

Figure 2.4: Mean DVH for all 10 patients showing PTV1-3 (a)-(c), for RA and static gantry IMRT.

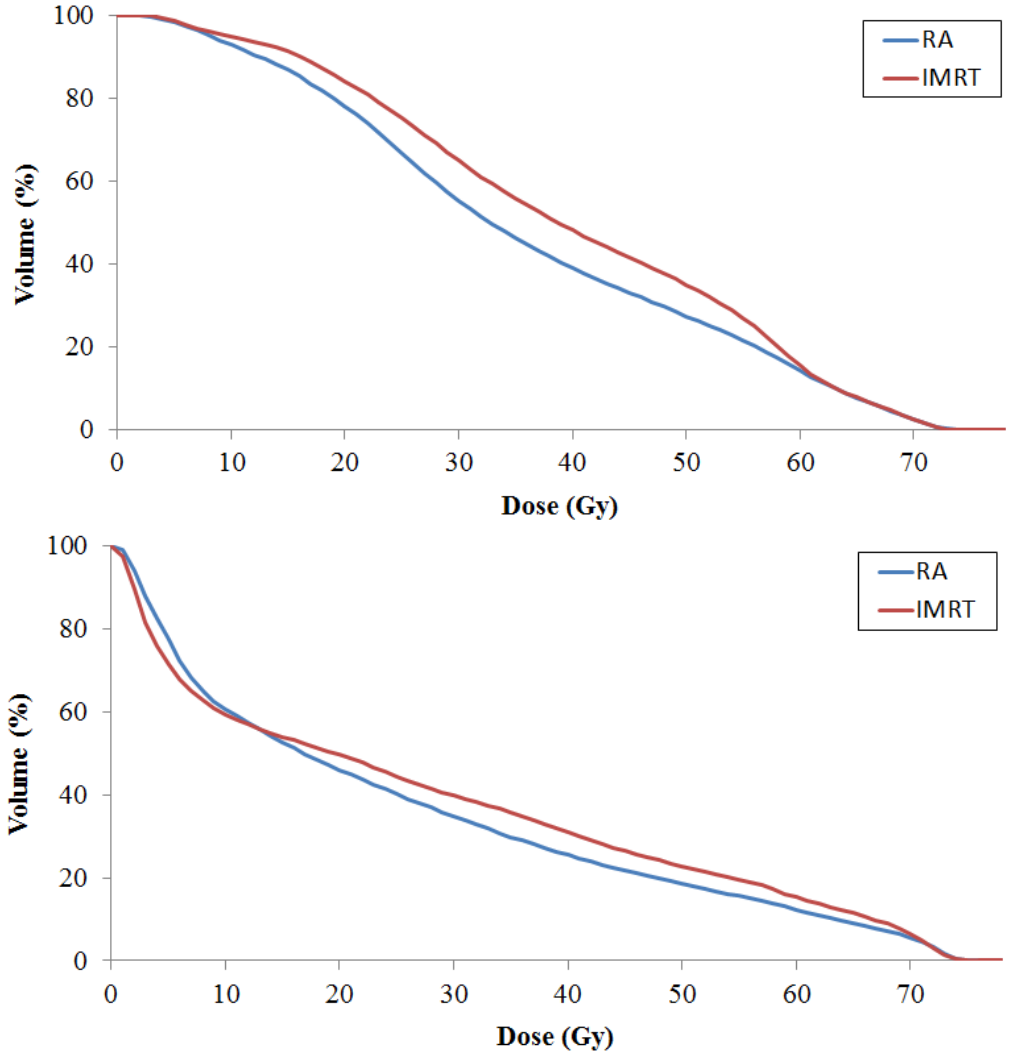

Figure 2.5: Mean DVH rectum (a) and bladder (b), comparing RA with static gantry IMRT.

Analysis of the three main OARs (rectum (Fig. 2.5 (a), bladder (Fig. 2.5 (b)) and the femoral heads) can be found in table 2.5. The RA plans spared the rectum better than IMRT over the whole range of dosimetric end points. The high volume end points ($V_{80\%}$-$V_{30\%}$) all showed a statistical difference while the low volume end points ($V_{15\%}$ and $V_{3\%}$) do not. Although the maximal dose point is larger for the RA plans, the mean dose and EUD is still significantly lower. Analysis of the bladder shows improvements for RA although all of the investigated parameters were deemed statistically insignificant. The single dosimetric end point ($V_{50\%}$), mean and maximum dose of the (representative) left femoral head were all significantly improved for the RA plans when compared with the IMRT plans.

The average volume of normal tissue (body minus largest PTV) receiving more than 2 and 5 Gy for RA is 8200 ± 1300 and 5650 ± 990 cm^3 respectively. These values were on average lower for IMRT (7728 ± 1343 and 5320 ± 891 cm^3), although both differences were not deemed significant.

		RA		IMRT		Significance
		Average	**Std dev**	**Average**	**Std dev**	
Rectum	$V_{3\%}$	68.7	2.4	68.8	2.3	NS
	$V_{15\%}$	59.1	3.0	60.3	2.8	NS
	$V_{30\%}$	47.2	5.4	52.8	4.4	RA<IMRT
	$V_{50\%}$	32.2	5.2	38.1	4.3	RA<IMRT
	$V_{60\%}$	27.5	4.7	32.3	4.3	RA<IMRT
	$V_{70\%}$	23.6	4.3	29.4	6.0	RA<IMRT
	$V_{80\%}$	19.8	3.8	24.0	3.4	RA<IMRT
	D_{max}	73.9	0.9	72.7	0.8	RA>IMRT
	D_{mean}	36.2	3.8	39.7	3.1	RA<IMRT
	EUD	40.6	3.1	43.7	2.7	RA<IMRT
Bladder	$V_{5\%}$	65.9	9.1	68.2	5.2	NS
	$V_{25\%}$	37.4	17.5	42.8	19.2	NS
	$V_{50\%}$	18.7	11.8	22.1	14.1	NS
	D_{max}	75.3	0.7	74.8	0.8	NS
	D_{mean}	25.7	10.0	27.5	10.8	NS
	EUD	52.8	4.6	54.0	4.6	NS
FH	$V_{50\%}$	18.1	6.3	23.9	9.9	RA<IMRT
	D_{max}	39.8	5.4	47.4	1.8	RA<IMRT
	D_{mean}	18.3	4.0	22.2	6.2	RA<IMRT

Table 2.5: Summary of planning study OAR analysis.

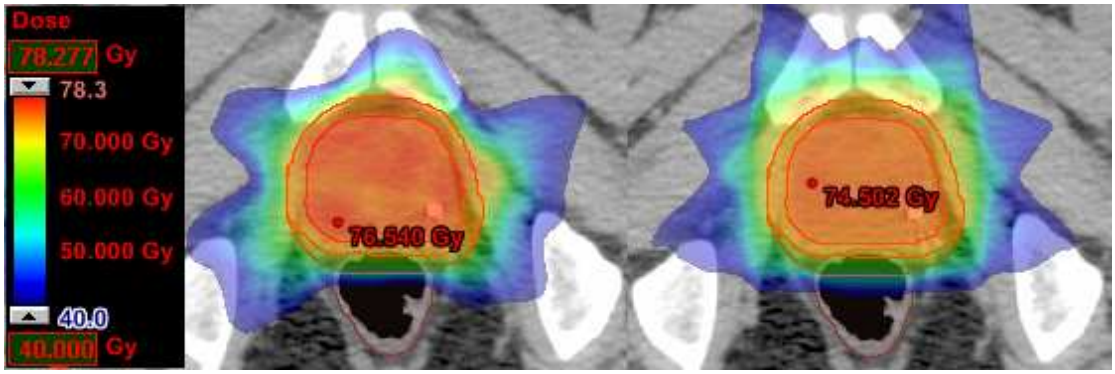

Figure 2.6: Representative sagittal dose distribution. RA (left) and five field IMRT (right). The dose colour wash runs from 40 through to 78.28 Gy.

(a)

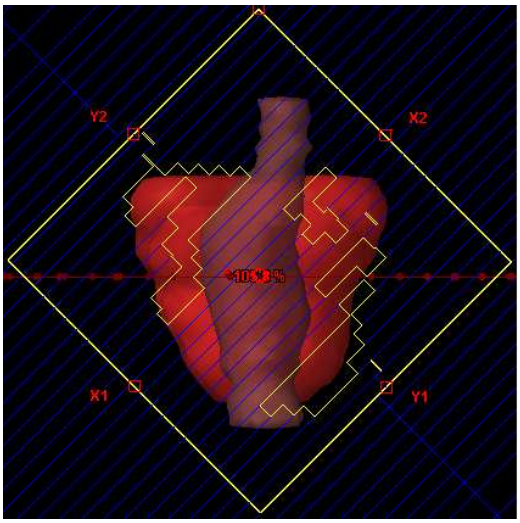

(b)

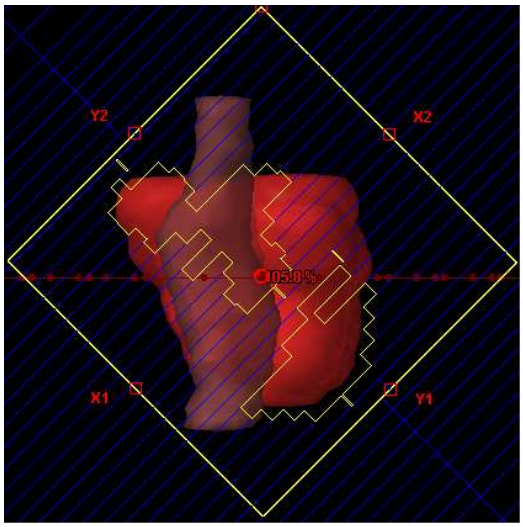

(c)

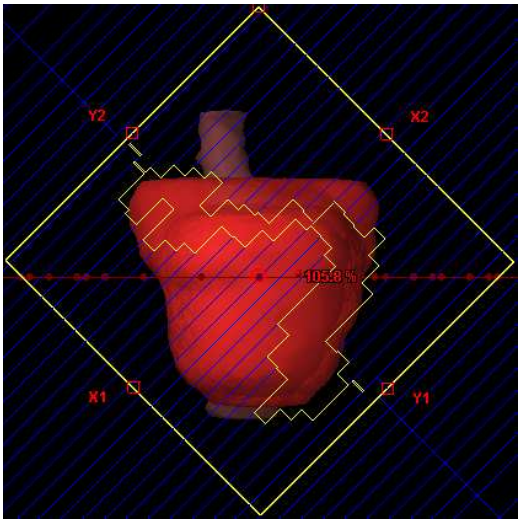

(d)

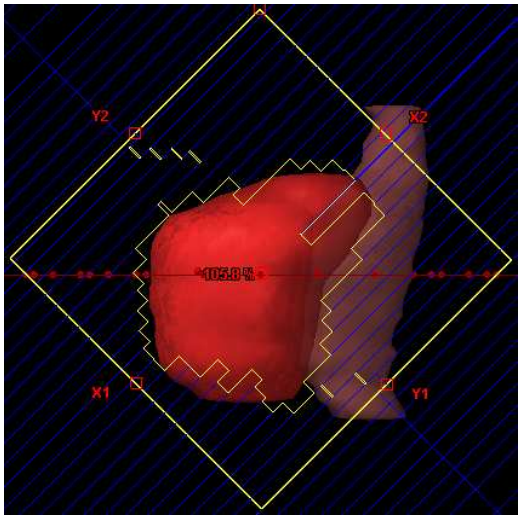

Figure 2.7: BEV control point examples taken from a single plan. Contours include the PTV and rectum.

When comparing the plans with and without user interactions, comparable PTV coverage was observed (D_{mean} and D_{max}, CI_{95} and HI) whilst the quality of OAR sparing was reduced. The mean rectal dose-volume points were lower across the range of points measured, significantly so for the $V_{50\%}$ point, as was the mean dose.

2.4 Discussion

An empirical planning strategy has been developed and implemented in an effort to streamline, standardise and improve the overall plan quality resulting from the RA inverse planning process. This process has both familiar and foreign aspects with regard to static gantry IMRT. The introduction of a resolution based optimiser means that solely employing standard IMRT class solutions and strategies does not produce the optimal plan. This is mainly due to the fact that RA planning uses a multi-step optimising process. It is paramount to understand this process, in order to know when and how to apply appropriate planning based parameters and to guide the optimiser in the desired direction. The development of new RA specific strategies is important to ensure consistency amongst plans and to streamline the planning process in general, whist producing clinically acceptable plans for a wide variety of patient anatomies. To the author's knowledge there is currently no published approach to class like solutions for RA planning and it is believed that development of these solutions will help departments reduce the time it takes to develop their own planning strategies when transferring from an existing static gantry IMRT program, or establishing a new dynamic IMRT program.

Application of the above strategy to 10 prostate patients has shown that all plans not only comply with the acceptance requirements of the planning protocol but are generally in line with previously published RA, prostate planning study data [35-38]. A direct comparison with published data is still required as evidence that both techniques are not off-set from published data. A summary of target and OAR comparisons can be found in table 2.6 and 2.7 respectively. Direct comparisons can be difficult due to variations in patients, target definitions and even dose prescriptions. With this in mind, the author believes that the presented justification planning study is not only generally but also directly comparable to previously published data. The comparison with static gantry IMRT is limited due to the fact that a 5-field technique was implemented. The observed differences in OAR sparing between the two techniques may be reduced or even removed with a more sophisticated 7 or 9-field IMRT technique, although this would increase both the MUs and TT even further. With the above strategy and the empirical set of parameters presented, the mean RA

optimisation time was 15.0 ± 1.3 minutes, a justifiable increase compared to the static gantry optimisation time of 8.0 ± 0.6 minutes, when the reduction in MUs and TT is considered.

	Planning study RA data	Published RA data
MU	541.0	454.2 [35], 477 [61]
***CI*$_{95}$**	1.08	1.12 [35]
HI	95.8	93.8 [35], 93.8 [61]
D_{max}	76.4	78.5 [35]
D_{mean}	73.0	75.0 [35], 74.0 [61]

Table 2.6: Plan and target volume comparison with published data. References indicated as superscript.

		Planning study RA data	Published RA data
Rectum	D_{mean}	36.2	40.2 [36], 40.3 [61]
	EUD	53.1	50.0 [35]
Bladder	D_{mean}	25.7	43.3 [36], 44.5 [61]
	EUD	32.6	32.1 [35]
FH	D_{mean}	18.3	19.4 [61]

Table 2.7: OAR comparison with published data. References indicated as superscript.

The results of the plan comparison with and without user interactions is further evidence to the point that interactions are required to (1) assign the optimum virtual OAR objectives, dependent on patient specific anatomy and (2) define appropriate MLC apertures in the lower resolution levels. Further to this point, the average virtual OAR constraints used for the re-planned optimisation were based on values that had already proven successful for this small group of patients, and therefore it can be envisioned that applying these values to a wider range of patient anatomies may produce results with even more dramatic advantages.

Although the data is not shown, further investigations revealed that the addition of a second full arc further improves OAR sparing but the improvement was deemed unnecessary when the associated increasing in both MU and TT is considered. Plans with two full arcs are investigated further in chapter 3. The above RA planning strategy has also been successfully trialled on a similar yet distinct disease site where the PTV wraps around an OAR (thyroid bed and spinal cord respectively), and even more complex treatment sites such as head & neck. Whilst the details go beyond the scope of this work, initial findings indicate that the virtual contouring, NTO, butterfly objective and optimisation user interactions can be transferred as presented here. However, more work is required to be able to determine the optimal number of arcs, collimator angle, jaw size, MU objective and avoidance sectors.

2.5 Concluding Remarks

The theoretical advantages of rotational techniques are well established but the detailed methods used to achieve these results – in the form of class solutions or otherwise – are yet to be published. In an attempt to supplement the literature, it has been shown that using the outlined field set up, starting objectives and optimisation strategy, prostate RA plans can be produced in a systematic manner to produce plans that are not only clinically acceptable but are generally and directly in line with previously published data. The slight increase in optimisation time of the PRO based inverse planning (compared with conventional inverse planning techniques) seems justified when other clinical advantages of RA are considered. Future iterations of the Eclipse TPS may also reduce this planning time gap. The MU and estimated TT are significantly reduced when compared with IMRT, whilst maintaining comparable target volume coverage and a slight improvement in conformity. RA OAR sparing is also shown to improve, although this may be reduced through comparisons to more sophisticated static gantry IMRT techniques. The presented planning strategy has been shown to work for the CHHiP protocol, but it can be easily modified and implemented to suit the specific requirements of other radiotherapy departments, in an effort to treat patients with high and intermediate risk carcinoma of the prostate in a highly conformal and time efficient manner.

Extensive RA planning study data has been published for a range of clinical sites, and now a streamlined planning strategy has been formulated to compliment these studies. A clinical site that is yet to be investigated (related to but independent of the prostate study presented above) is treatment of the prostate bed in the post operative setting. This treatment site provides many of its own challenges and problems, some of which may benefit from the implementation of the presented RA planning strategy. The feasibility of this application is the focus of the subsequent chapter.

Chapter 3 – Prostate Bed Feasibility and Dose Escalation Study.

3.1 Introduction

The focus of chapter 2 was to develop a RA planning strategy whereas chapter 3 switches tact to focus on the implementation of this strategy to an existing – and persistent – clinical problem within the WBCC, and is therefore more clinical in nature. The use of prostate bed radiotherapy as adjuvant therapy in men with adverse risk factors following radical prostatectomy, or in the salvage setting, offers a potentially curative treatment after an unsuccessful radical prostatectomy. In the adjuvant setting recent prospective randomised clinical trials have demonstrated significant improvements in both progression free and overall survival [73-76]. In the salvage setting, with either a rising prostate specific antigen (PSA) post surgery or a persistently elevated PSA following surgery, there have been no prospective randomised controlled trials investigating its use. However, numerous retrospective studies of salvage radiotherapy have demonstrated its efficacy. Furthermore, this data has been supported in both a multi-institutional pooled data analysis [77] and a comprehensive review of published studies [78].

Assuming that the residual tumour burden is much smaller than is the case with radical irradiation, modest doses of radiotherapy have generally been employed in post prostatectomy radiotherapy. In randomised clinical trials of adjuvant radiotherapy, patients were irradiated to doses of 60-64 Gy using 3DCRT and severe toxicity was unusual. For example, in the European Organisation for Research and Treatment of Cancer (EORTC) study at 5 years following treatment the cumulative incidence of grade 3 toxicity was 4.2% in the adjuvant arm and 2.6% in the observation arm ($p = 0.073$). However, the cumulative incidence of any grade of toxicity was significantly higher in the adjuvant arm compared to observation (64.9% versus 54.3%; $p = 0.05$) [76]. In the Southwest Oncology Group (SWOG) trial, although graded toxicity was not reported, rates of complications known to be related to treatment were also more common in the adjuvant radiotherapy arm (23.8% versus

11.9%; p = 0.002) [73].

At the dose levels used in both the SWOG and EORTC trials approximately 25% of patients will develop biochemical failure within 5 years. Moreover, in this group of patients local failure was the predominant site of relapse, suggesting that more aggressive local treatment might improve both biochemical control and survival. Although there is a considerable amount of data to support dose escalation for radical radiotherapy for localised prostate cancer [79-82], there is less data in the postoperative setting. Several small retrospective studies suggest that a dose response effect is seen with both adjuvant and salvage radiotherapy [83-86] and is supported by tumour control probability (TCP) modelling [87].

Following prostatectomy, the whole surgical bed may harbour microscopic disease and is therefore at risk of subsequent relapse [88, 89]. A number of consensus guidelines for target volume definition have been developed, based upon known patterns of recurrence [68, 90-92]. In these guidelines the posterior extent of the CTV often extends caudally either up to or behind the anterior edge of the rectal wall. With volumetric expansion to produce a PTV, this commonly creates a concave target volume that wraps around the rectum. Clinically, target volumes of this nature are difficult to treat effectively without significant rectal irradiation using simple 3DCRT. Compounding this problem is the fact that target volumes can show large inter-fraction motion due the variability in OAR filling in close proximity [93]. As a result, the integrity of the PTV is often compromised as to reduce the dose to the rectum. However, IMRT techniques can produce isodose distributions with concave shapes, and therefore allow for a reduction in rectal irradiation [94-96] and may provide solutions to these issues.

Fixed gantry IMRT has been extensively investigated as a primary treatment modality for prostate cancer [97-103], but there is less data on its use in the postoperative setting [104-106]. However, the limited clinical data available suggests a favourable toxicity profile in comparison to historical controls treated with 3DCRT and has been shown to allow for significant dose escalation. As an alternative form of IMRT, VMAT techniques similarly improves the conformity of radiotherapy [6, 34, 35], as presented in chapter 2. Rotational forms of IMRT are yet to be investigated in the

post-prostatectomy setting, and therefore in this planning study it has been retrospectively studied in a cohort of patients - previously treated with 3DCRT - in order to assess its ability to reduce rectal irradiation, whilst maintaining the integrity of the target volume and potentially allow for escalation of dose.

3.2 Patients and Methods

3.2.1 Patient Cohort

Data from ten consecutive patients who had previously undergone 3DCRT following radical prostatectomy at the WBCC were selected for the study.

3.2.2 Treatment Planning

All patients were prepared for simulation according to WBCC protocols as to ensure a constant bladder volume and an empty rectum. Patients were then CT scanned at 1.5 mm slices in the supine position. A single clinician defined the CTV (see figure 3.1 for examples of CTV and PTV definition) which comprised the whole prostatectomy surgical bed according to the consensus guidelines of the Australian and New Zealand radiation oncology Genito-Urinary group [68]. In brief, the inferior border of the CTV was defined as 6 mm inferior of the vesicourethral anastomosis (defined as the first slice below which urine was visible in the bladder), extended superiorly to include the seminal vesicle bed and laterally to the medial border of the levator ani muscle or the obturator internus. From the inferior border of the CTV to 3 cm superiorly the anterior border of the CTV was the posterior aspect of the symphysis pubis, and more superiorly included the posterior 1.5 cm of the bladder. In order to limit the amount of rectal irradiation the posterior extent of the CTV allowed a minimum 2 cm margin from the posterior extent of the CTV to the posterior rectal wall. The CTV included all non-vascular tumour bed clips wherever possible. The optimal CTV expansion during the original 3DCRT based treatment was 1 cm in all directions, reducing to 0.5 cm in the posterior direction where it was not possible to meet the rectal dose constraints. In some cases, reducing the posterior expansion to 0.5 cm still did not allow the rectal dose constraints to be met and clinical judgement was used on a patient-by-patient basis to manually reduce this posterior border further. For the purposes of the planning study two separate PTVs were defined but only one is used for any single treatment plan. PTV_{1cm} is a 1cm CTV → PTV geometric expansion and PTV_{treat} is a 1cm CTV → PTV expansion, except in the posterior border where 0.5 cm was implemented, followed by a further reduction based on the clinician's judgment.

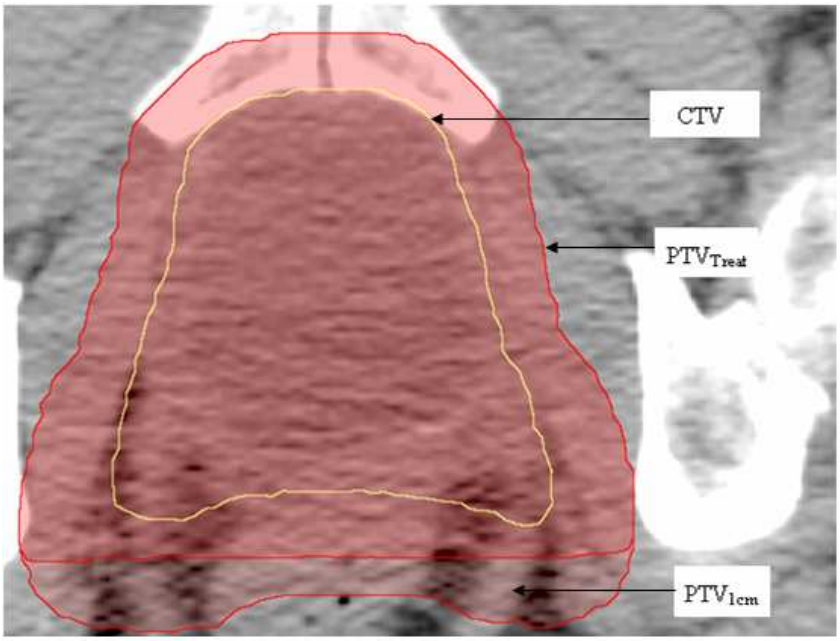

Figure 3.1: Target volume definition indicating CTV, PTV_{Treat} and PTV_{1cm}

The planning data set consists of 40 treatment plans (summary in table 3.1), with each patient in the cohort having four individual plans. All 3DCRT plans consist of three (anterior-posterior, left and right lateral) 18 MV beams with MLCs conforming to the PTV and enhanced dynamic wedges (EDWs) on the lateral fields. Plan normalisation was achieved through a single representative ICRU 50 point within the target volume. Two separate plans were produced with a conformal technique, the first plan ($3D_{1cm}$) having PTV_{1cm} as the primary target, and the second ($3D_{treat}$), PTV_{Treat}. Both of the above plans were prescribed 64 Gy in 32 fractions.

All RA plans were optimised based on an previously published planning strategy [107], as presented in chapter 2. Modifications were made to this strategy as to reflect the planning goals of the treatment site in question. Doses to the rectum are often pushed very close to the planning dose constraints ($D_{60\%} < 40$ Gy and $D_{40\%} < 60$ Gy) [68] and therefore an additional 6 MV CCW arc was added, along with removing any restriction on the number of MUs. These modifications allow for higher degrees of modulation and therefore organ sparing. The resulting plans were globally normalised such that the $D_{50\%}$ equalled the prescribed dose. A deviation of 0.5% from this point was allowed, as to meet other planning constraints. Again, two RA plans were produced for each patient but both have PTV_{1cm} as the primary target volume. The

difference between the two plans comes in the prescribed dose, the first (RA_{64}) having an identical prescription as the 3DCRT plans above, and the second (RA_{70}), escalation this dose to 70 Gy in 35 fractions.

Plan	Technique	Prescription (Gy)	PTV volume
$3D_{1cm}$	3DCRT	64	PTV_{1cm}
$3D_{Treat}$	3DCRT	64	PTV_{Treat}
RA_{64}	RA	64	PTV_{1cm}
RA_{70}	RA	70	PTV_{1cm}

Table 3.1: Summary of treatment plan data set

3.2.3 Evaluation Tools

A range of planning evaluation tools were implemented to inter-compare the four distinct sets of treatment plans to assess the techniques ability to treat the target volume, and spare critical normal structures. Dosimetric verification tools have also been used to assess the techniques ability to physically deliver the planned dose distribution. Acceptance criteria have been assigned for all of these parameters, a summary of which can be found in column 2 of table 3.2. Many of these evaluation tools have been used in previous chapters but are reproduced here for completeness.

The dose-volume parameters were reported to assess PTV coverage, along with the conformity and homogeneity indices. $D_{XX\%}$ represents the dose to XX of the target volume and is reported for the 98, 50 and 2% volumes. The conformity index (CI_{95}) was calculated as a ratio of the 95% isodose line to the volume of the plan PTV [70]:

$$CI_{95} = \frac{V_{95\%}}{V_{PTV}} \tag{6}$$

Previously published studies [34, 35] have shown RA to be more conformal than 3DCRT and therefore more strict CI_{95} constraints are assigned to RA plans than 3DCRT. The homogeneity index (HI) was defined as follows:

$$HI = 100 * \left[1 - \left(\frac{D_{5\%} - D_{95\%}}{D_{mean}} \right) \right], \tag{7}$$

where $D_{5\%}$ and $D_{95\%}$ are the doses to 5 and 95% of the PTV respectively, and D_{mean} is the mean PTV dose. *HI* values closer to 100% indicate a more homogeneous distribution of dose within the target volume. The number of MUs required for each plan is also reported.

The ability of the treatment plans to spare the rectum was assessed through two dose-volume points, the mean (R_{mean}) and maximum (R_{max}) doses, and the EUD. The two dose volume points correspond to the two rectal constraints suggested by Sidhom et. al. [68], $R_{YY\%}$, where YY is equal to either 40 or 60% of the rectal volume. As presented in chapter 2, the EUD is defined as the uniform dose that will produce the equivalent radiobiological effect as the organ specific non-uniform dose distribution, and is a useful tool when inter-comparing plans with differing dose prescriptions and/or steep dose gradients. The generalised EUD formalism is defined as:

$$EUD = \left(\frac{1}{N} \sum_i D_i^a \right)^{\frac{1}{a}}, \tag{8}$$

where N is the number of voxels within the investigated structure, D_i represents the dose to each individual voxel within the structure, and a is an organ specific dose volume parameter. For the organ in question, it has been suggested that this organ specific parameter is equal to 8.3 [35, 108].

To assess the feasibility of delivering the highly modulated RA_{70} plans, patient specific verification measurements were done using the diode based ArcCHECK^{TM} device (Sun Nuclear, Melbourne, FL) [109, 110]. This novel verification tool consists of 1386, 0.8 x 0.8mm diodes, helically distributed in a cylindrical Perspex phantom with dimensions of 26.6 cm diameter and 32.4 cm long. The diodes have a spatial resolution of 1cm in the axial and rotational axes. All 10 RA_{70} plans were transferred to a CT image of the phantom and re-calculated. These plans were then delivered to the phantom on a Varian Trilogy iX. Gamma comparisons were made between the TPS calculated and measured dose for gamma-index acceptance criteria of 3% dose-difference and 3mm distance to agreement (DTA). Given this criteria we set a 90% pass rate for all points over a 10% dose threshold.

Verification measurements of this nature are novel and therefore comparable published data does not currently exist, although Iftimia *et. al.* [111] assessed RA verification for the corresponding 2D device, MapCHECK (Sun Nuclear, Melbourne, FL) 2D diode array. Reported MapCHECK gamma indexes (3%/3mm, threshold of 10%) are in the range of 89.1-99.1%, with a mean of 94.4%. Although these methods are not directly comparable, the results are consistent with the constraints imposed above.

Statistical comparisons of the above evaluation parameters were assessed using a one sided paired t-test, and deemed statistically significant when p-values were ≤ 0.05.

3.3 Results

An example dose distribution for each planning technique can be found in figure 3.2. The volume of PTV_{1cm} was significantly larger than PTV_{Treat} with mean values of 306.6 ± 70.4 and 275.8 ± 60.1 cm^3, respectively. A summary of all plan acceptance criteria can be found in table 3.2, noting that not all comparative permutations have been calculated, with obvious or nonsensical comparisons omitted. Average and statistical comparisons of the above planning parameters can be found in table 3.3, whilst average DVH data for the PTV and rectum can be found in figure 3.3(a) and (b) respectively. A representative ArcCHECK dose difference comparison can be found in figure 3.4, indicating the measurements points that failed the upper or lower bounds of acceptance.

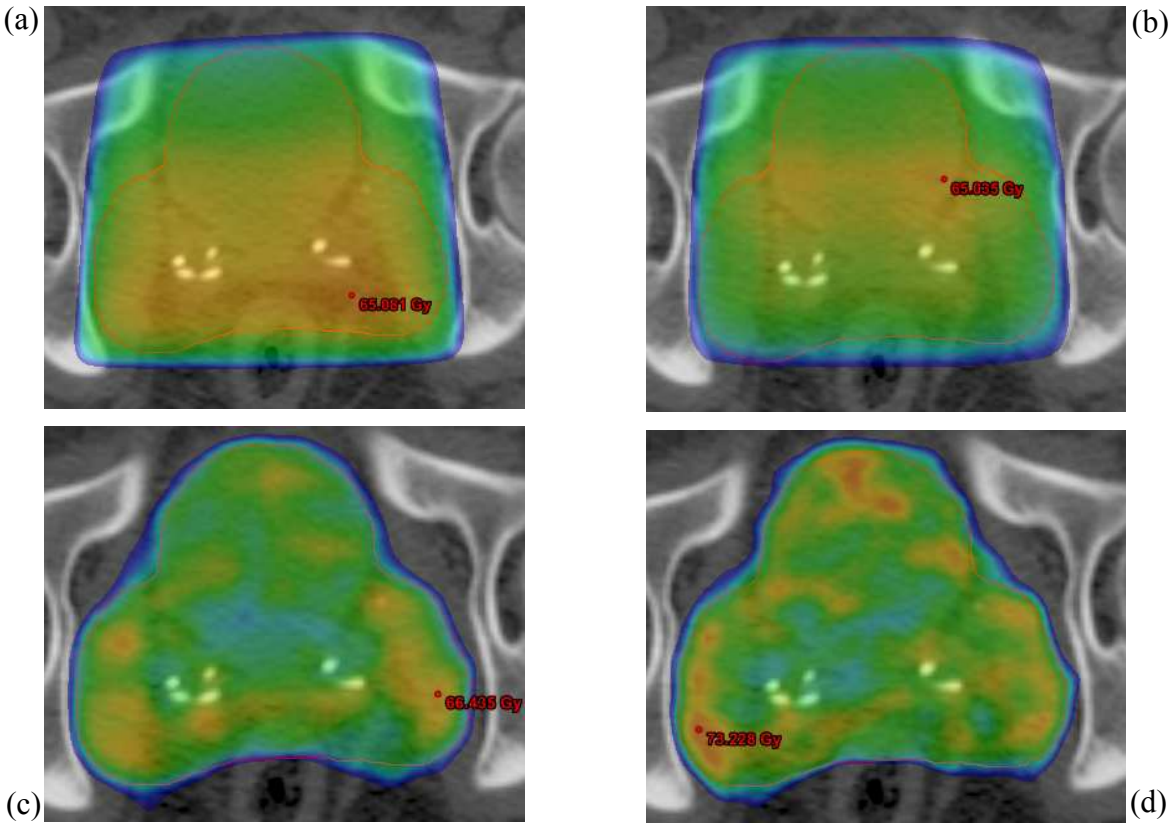

Figure 3.2: Example dose distributions for a single patient, showing $3D_{1cm}$ (a), $3D_{Treat}$ (b), RA_{64} (c) and RA_{70} (d). PTV_{1cm} is shown in all plans. The dose colour wash runs from the 90% isodose line through to the respective dose maximum.

The investigated clinical problem is evident in the above results with seven $3D_{1cm}$ plans failing at least one rectal dose constraint and only three passing all the imposed acceptance criteria, evidence to the point that 3DCRT is unable to treat an uncompromised treatment volume without failing dose constraints (table 3.2) and over dosing the rectum. This issue is resolved through the reduction of the posterior PTV border, as nine out of ten $3D_{treat}$ plans meet both the rectal constraints, although the risk of geographical miss is significantly increased. Only six of these plans passed all the acceptance criteria, although nine did pass the rectal constraints, conformity and homogeneity acceptance. The compromise in PTV volume is completely avoided through the use of RA planning techniques, with all 10 RA_{64} plans meeting the imposed acceptance criteria. Nine of the RA_{70} plans met both of the rectal dose constraint whilst a single plan failed the verification acceptance criteria, resulting in a total of eight plans meeting all the imposed criteria. The mean value for the ArcCHECK absolute gamma was 94.1%.

		Number of plans meeting criteria			
	Acceptance criteria	RA_{70}	RA_{64}	$3D_{Treat}$	$3D_{1cm}$
Rectum	$D_{40\%}$<60Gy	9/10	10/10	10/10	4/10
	$D_{60\%}$<40Gy	10/10	10/10	9/10	4/10
PTV	$D_{50\%}$=P±0.5%	10/10	10/10	8/10	8/10
	$D_{98\%}$>0.95*P	10/10	10/10	9/10	9/10
	$D_{3\%}$<1.05*P	10/10	10/10	9/10	9/10
	CI_{95}<1.5	-	-	10/10	10/10
	CI_{95}<1.2	10/10	10/10	-	-
	HI>90%	10/10	10/10	10/10	10/10
ArcCHECK	$\gamma_{3\%,3mm}$>90%	9/10	-	-	-
All criteria	Pass all above	8/10	10/10	6/10	3/10

Table 3.2: Plan acceptance criteria summary.

P = prescribed dose

		RA_{70}	RA_{64}	$3D_{Treat}$	$3D_{1cm}$	Significance
Rectum	$R_{40\%}$	47.6	43.2	51.8	58.6	α γ θ ι
	$R_{60\%}$	24.0	22.3	34.1	43.4	α γ ζ ι
	R_{mean}	38.2	34.9	41.2	45.7	α γ ζ ι
	R_{max}	73.4	67.4	65.1	65.2	ε
	EUD	58.6	52.9	54.2	57.1	α γ η κ
PTV	$D_{50\%}$	70.0	64.0	63.8	64.2	-
	$D_{98\%}$	67.1	61.4	61.8	61.7	δ
	$D_{2\%}$	72.4	66.5	65.8	66.2	Δ
	CI_{95}	1.1	1.1	1.3	1.3	λ μ
	HI	93.8	93.3	94.3	94.2	β γ λ μ
	MU	867.6	810.7	271.3	268.6	λ μ

Table 3.3: Planning parameter comparison. Statistical comparisons are outlined in column 7. $^{\alpha}RA_{70} < 3D_{1cm}$, $^{\beta}RA_{70}$ vs. $3D_{1cm}$ NS, $^{\gamma}RA^{64} < 3D_{1cm,}$ $^{\delta}RA_{64}$ vs. $3D_{1cm}$ NS, $^{\varepsilon}RA_{64} > 3D_{1cm}$, $^{\zeta}RA_{70} < 3D_{Treat}$, $^{\eta}RA_{70} > 3D_{Treat}$, $^{\theta}RA_{70}$ vs. $3D_{Treat}$ NS, $^{\iota}RA64 < 3D_{Treat}$, $^{\kappa}RA64$ vs. $3D_{Treat}$ NS, $^{\lambda}RA_{70}$ vs. RA_{64} NS, $^{\mu}3D_{Treat}$ vs. $3D_{1cm}$ NS.

Across the patient cohort, the rectal sparing parameters ($R_{40\%}$, $R_{60\%}$, R_{mean} and EUD) were significantly less for RA_{64} than both conformal techniques, although the maximal dose point (R_{max}) was slightly higher. This significant improvement over conformal was mirrored for RA_{70}, excluding the EUD. On average the RA_{70} EUD was 1.5 and 4.5 Gy more than $3D_{1cm}$ and $3D_{treat}$ respectively, mainly due to the fact that volumes of the rectum received doses above 64 Gy (the prescribed dose of all the other plans). The conformity of the RA plans was better than that of the 3D techniques, but the reverse is true with respect to homogeneity. More MUs (table 3.3, row 12) were required for both RA plans over both 3D plans but no significant intra-technique differences were observed.

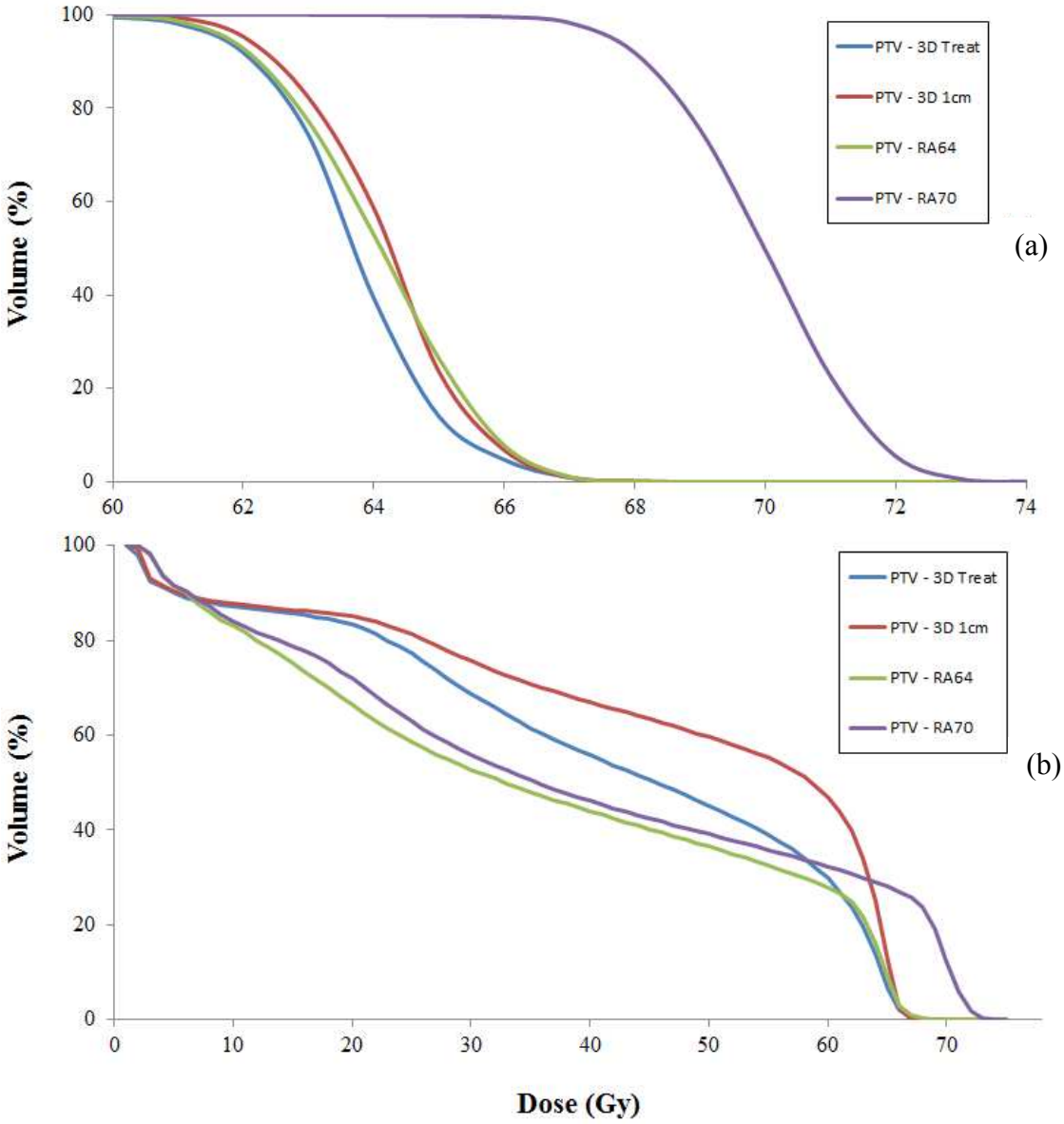

Figure 3.3: Mean DVHs for the target (a) and rectal (b) volumes.

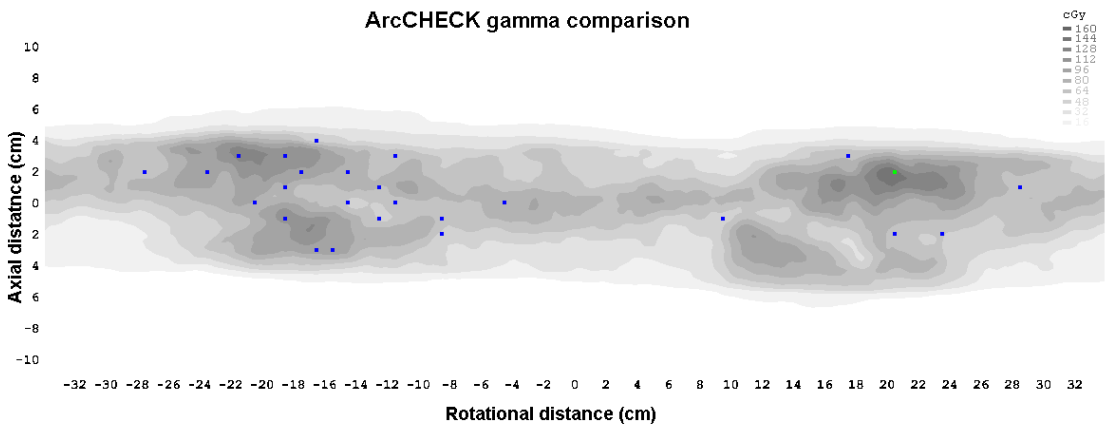

Figure 3.4: Example ArcCHECK gamma comparison for a single patient. Shown is the planned dose map with failed points superimposed. In this example the failed points represent 3.7% of all investigated points.

3.4 Discussion

The major advantage of intensity modulated radiotherapy techniques is their ability to reduce the dose to critical normal tissues. In prostate bed radiotherapy the rectum is a major dose limiting structure and reducing the dose it receives may reduce toxicity. Safe dose escalation has been shown to be feasible using fixed gantry IMRT in this setting and low rates of toxicity are reported even with significant dose escalation [106, 112, 113]. However, the increased MU required for these techniques can prolong the time required for treatment and thus reduce efficiency. The average RA (RA_{64} and RA_{70}) beam on time was 2.3 minutes and although no quantitative comparisons with 3D techniques are made, it is expected that RA plans would be treated in the same 10 minute time slot as conformal treatments and thus negating the historical disadvantage of intensity modulated deliveries.

This planning study investigated prostate bed irradiation in 10 patients previously treated with conformal radiotherapy. Using conformal radiotherapy and a uniform 1 cm CTV→ PTV expansion it was difficult to meet the pre-defined rectal dose constraints in most patient cases. Moreover, even with a reduction of the posterior PTV expansion to 0.5 cm it was still not possible to meet these constraints in many cases. Decreasing the PTV further has allowed the defined rectal dose constraints to be met but at an increased risk of geographical miss. Using surgical clips and on board imaging to study prostate bed motion, one study has suggested that movement of more than 5 mm may be seen in 27% of patients in this setting [106]. Similar findings have also been reported by Schiffner et. al. who used fiducial markers to describe movement in the prostate bed; their study suggests that using bone localisation more than 5 mm of movement may occur on nearly 40% of treatment days [114], suggesting that at a bare minimum of 5 mm expansion should be used, with 1 cm being preferable. Although not the concentration of the current work, the potential for reducing these margins may also be safely achieved through the implementation of daily image guidance (cone-beam CT and orthogonal 2D kV images) and soft tissue matching. Due to the conformal nature of RA techniques, imaging of this nature is also a pre-requisite for successful implementation, within the clinic.

This planning study has shown that RA techniques provide the ability to treat the prostate bed without comprising the target volume, whilst at the same time improving rectal sparing, compared to what has been previously treated locally. Moreover, it has been shown that escalating the prescribed dose to this volume by a further 6 Gy is feasible, in the majority of patients. As seen in figure 1, the average rectal dose for RA_{70} is less than both conformal techniques for 70% of the volume, although almost 30% of the volume receives more than the conformal prescribed dose of 64Gy. As a result, the RA_{70} rectal EUD is larger than of the previously treated cohort. This increase seems justified due to current toxicity data and the results of previously published studies. Escalation of this nature still needs to be considered on a patient-by-patient basis due to the fact that two of the ten RA_{70} plans failed one of the imposed acceptance criteria. One patient failed a rectal dose constraint and one the pass criteria of the ArcCHECK verification. These failures were rectified by reduction of the PTV posterior border to 8 mm and restricting the optimisation MUs to less than 650, as to improve rectal sparing and reduce over modulation respectively. In both cases the integrity of the plans were maintained whilst in the former the $R_{60\%}$ reduced below 40 Gy and the latter, the gamma improved to a point where agreement was above the 90% criteria. Conclusions based on ArcCHECK measurements are limited due the fact that the devise is novel and the associated measurement capabilities and limitations are still unknown (discussed further in 5.1). Further RA verification measurements using other devices are conducted as part of the subsequent chapter.

3.5 Concluding Remarks

The planning strategy presented in chapter 2 has been modified to fit the needs of a related but independent patient group with the goal of maintaining target volume integrity and investigating the feasibility of safe dose escalation. The ability of RA optimisation to produce concave and sharp dose gradients has completely satisfied the former goal, with the full patient cohort meeting OAR dose and plan constraints, even when a 1 cm CTV→PTV expansion was implemented, and hence the risk for geographical miss is reduced without increasing the expected toxicity. Implementation of RA optimisation has also shown that dose escalation up to 70 Gy is feasible on a patient-by-patient basis. Care needs to be taken not to over-modulate plans or produce patient geometries where large volumes of rectum overlap with the PTV. If these issues do arise the potential to restrict the plan MUs and reduce the PTV's posterior border exists, although further work on the former is still required. The increased rectal EUD in this dose escalated patient group may result in an increased level of toxicity, although previously published data suggests that this may be justified. It is suggested that escalation of this type be accompanied by daily soft tissue registration image guidance and extensive early and late patient follow up.

Plan verification is essential for complex delivery techniques such as RA whereby discrepancies between the planned and measured dose may be a culmination of many parameters including: the ability for the TPS to model the dose from complex and often small MLC apertures (Figure 2.7), accuracy of the measurement (ArcCHECK) hardware, linac variations and experimental uncertainty. If we are to reduce many of these discrepancies involved with this still novel and complex delivery techniques then the origin of these must be further investigated. To address only one of these issues, the ability and accuracy of the Eclipse TPS to model complex dose distributions and delivery techniques, is the concentration of the subsequent chapter.

Chapter 4 – Configuration of the Anisotropic Analytic Algorithm

4.1 Introduction

The anisotropic analytic algorithm (AAA) is Varian Medical System's implementation of the superposition/convolution type algorithm, originally developed by Ulmer et. al. [115, 116]. This type of algorithm currently dominates commercial TPSs due to its improved calculation of lateral electron transport when compared with other dose calculations algorithms; such as the pencil beam convolution (PBC) algorithm [117, 118]. This improvement in lateral electron transport is especially important when dealing with heterogeneous media [118], such as lung and bone. In saying this, the gold standard of dose calculation is still regarded as Monte Carlo (MC) models [119, 120]. The main reason full MC calculation models are not implemented in commercial TPSs is due to the fact that they are computationally heavy, resulting in increased calculation times when compared with AAA.

Configuration of the AAA in the Eclipse TPS requires a variety of linac beam parameters as input data [67]. As a minimum this includes: beam profiles at a range of depths (D_{max}, 50, 100, 200, and 300 mm) for field sizes ranging from 3x3 to 40x40 cm, diagonal 40x40 cm profiles, percentage depth doses (PDDs) and output factors (OF) for the full range of field sizes. Generally, this beam data is manually measured and is therefore linac - or at least institution – dependent, and as a result, separately configured algorithms are unique in nature. As per Varian's recommendation, beam data is conventionally collected with the linac jaws (secondary collimator) defining the field edge [66, 67]. The physical penumbra of fields defined by either the jaw or MLC vary from one another due to multiple factors, including inter-leaf leakage and the transmission and scatter off the rounded leaf tips (see figure 1.4). Conventionally, these variations are accounted for within the Eclipse TPS, by leaf transmission and dosimetric leaf gap (DLG) factors. The MLC transmission factor accounts for transmission through the leaves and mainly affects the umbra region (defined as the region outside the lower penumbral point, 20%). The DLG accounts for the increased

transmission through the rounded leaf tips, whereby fields defined by the MLC are effectively made wider by the magnitude of the DLG [121, 122]. Neither of these factors account for differences in penumbral shape of the jaws and MLCs.

Although good agreement between the AAA and novel verifications measurements (ArcCHECK) has been observed over the whole arc (chapter 3), observations by other authors (Gange et. al. [123]) have indicated large errors for single RA control points, despite the fact that MLC transmission is modeled by transmission factors. Part of the study by Gange et. al. benchmarked a single irregular MLC control point against MC calculations. Consistent discrepancies on the order of 5% were observed across a single leaf end penumbra, and 12% across an isolated leaf edge. The authors postulate that the errors in MLC modeling may results in errors on the order of 1.5% over the full arc [123].

The AAA has been previously verified for fields defined by static MLCs [124] but the question still remains if the AAA more accurately models MLC defined fields if the configuration beam data is collected with the MLC rather than the jaws defining the field. This question is especially pertinent when considering highly modulated fields where the MLC constantly defines the field edge, as is the case with both static and rotational IMRT (figure 2.7). In the present study, two separate AAAs are configured using beam data collected with either the jaw or the MLC defining the field edge with the hypothesis that this may improve the modeling of MLCs and reduce potential calculation errors that are involved with highly modulated plans. An extensive comparison between the two algorithms follows, including comparisons with static and dynamic fields in solid water, anthropomorphic phantoms and patient anatomies. Comparisons with physical verification methods are also performed.

4.2 Materials and Methods

4.2.1 The AAA

When calculating the dose from a single field (or control point) the AAA splits the field into multiple smaller sub-fields, or beamlets *(β)* [67]. The dose contribution from each beamlet is then calculated using convolution methods. Throughout this process, the energy fluence from each beamlet is split into three separate dose contributing components; primary photons, extra-focal photons and contamination electrons (originating in the flattening filter, ion chamber, collimator and air) [125]. The relevant convolution equation is as follows:

$$D_\beta(x,y,z) = \Phi_\beta \times I_\beta(z,\rho) \times \iint_\beta K_\beta(x' - x, y' - y, z, \rho) dx' dy' \quad (9)$$

where the dose contribution from each beamlet is $D_\beta(x,y,z)$, Φ_β is the beamlet fluence, $I_\beta(z,\rho)$ is the energy deposition density function, and $K(x,y,z,\rho)$ is the MC derived scatter kernel [66, 67, 115]. Each of these functions are defined separately for the three dose components and therefore calculated independently from one another. Not only are the energy fluence and the scatter kernel analytic functions, the convolution integral has been solved analytically, hence the leading *A* in the algorithms name. The second *A* comes from the fact that each scatter kernel is evaluated in multiple anisotropic directions from the beamlet. Following each individual convolution, the dose at a point, $D(x,y,z)$, is calculated as the superposition of all three dose components over all beamlets [66].

4.2.2 Beam Configuration

All beam cross-plane profiles and PDDs (unless otherwise stated all presented PDDs are normalised to 5cm) were measured at 100 cm source-to-skin distance (SSD) in a PTW (Freiburg, Germany) MP3 water tank using a 0.125 cm^3 PTW semiflex chamber and the software analysis and conversion done using the matched PTW Mephysto Mc^2 program. OFs were measured in either the Med-tec (TruMed Healthcare, Orange city, Iowa, USA) or PTW MP3 water tanks (dependent on field size) using the same semiflex chamber, at 100 cm source-to-axis distance (SAD) with a reference depth of

5 cm in a 10x10 cm field. The chamber was offset to the effective point of measurement in the depth axis.

Two independent sets of beam data were collected on separate occasions, one with the jaws defining the field and one with the MLC. In the case where the MLC was defining the field, the jaws were placed at least 4 cm outside the MLC field edge. The largest field size being the only exception to this rule, whereby the jaw and MLC overlap due to the construction of the linac head. Positioning the jaws in this fashion meant that the jaws were a large enough distance away from the field edge as not to affect the measurement whilst not exposing the end of the leaf bank to radiation. Profile measurements ran perpendicular to the MLC, with the converging point of the MLC, off-set from the axis of chamber motion. Both of these data sets were restricted to 6 MV only. Beam profiles were measured at depths of D_{max}, 5, 10, 20 and 30 cm for field sixes 3x3, 4x4, 6x6, 8x8, 10x10, 20x20, 30x30, and 40x40 cm and diagonal scans for the largest field. All profiles were measured at least 3.5 cm past the field edge (defined at 50% of full width at half maximum (FWHM)). In the case where measurements were limited by the tank geometry (40x40 cm), half profiles were measured and then symmetrised. Central axis PDDs were also measured for each of the above stated field sizes. All of this data were then symmetrised and smoothed in the Myphesto Mc^2 software. As a representative example of these data sets, the full MLC defined half-beam profile and PDD set can be found in figure 4.1 (a) and (b) respectively. OFs for a sample of the above field sizes were measured and then the remainder of the data set interpolated in Microsoft Excel. Both of these data sets were then converted to Ascii format in preparation for importation into the Eclipse TPS for beam configuration.

The first algorithm was configured using the jaw defined data set, henceforth referred to as AAA_{Jaw}. This algorithm was subjected to an extensive commissioning program including inter-comparisons with the then clinical PBC, in homogeneous and inhomogeneous media (bone and lung) using point dose chamber measurements as a benchmark. The results of this study were inline with previously published data [118, 119, 124, 126]. The majority of AAA_{Jaw} calculated point doses were within 3% of the measured data, and in general improved over the PBC. This algorithm was subsequently released for clinical use for 3DCRT calculations. The second algorithm,

$AAA_{MLC,}$ was later configured using the MLC collected data set and identical OFs. All other user defined parameters such and the MLC leaf transmission and DLG were set as to align with locally measured values (1.4% and 2.1 mm respectively) and were consistent across both algorithms. To reiterate from 2.1.2.3, the dose grid size used in all AAA calculations was 2.5 mm.

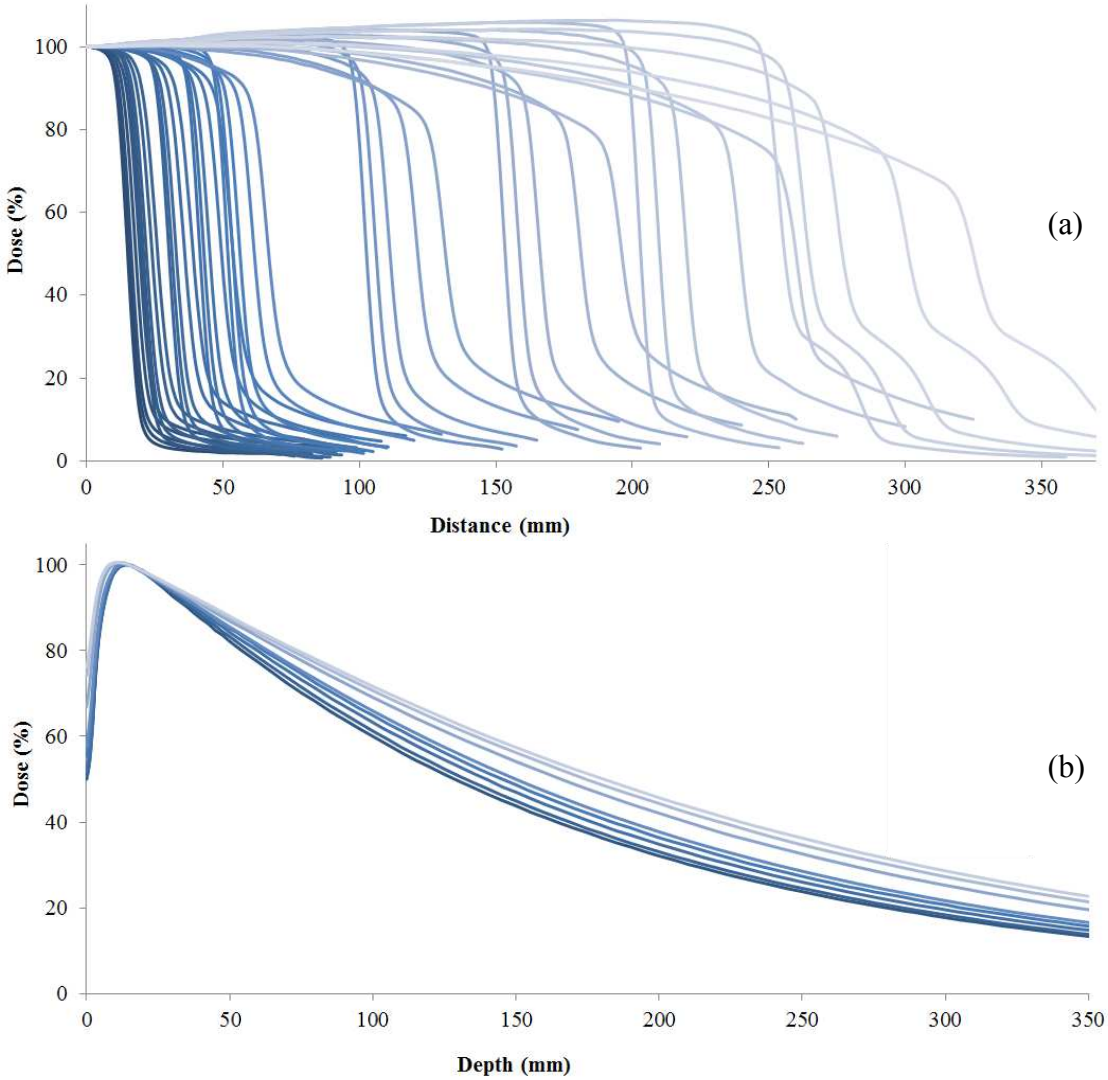

Figure 4.1: Half-beam profiles (a) and central axis PDDs (b) (normalised to d_{max}) for the full AAA_{MLC} data set.

4.2.3 Algorithm Comparison

4.2.3.1 Measured Data

The first step in establishing differences between the two AAAs was to compare the measured data that went into configuring them. The field sizes and physical penumbras (defined as the distance between the 80 and 20% points) was tabulated for all input data. The measured PDDs were compared at three depths, D_{max}, D_{80} and D_{50}, where D is the depth denoted by the subscript, as a percentage of dose. Following configuration, the Eclipse TPS calculates average gamma errors between the input and output data for points including: within the field, in the penumbra region and outside the field. A comparison of these errors is also presented.

Statistical analysis done throughout used a one sided, two paired sample T test and differences were deemed statistically significant if $p \leq 0.05$.

4.2.3.2 Phantom Comparisons

Various inter-comparisons were made between the two AAA algorithms in virtual and physical CT scanned phantoms. This process started with simple comparisons between open fields simulating the geometry under which the original data was acquired (jaw and MLC defined fields). A virtual water phantom (cube) of dimensions 50 cm^3 and uniform density (HU=0) was created in the Eclipse TPS and ant-post fields of sizes 3x3 and 10x10 cm added. Two separate plans were inserted for each size, one with the jaws defining the field and one with the MLC, and calculated with both algorithms, resulting in a total of eight individual plans. Beam profiles at depths of 1.5, 5 and 30 cm were then extracted through the central axis and PDDs at the centre of the field. Comparisons of the beam penumbra, field size and dose subtractions were made between the two algorithms and the corresponding measured data.

4.2.3.3 Patient Treatment Plans

All AAA calculations presented in the preceding chapters were done using the AAA_{Jaw} algorithm. To assess the differences in the two algorithms when calculating more complex RA plans, the 10 prostate patients from chapter 2 were recalculated

with AAA_{MLC} and differences assessed through the global and PTV maximum point dose differences, volumetric dose subtraction (AAA_{Jaw} -AAA_{MLC}), dose difference profiles and the mean PTV3 dose. The clinical significance of any observed difference in the PTV dose was assessed through calculation of EUD based TCPs using methods published by Gay and Niemierko [127]. This method requires PTV DVH data and several radiobiological parameters such as the alpha beta ratio (α/β), the dose-response curve parameter (γ_{50}), the mean dose to control 50% of tumors (TCD_{50}) and the previously described tumor specific parameter, a. Prostate specific values for these parameters were taken from the literature: α/β = 3.1 [128], γ_{50} = 2.9 [129], TCD_{50} = 70.5Gy [129] and a = -10 [130]. A sub set of these comparisons were completed for more complex treatment plans including double arc treatments of the thyroid bed and brain.

4.2.3.4 Verification Measurements

Ion chamber point dose measurements were completed to assess the accuracy of the two algorithms. Verification plans for a random selection of five prostate RA plans (from chapter 2) were created in the Eclipse TPS. These verification plans used a CT scan of the Computerized Imaging Reference Systems Inc. (CIRS) pelvis phantom (Fig 4.2) and the RA plan calculated using both algorithms. Farmer (0.6 cm^3) (points 1, 2 and 4) and semiflex (0.125 cm^3) (point 3) chamber volumes were contoured at four locations corresponding to the bladder - PTV interface, PTV, rectum - PTV interface and femoral head. The mean dose of each chamber volume was extracted. Each plan was then delivered a total of 12 (four points by three repeat measurements) times on a Varian iX linac and the measured chamber values compared with those calculated by the two algorithms. To stress the algorithms further, the above verification process was repeated for a simulated lung treatment in a thorax CIRS phantom at three points (Figure 4.3) again using both the farmer (point 5) and semiflex (point 6 and 7) chambers, and again compared with both AAA calculated mean dose values. All percentage differences are calculated using AAPM Task Group 119 formalism (100*[(measured dose)-(planned dose)]/prescribed dose) [131].

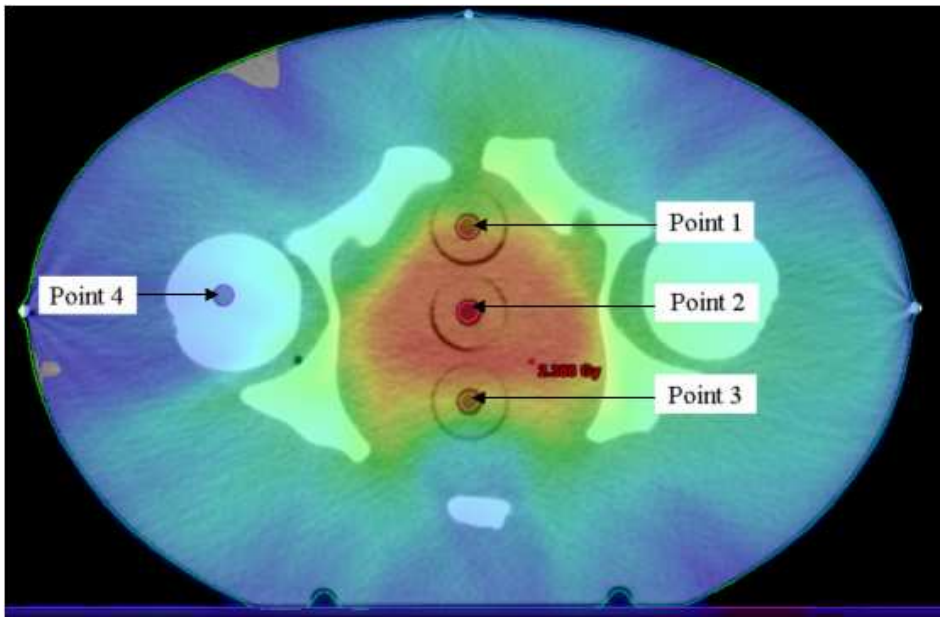

Figure 4.2: AAA verification using the CIRS pelvis phantom and chamber point measurements

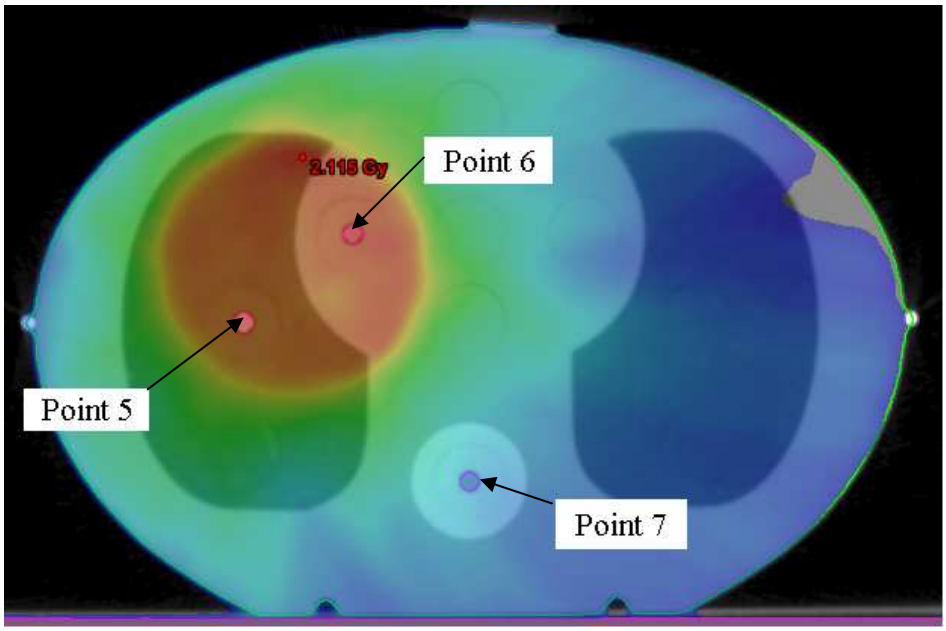

Figure 4.3: AAA verification using the CIRS thorax phantom and chamber point measurements.

4.3 Results

4.3.1 Algorithm Comparison

4.3.1.1 Measured Data

Example comparisons of the measured beam profiles can be found in Figure 4.4 (3x3cm) and Fig 4.5 (10x10 cm) and a full summary of the field size and penumbral values in table 4.1. There is no overall trend between the measured jaw and MLC defined field sizes. Some jaw defined fields are larger, other MLC defined fields are larger and some show non-significant differences. However, consistent with MLC and jaw radiation transmission, this is not the case when it comes to the measured penumbras. A strong trend is observed, indicating that the MLC defined fields have a lager penumbra over the range of field sizes (except the largest 40x40 cm due to the fact that the geometry is identical for both (jaw and MLC overlap)). Although not quantitatively addressed, it can be seen from figures 4.4 and 4.5 that the MLC defined fields not only have larger penumbras but higher doses in the umbra region.

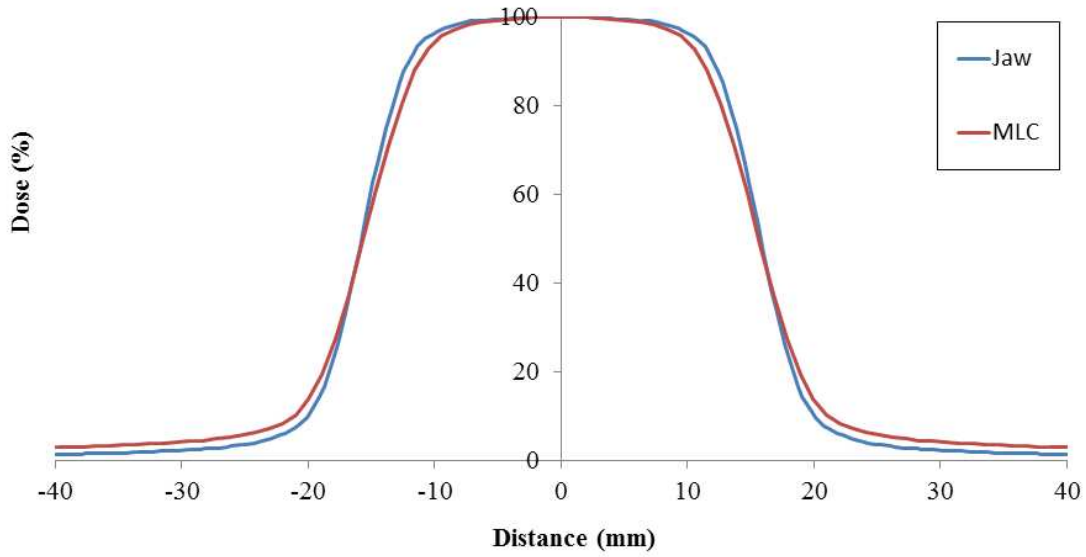

Figure 4.4: Comparison of measured jaw and MLC defined 3x3cm profiles at 5cm depth.

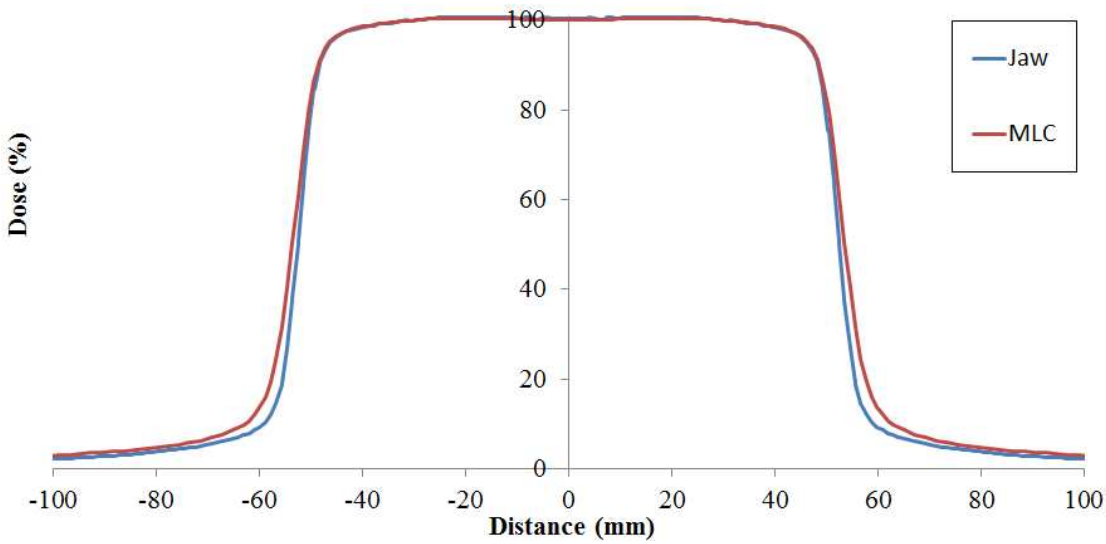

Figure 4.5: Comparison of jaw and MLC defined measured 10x10cm profiles at 5cm depth.

Field size (cm)	Depth (mm)	Field size (cm)		Significance	Penumbra		Significance
		Jaw	MLC		Jaw	MLC	
3x3	15	3.05	3.01	Jaw>MLC	4.71	5.80	Jaw<MLC
	50	3.16	3.13		5.02	6.18	
	100	3.31	3.28		5.21	6.35	
	200	3.62	3.60		5.64	6.92	
	300	3.93	3.90		5.87	7.13	
4x4	15	4.06	4.02	Jaw>MLC	4.38	6.35	Jaw<MLC
	50	4.20	4.17		5.16	6.99	
	100	4.42	4.39		5.44	7.35	
	200	4.83	4.81		5.95	8.16	
	300	5.24	5.21		6.38	8.70	
6x6	15	6.10	6.05	Jaw>MLC	4.94	6.57	Jaw<MLC
	50	6.31	6.26		5.38	7.31	
	100	6.62	6.57		5.86	7.96	
	200	7.24	7.20		6.65	9.17	
	300	7.85	7.81		7.38	9.97	
8x8	15	8.12	8.31	Jaw<MLC	5.07	6.49	Jaw<MLC
	50	8.41	8.61		5.57	7.20	
	100	8.82	9.03		6.22	8.15	
	200	9.64	9.89		7.45	10.00	
	300	10.45	10.74		8.64	11.89	
10x10	15	10.15	10.36	Jaw<MLC	5.08	6.51	Jaw<MLC
	50	10.50	10.72		5.67	7.28	
	100	11.01	11.25		6.49	8.46	
	200	12.03	12.30		8.15	10.88	
	300	13.05	13.35		10.16	13.77	
20x20	15	20.37	21.52	NS	5.24	6.73	Jaw<MLC
	50	21.07	21.23		6.13	7.86	
	100	22.07	22.24		7.65	9.98	
	200	24.08	24.28		12.69	16.22	

	300	26.08	26.31		20.55	24.46	
30x30	15	30.57	30.38	NS	5.28	6.81	Jaw<MLC
	50	31.62	31.74		6.38	8.32	
	100	33.11	33.24		8.65	11.50	
	200	36.08	36.24		17.74	21.10	
	300	39.05	39.23		32.92	35.05	
40x40	15	40.83	40.62	Jaw>MLC	5.25	6.13	NS
	50	42.23	42.01		6.63	7.15	
	100	44.19	43.99		9.83	10.15	
	200	48.24	47.93		21.48	21.50	
	300	52.25	52.00		45.76	43.83	

Table 4.1: Measured profile comparison for jaw and MLC defined fields. Fields sizes and penumbral vales are presented for the full range of field sizes and depths in the data set along with statistical comparisons.

Comparisons of the measured PDDs can be found in Figure 4.6 (a) (3x3 cm) and Figure 4.7 (10x10 cm) and a summary of the percentage depth values in table 4.2. An example PDD subtraction (measured jaw PDD - MLC PDD) is also presented in Figure 4.6 (b). No statistical differences are seen in the build up region however variations are seen at depth. Both the D_{50} and D_{80} are larger for the jaw defined field, across the range of field sizes. As these differences are small, the trend can be more easily visualised in figure 4.6 (b), with the jaw defined field PDD consistently larger than that of the MLC for depths larger than 50 mm. The maximum percentage differences for D_{50} and D_{80} are 1.0 and 1.5% for respectively. The potential orientation of these small yet significant variations will be discussed in further detail below. Average gamma errors between each algorithm and the measured data can be found in table 4.3. As observed, the largest errors occur in the penumbra and outside the field, with larger differences between the measured MLC data and the configured AAA_{MLC}.

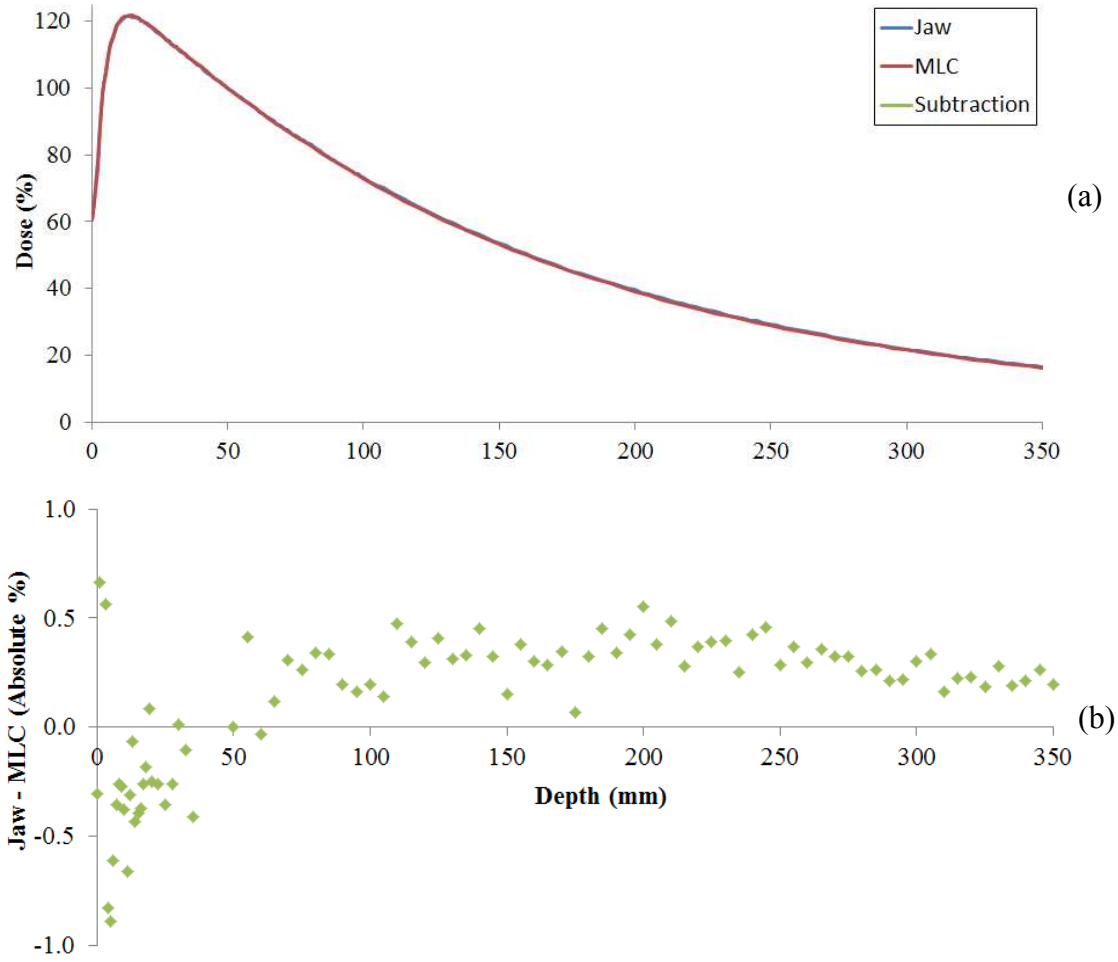

Figure 4.6: Measured 3x3 cm jaw (largely obscured) and MLC PDDs for a 3x3 field (a). PDD subtraction (jaw-MLC) showing small yet consistent differences at depths larger than 50 mm (b).

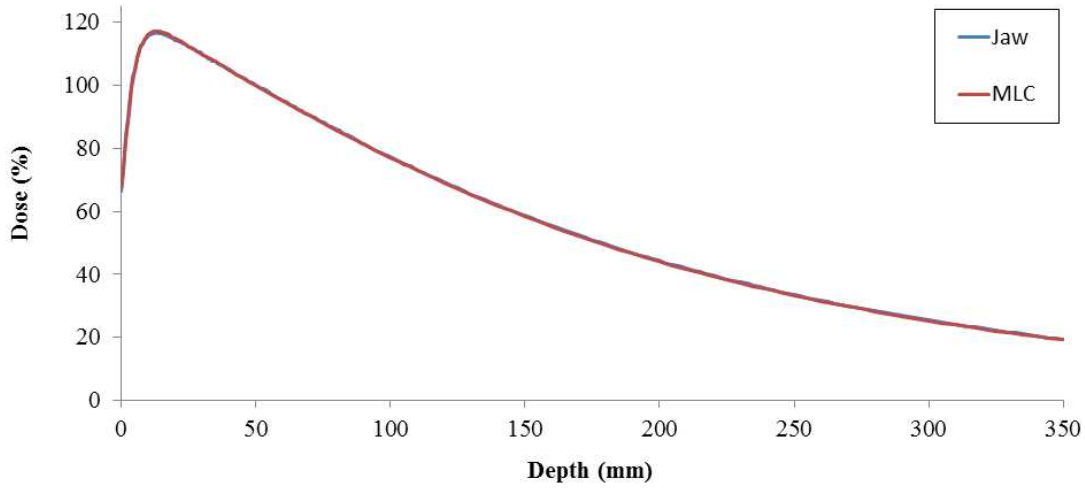

Figure 4.7: Measured jaw (largely obscured) and MLC PDDs for a 10x10 cm field.

Filed size	D_{max} (mm)		D_{80} (mm)		D_{50} (mm)	
(cm)	Jaw	MLC	Jaw	MLC	Jaw	MLC
3x3	13.5	14.0	54.8	54.1	129.7	128.4
4x4	14.5	13.0	56.9	56.4	133.6	132.3
6x6	13.5	14.0	59.7	59.6	140.0	139.5
8x8	13.1	13.0	61.9	61.7	146.2	145.0
10x10	14.0	13.0	64.1	63.1	151.0	149.7
20x20	11.1	12.0	68.5	67.5	166.2	164.7
30x30	12.0	11.0	70.7	70.3	174.1	173.2
40x40	11.0	11.0	72.6	72.4	180.2	179.4
Significance	NS		Jaw>MLC		Jaw>MLC	

Table 4.2: Comparison of measured PDDs.

	AAA_{Jaw}	AAA_{MLC}	Δ (AAA_{Jaw}-AAA_{MLC})
Within field	0.15	0.12	0.03
Penumbra	0.21	0.36	-0.15
Outside field	0.34	0.87	-0.53

Table 4.3: Average gamma errors between measured and configured data for the respective algorithms, within the field, penumbra and outside the field.

4.3.1.2 Phantom Comparisons

Figures 4.8 is presented as a comparison between a 3x3 cm MLC defined field calculated with the two AAA algorithms, although as can be observed any differences are indistinguishable. Figures 4.9 (a)-(b) are in analogy with figures 4.6 (a)-(b) but are presented as a comparison between the PDD of the two algorithms. The observed inter-algorithm values are small and insignificant. Figures 4.10-4.13 give comparisons between measured and calculated (AAA_{Jaw}) profiles for 3x3 and 10x10 cm jaw and MLC defined fields. Relatively good agreement is observed for the MLC and jaw defined 10x10 cm fields and the jaw defined 3x3 cm field (differences mainly a result

of the fact that the calculation grid size is large relative to the field size), although larger differences are observed for the 3x3 cm MLC defined field. A quantitative analysis of measured and configured field size and penumbra can also be found in tables 4.4 and 4.5 respectively. The agreement between measured and configured field size is generally good although large discrepancies are seen for small (3x3 cm) MLC defined fields, with the configured size consistently larger than the measured data. Larger errors between the measured and configured penumbra are observed across all investigated fields and depths. The overall trend in this data is that the configured penumbras are smaller than that of the measured, a result consistent with the observations of other authors [123].

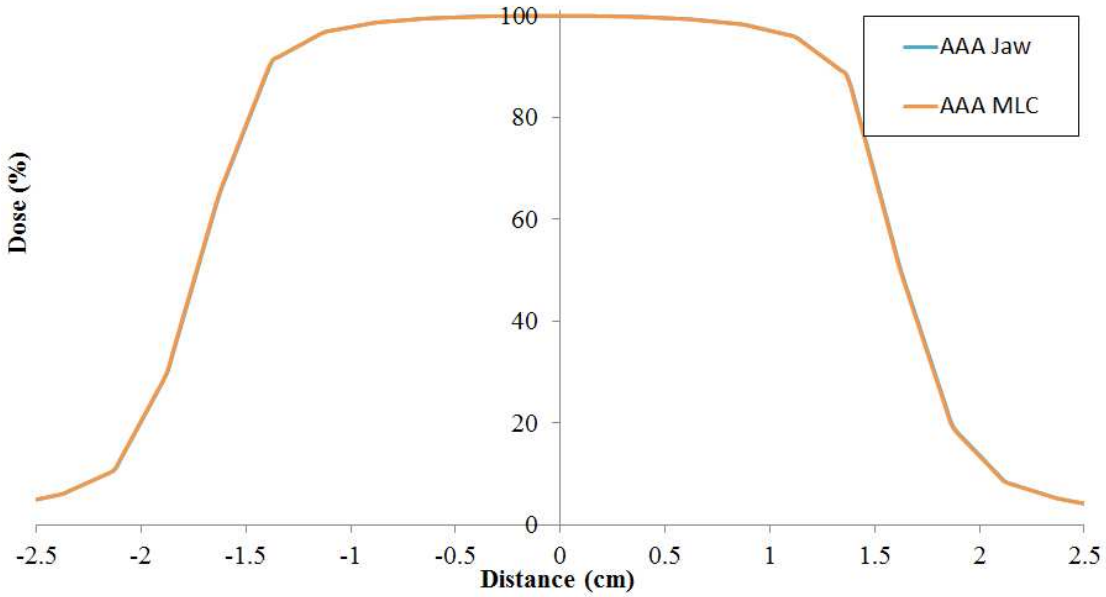

Figure 4.8: Profile comparison for a MLC defined field calculated with both AAA_{Jaw} (largely obscured) and AAA_{MLC}. The profile presented is a 3x3 cm field and 5 cm depth.

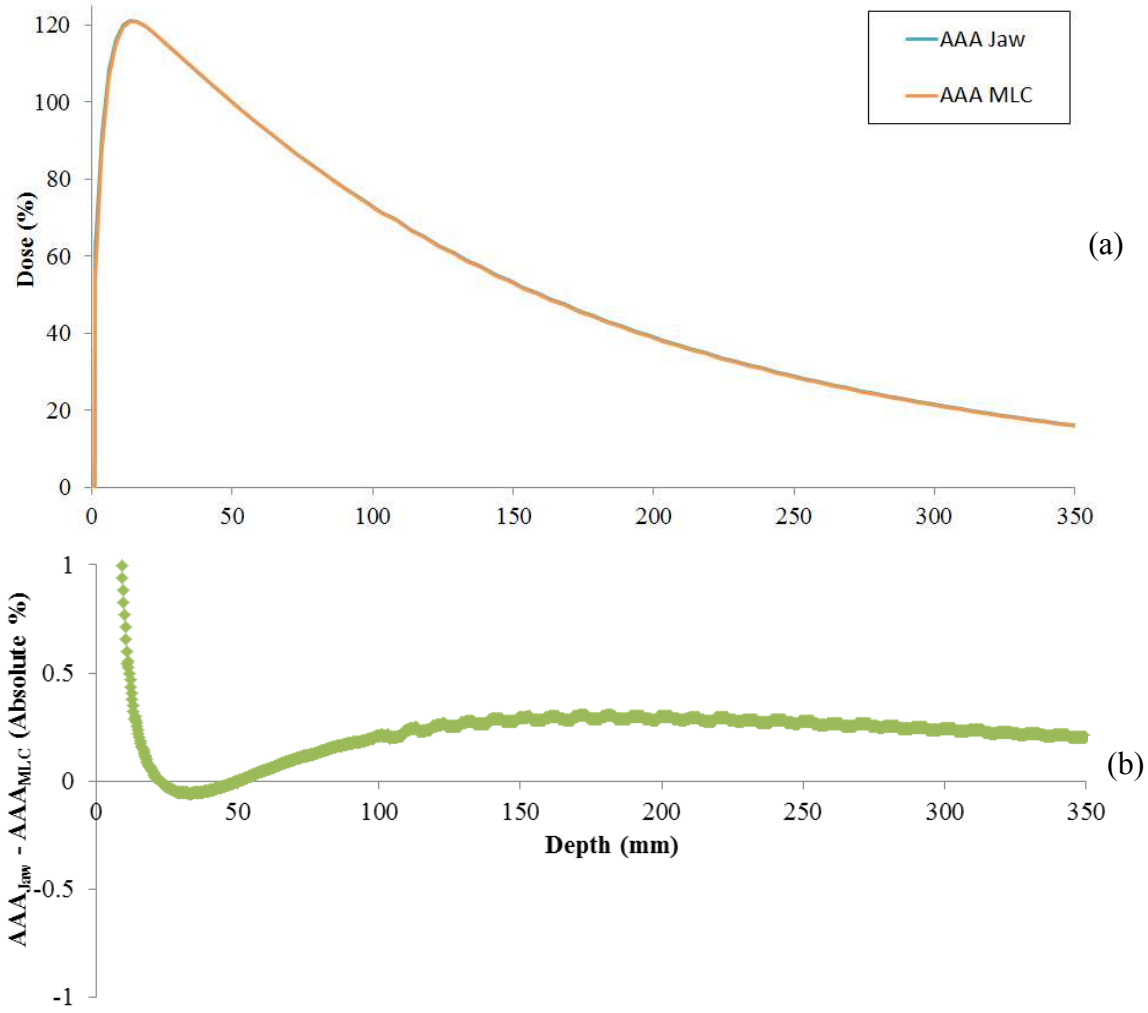

Figure 4.9: AAA_{Jaw} (largely obscured) and AAA_{MLC} PDDs for a 3x3 cm jaw defined field (a). Corresponding PDD subtraction (AAA_{Jaw}-AAA_{MLC}) (b).

Field size (cm)	Depth (mm)	Jaw defined field					MLC defined field				
		Measured	AAA_{Jaw}	Rel Δ (%)	AAA_{MLC}	Rel Δ (%)	Measured	AAA_{Jaw}	Rel Δ (%)	AAA_{MLC}	Rel Δ (%)
3x3	15	3.05	3.01	1.2	3.03	0.60	3.01	3.23	-7.2	3.25	-7.9
	50	3.16	3.13	0.8	3.11	1.4	3.13	3.34	-6.9	3.33	-6.5
	300	3.93	3.93	0.0	3.93	0.0	3.90	4.15	-6.4	4.16	-6.7
10x10	15	10.15	10.15	0.0	10.14	0.1	10.36	10.43	-0.7	10.43	-0.7
	50	10.50	10.51	-0.1	10.52	-0.2	10.72	10.81	-0.9	10.82	-1.0
	300	13.05	13.04	0.1	13.05	0.0	13.35	13.42	-0.5	13.43	-0.6

Table 4.4: Comparison between Eclipse calculated fields sizes for AAA_{Jaw} and AAA_{MLC} and jaw and MLC defined fields. Percentage differences are presented relative to the corresponding measured data.

Field size (cm)	Depth (mm)	Jaw defined field					MLC defined field				
		Measured	AAA_{Jaw}	Rel Δ (%)	AAA_{MLC}	Rel Δ (%)	Measured	AAA_{Jaw}	Rel Δ (%)	AAA_{MLC}	Rel Δ (%)
3x3	15	4.71	2.85	39.5	2.85	39.5	5.80	4.26	26.6	4.26	26.6
	50	5.02	3.82	23.9	3.81	24.1	6.18	4.89	20.9	4.89	20.9
	300	5.87	4.13	29.6	4.14	29.5	7.13	5.92	17.0	5.92	17.0
10x10	15	5.08	3.88	23.6	3.88	23.6	6.51	5.00	23.2	5.00	23.2
	50	5.67	3.70	34.7	3.69	34.9	7.28	5.20	28.6	5.19	28.7
	300	10.16	8.81	13.3	8.82	13.2	13.77	10.76	21.9	10.76	21.9

Table 4.5: Comparison between Eclipse calculated penumbras (mm) for AAA_{Jaw} and AAA_{MLC} and jaw and MLC defined fields. Percentage differences are presented relative to the corresponding measured data.

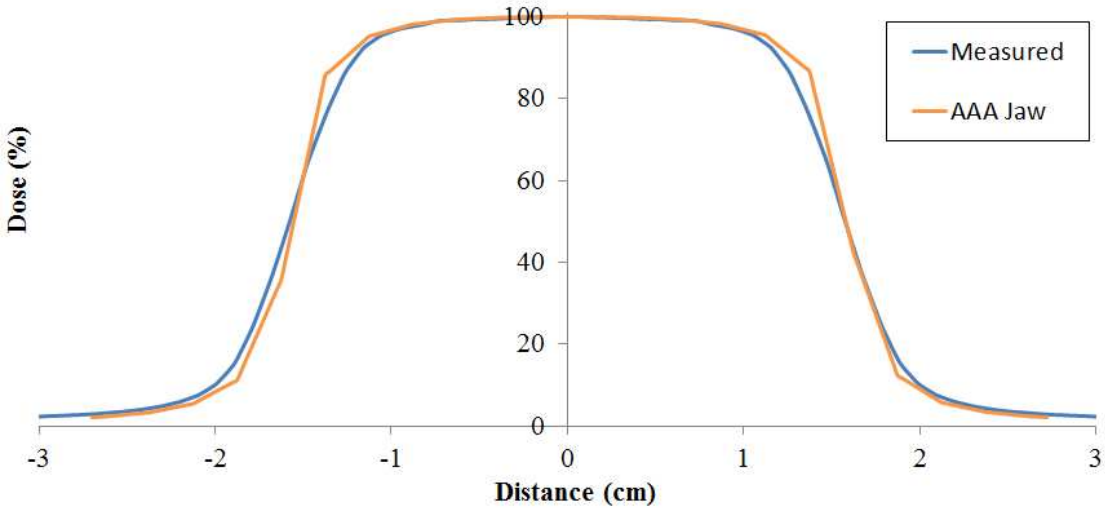

Figure 4.10: Comparison of AAA_{Jaw} calculated and measured 3x3 cm profiles with the jaw defining the field. Depth of measurement = 5cm.

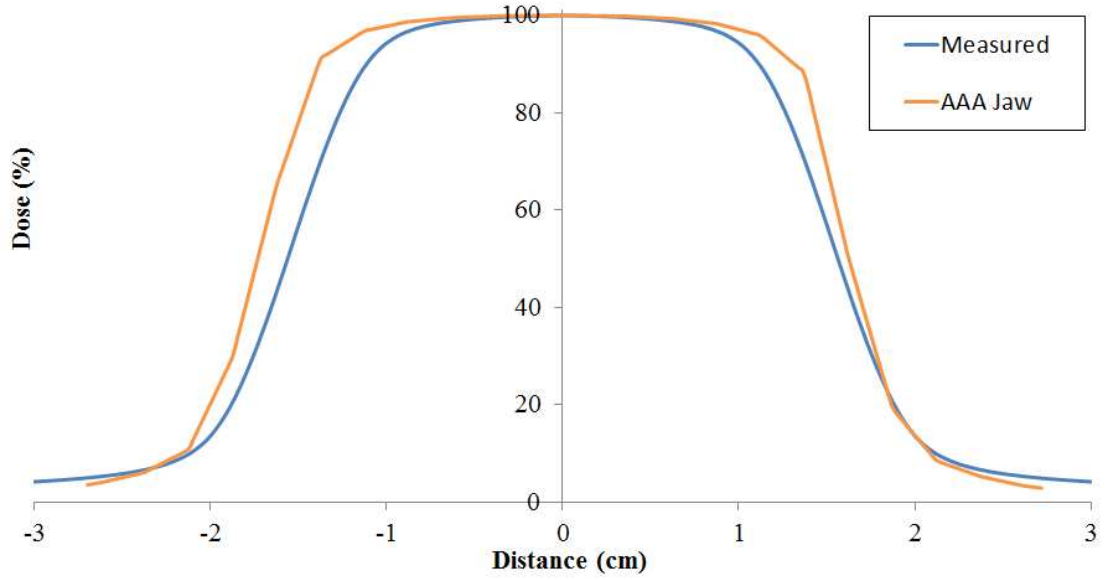

Figure 4.11: Comparison of AAA_{Jaw} calculated and measured 3x3 cm profiles with the MLC defining the field. Depth of measurement = 5cm.

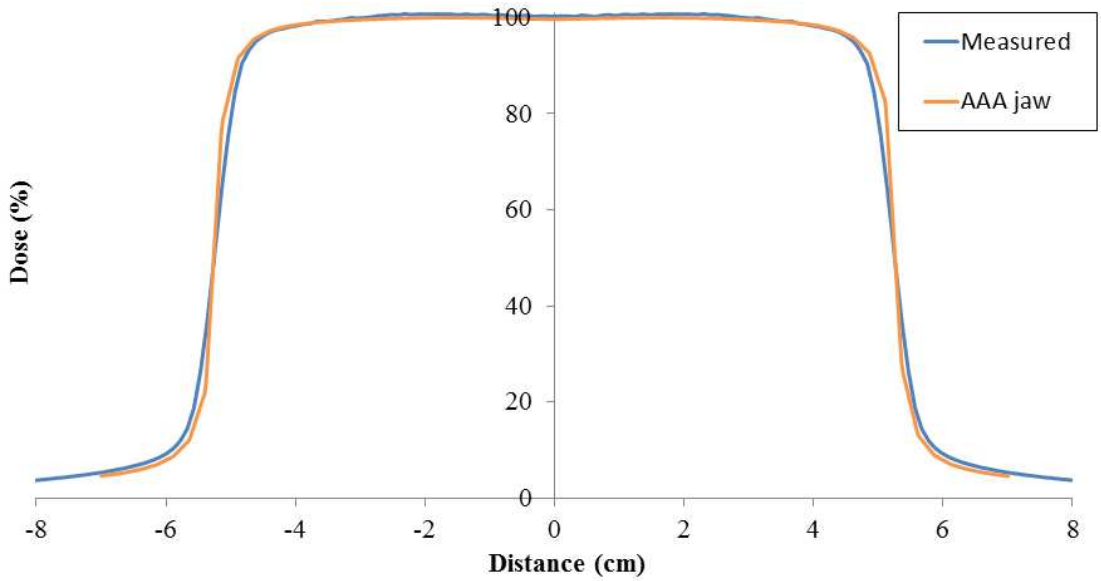

Figure 4.12: Comparison of AAA_{Jaw} calculated and measured 10x10 cm profiles with the jaw defining the field. Depth of measurement = 5cm.

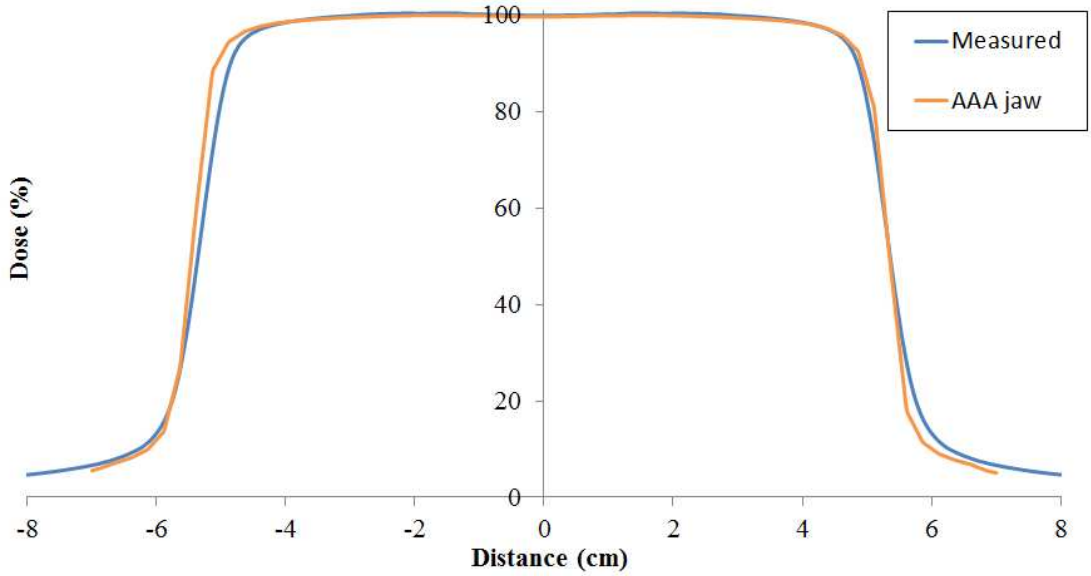

Figure 4.13: Comparison of AAA_{Jaw} calculated and measured 10x10 cm profiles with the MLC defining the field. Depth of measurement = 5cm.

4.3.1.3 Patient Treatment Plans

A summary of data collected for the 10 prostate patient data set can be found in table 4.6. This data reveals that the AAA_{Jaw} algorithm produces a significantly larger mean PTV3 dose. The mean global maximal point difference between the two plans - over the full 74 Gy treatment - is 0.90 Gy or 1.22%. The difference in maximum PTV dose is 0.52 Gy or 0.71%. As an assessment of the clinical significance of these differences the TCPs can be found in table 4.6. Plan and profile subtractions for prostate, thyroid bed and brain can be found in figures 4.14-16.

Patient	**Mean PTV3 dose (Gy)**		**TCP (%)**		**Plan subtraction**			
	AAA_{Jaw}	AAA_{MLC}	AAA_{Jaw}	AAA_{MLC}	Abs max Δ (Gy)	Abs max Δ (%)	PTV max dose Δ (Gy)	PTV max dose Δ (%)
1	75.90	75.46	72.1	70.2	0.80	1.08	0.52	0.70
2	74.59	74.14	66.0	63.8	0.60	0.81	0.53	0.71
3	73.70	73.33	61.6	59.7	0.95	1.28	0.49	0.66
4	73.32	72.25	59.7	57.1	0.86	1.16	0.54	0.73
5	73.88	73.47	62.6	60.5	0.95	1.28	0.50	0.68
6	73.72	73.24	61.6	59.1	0.85	1.15	0.55	0.74
7	75.19	74.71	69.0	66.7	0.88	1.19	0.53	0.72
8	75.21	74.77	68.9	66.8	1.11	1.50	0.52	0.70
9	73.88	73.43	62.5	60.2	1.07	1.45	0.52	0.71
10	73.77	73.37	59.5	58.3	0.97	1.31	0.55	0.74
Average	74.31	73.82	64.3	62.2	0.90	1.22	0.52	0.71
Significance	AAA_{Jaw}>AAA_{MLC}		AAA_{Jaw}>AAA_{MLC}		-	-	-	-

Table 4.6: PTV3 and plan subtraction data for differences in dose calculated with AAA_{Jaw} and AAA_{MLC} for 10 prostate RA plans. Dose differences are presented as absolute values.

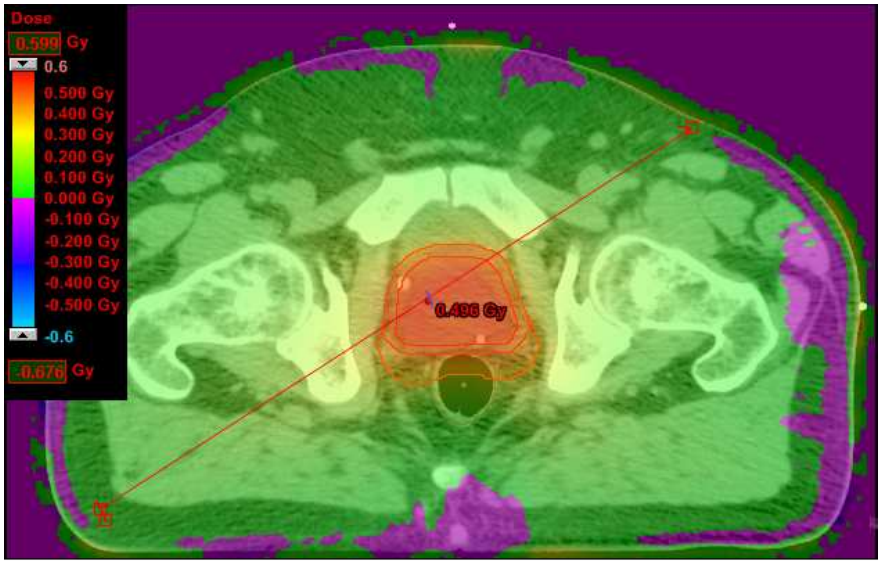

(a)

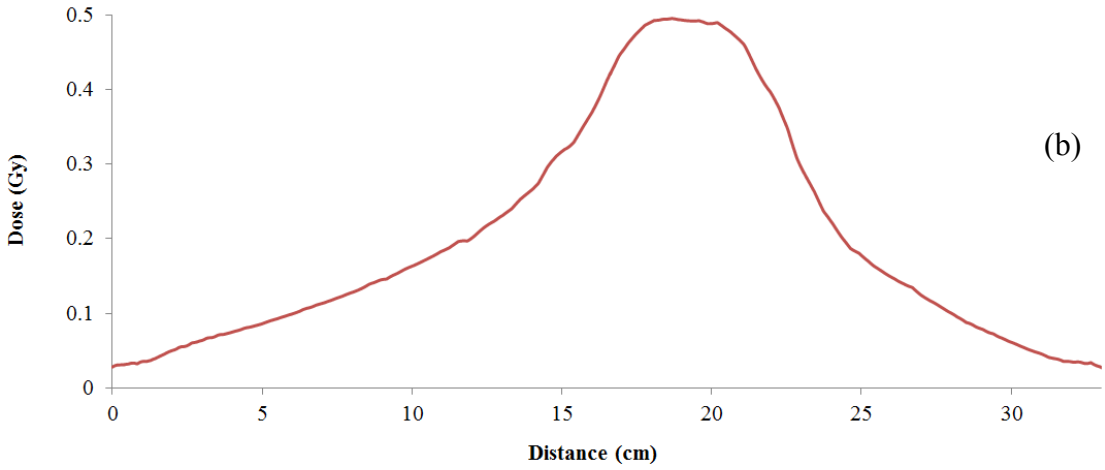

(b)

Figure 4.14: RA prostate doe subtraction (AAA_{Jaw} - AAA_{MLC}) (a). The red line represents the plane and direction in which a dose subtraction profile was taken, as presented in (b).

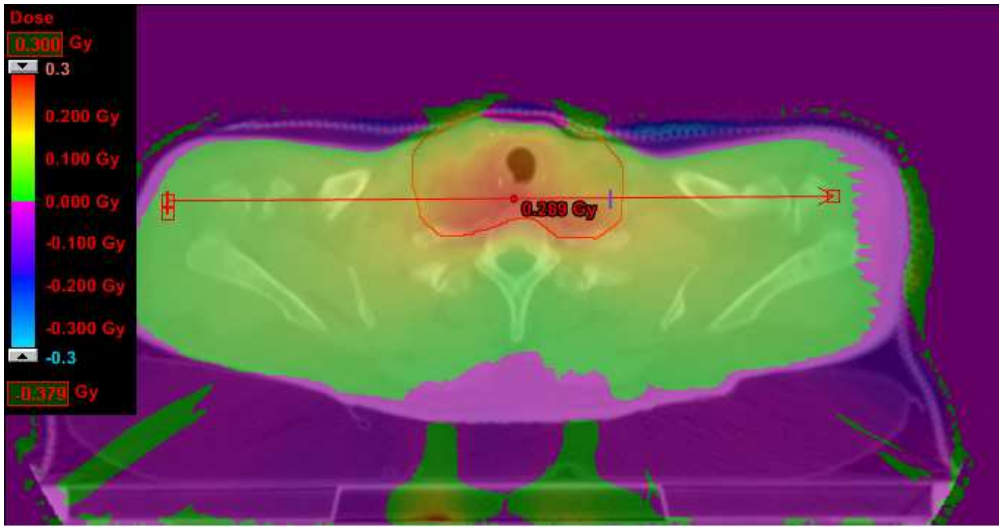

(a)

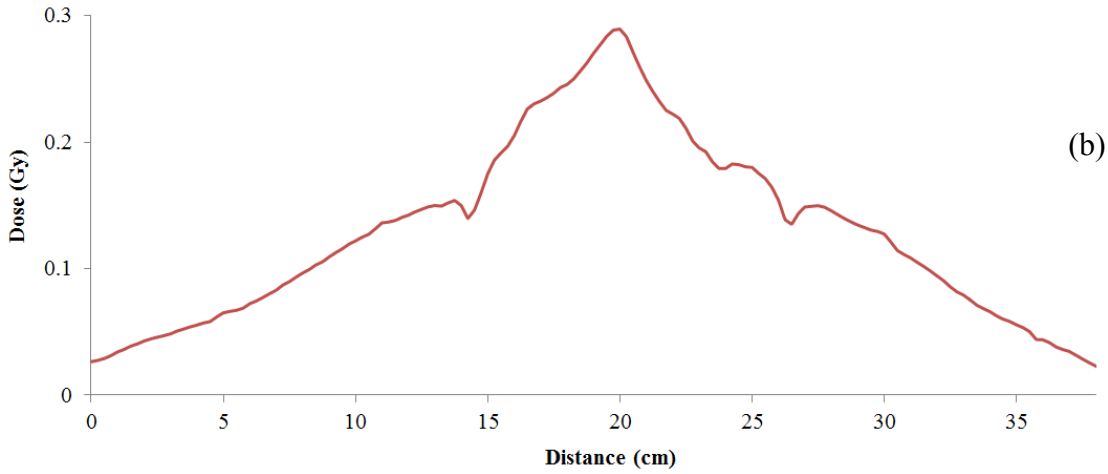

(b)

Figure 4.15: RA thyroid bed doe subtraction (AAA_{Jaw} - AAA_{MLC}) (a). The red line represents the plane and direction in which a dose subtraction profile was taken, as presented in (b).

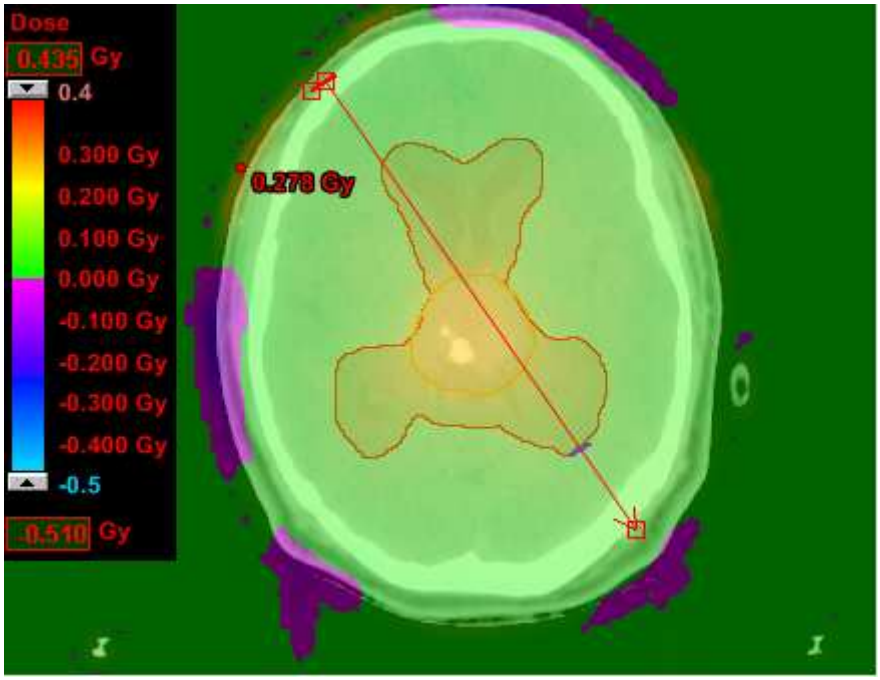

(a)

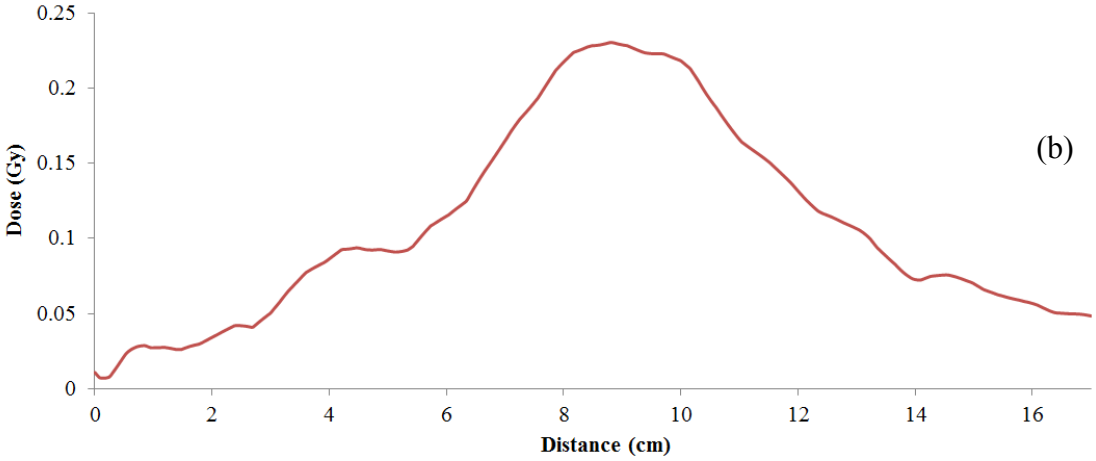

(b)

Figure 4.16: RA brain doe subtraction (AAA_{Jaw} - AAA_{MLC}) (a). The red line represents the plane and direction in which a dose subtraction profile was taken, as presented in (b).

4.3.1.4 Verification Measurements

A summary of point dose verification measurements can be found in table 4.7. Across both the prostate verification and lung simulation measurements 23 points were investigated. AAA_{Jaw} more accurately predicted the measured dose on 10 occasions and AAA_{MLC} on 13. The mean absolute difference between the presented values was 0.34%, within the experimental uncertainty of the measurement process. In general measurements for both algorithms were in good agreement with the exception of point 3 (rectum - PTV interface), largely due to the fact that the chamber often fell in a steep dose gradient. No other intra-patient or single point trends were observed.

Patient	Chamber point	Δ AAA_{Jaw} (%)	Δ AAA_{MLC} (%)
1	1	-0.20	0.20
	2	0.06	0.61
	3	-4.05	-3.65
	4	0.01	0.21
2	1	-0.97	-0.17
	2	-1.04	-0.44
	3	-10.35	-10.10
	4	-0.55	-0.35
3	1	2.81	3.26
	2	1.68	2.13
	3	-6.99	-6.79
	4	-0.10	0.05
4	1	1.14	1.64
	2	-0.01	0.59
	3	-10.23	-9.98
	4	1.51	1.66
5	1	1.20	1.60
	2	-0.78	-0.23
	3	-2.91	-2.41
	4	-1.36	-1.16
-	5	0.63	0.80
	6	-0.29	-0.01
	7	2.10	2.20

Table 4.7: Summary of point dose verification measurements. Prostate verification measurements (points 1-4) are presented as patients 1-5 whereas the simulated lung treatment (points 5-7) does not have an assigned patient number.

4.4 Discussion

The observed differences in the measured beam profiles is consistent with the known difference in transmission of the jaw and MLC field defining ends [132], whereby the penumbra of the MLC defined field being larger than that of the jaw, for all field sizes smaller than 40x40 cm. The difference between the mean penumbral values of the measured jaw and MLC fields was 2.1mm. Although this value is small, it may be significant when field sizes are small, as is the case with highly modulated static and dynamic IMRT plans. The small yet significant difference between the measured PDDs was unexpected, as central axis radiation transport is often at a distance large enough not to be effected by the field edge. Further investigations has revealed no consistent variation in energy (and therefore depth dose) when either the jaws or MLCs are defining the field. Thus, it is concluded that the observed differences are a result of discrete measurement set-up and not the linac head geometry itself.

Various conclusions can be drawn from analysis of the two algorithms, given the observed differences in the profile and PDD input data. This configuration process seems to be very sensitive to the PDD input data but not that of the beam profiles. The differences in measured dose at depth have carried through the configuration process, but the observed penumbras for both jaw and MLC defined fields are almost identical for both algorithms, even though the input data was distinctly different. This is an important result, as any further differences between the algorithms can no longer be fully associated with the differences in measured beam profiles (and therefore the jaw or MLC defining the field), but must be largely due to the observed differences in the PDDs at depth. Both of the algorithms model the field edge and penumbra of jaw defined fields well across all the investigated field sizes, but this is not the case for MLC defined fields. Larger field sizes are modeled well but more significant discrepancies are observed for smaller field sizes. This fact again reinforcing the notion that highly modulated IMRT plans - or single control points - may not be modeled well by either AAA.

The largest differences between the calculated RA plans were observed on the patient surface and at depth. The differences at the surface often fluctuated between either algorithm calculating more or less dose. However, AAA_{Jaw} consistently calculated

more dose than AAA_{MLC}, at depth. These observations were consistent for all the investigated plans: including all 10 prostate plans, the thyroid bed and brain case. Measurement and modeling of the build-up region is challenging and inaccurate, and with the low doses involved, is likely to be clinically insignificant. The observed differences at depth are consistent with the differences in measured and AAA calculated PDDs for static fields. The mean PTV dose and TCP is significantly larger for AAA_{Jaw} than for AAA_{MLC}, although the chamber point dose investigations reveal that neither algorithm systematically predicts the dose more accurately than the other. Without a measurement device accurate enough to discriminate the accuracy of these small differences, no conclusions can be drawn as to weather one algorithm is preferred over the other.

Although no major differences have been observed between the two algorithms, further investigation have been performed as to improve the understanding of how the AAA is configured and how dose is calculated. As a measure of the sensitivity of individual configurations a third algorithm was configured using the exact same beam data that went into the original algorithm (AAA_{Jaw}). Subsequently, this AAA was used to retrospectively re-calculate already existing RA plans - such as those presented throughout the manuscript - and plan subtractions acquired. An individual RA plan was also repetitively calculated 10 times with a single algorithm and different permutations of plan subtractions acquired. In both of the above investigations negligible differences in calculated dose were observed and therefore it is concluded that both the configuration of and individual AAA calculations are a stable processes, and as a corollary, the observed minor differences in AAA_{Jaw} and AAA_{MLC} are not a result of variations in either of these processes.

Although conclusions can be drawn from the present study, there are major limitations and outstanding work that remains. Firstly, the configuration process is obviously a complex process and conclusions regarding the input data are convoluted with other related parameters such as the jaw and MLC transmission factors and the DLG. Secondly, the verification measurements are of a very discrete nature and the detector is of a one-dimensional (1D) nature. A more comprehensive verification comparison would set a more robust benchmark for the two algorithms to be compared against. This should include comparisons with 2D (film) or 3D (polymer gels) dosimeters and

independent MC calculations. It would be expected that with these verification techniques a robust and collective benchmark for both algorithms would be formed although these measures may still not be sensitive enough to inter-compare the two algorithms. A semiflex ion chamber has been employed to measure the majority of beam data utilised in this study and although this detector is small relative to a Farmer chamber, the accuracy of measurements of small field sizes (≤3x3 cm) is reduced [133]. Further work includes expanding the data set into smaller field sizes, through the use of a photon diode, diamond detector, liquid ion chamber or similar detector appropriate for measuring small field sizes. Further investigations to analyze the effect this extra input data has on the configuration of the AAA, would follow. A quantitative study comparing the accuracy of AAA dose calculation and verification measurements (ArcCHECK and other) dependent on the number of MUs and level of plan modulation is also of high importance. Comparisons with non superposition/convolution algorithms – such as Acuros [134] – is also of interest.

The major limiting factor in the above study is that the two data sets were collected during different measurement sessions, possibly resulting in variations that convolute the property that was being investigated, namely the variation in the penumbra for jaw and MLC defined fields. This complicating factor could be removed – and more robust conclusions drawn – by measurement of the two data sets during the same measurement session, or configuration of two algorithms using two identical sets of PDDs. Varian provides so called ‘golden beam data’ that is representative of a linac type but not an individual machine (or set of beam matched machines). The observed configuration insensitivity to input beam profiles begs the question; are user measured profiles required at all, or should golden beam data be used as a surrogate? Configuration and analysis of a golden AAA is also in the realms of interesting future work.

4.5 Concluding Remarks

Configuration of the AAA in the Eclipse TPS has been shown to be sensitive to PDD input and insensitive to profile input. This extreme sensitivity to PDD input has important consequences for institutions with multiple linacs. Unless the energy matching of these machines is very close it is recommended that multiple machine dependent algorithms be configured, as to reduce potential differences in dose at depth. As a result of the insensitivity to beam profile input, beam data can be collected with either the jaws or MLCs defining the field edge, although the former is recommended. Measurement in this manner is more robust, as measurements are insensitive to MLC positional errors and are less complex. The need for multiple algorithms (one for intensity modulated and conformal calculations) is also removed. Although the investigations in this chapter have produced a null result, the significance of this result is important with several recommendations coming as a consequence. The medical physics community must be vigilant when it comes to understanding the accuracy and limitations of the algorithms used to calculate dose, especially when complex and novel techniques such as RA are being utilised. The work presented in this chapter is just one of many steps that must be taken to improve this understanding.

Chapter 5 – Concluding Remarks

The work presented herein has improved the overall knowledge of RA optimisation and dose calculation whilst exploring new clinical applications. Several previously unanswered questions (1.4) relating to these topics have also been addressed. However, this was not achieved without limitation. The goal of the subsequent sections is to outline these limitations, expand on future work and conclude the overall findings.

5.1 Critical Analysis

As outlined in chapter 2, there are many user defined parameters that affect the quality of the resulting optimisation. A specific combination of these parameters is outlined in the planning strategy, the results of which are inline with previously published data, at least for the treatment of prostate. It is difficult to isolate each of these parameters and therefore independently quantify the effect of variations in them. Formal planning studies would at least go some way to improving the understanding of what values should be selected, and potentially improve the possibility for the most optimum plan resulting. First and foremost, the effect of collimator angle requires more attention, with plans ranging from 5° through to 45° being produces for a range of patient anatomies, with plan quality assessment using methods used throughout preceding chapters. The affect of beam energy (10 or even 18MV) is also of interest, along with flattening filter free treatments. Investigation on how the number of MUs affects plan quality, overall modulation and agreement with verification measurements is the topic of other outstanding work. Investigating these effects could be achieved through manually restriction the MU value during repeated optimisations. The final planning limitation is related to the fact that only prostate and prostate bed treatments have been formally investigated. Further work is required to extend the presented data to other and often more complicated treatment sites such as head & neck.

The verification measurements presented in chapters 2 and 3 were limited to ion chamber and novel diode based measurements. Further verification measurements using a larger variety of detectors such as radiochromic film (currently unavailable in the WBCC) for both the investigated treatment sites is required. This would provide more confidence in the optimisation, modeling and delivery chain, and give more weight to the feasibility of delivery. With the highly modulated and irregular fields involved improvement in small field dosimetry is also of high importance, as outlined in 4.5. The fact that the ArcCHECK device is novel in nature also limits its use and the conclusions that can be drawn from it. This currently included the devises ability to accurately measure exit dose and the issue of the diode spatial resolution (1 cm) – in a single plane – being able to sufficiently resolve many of the small fields involved with delivery (figure 2.7). Further work is also required on the analysis of ArcCHECK results and what action levels should be set. Discrepancies between the planned and ArcCHECK measured dose is a convolution of many factors including; errors in CT acquisition, AAA dose calculation, set-up errors, diode response and spatial resolution. Deconvolving some of these factors may prove difficult, but still requires attention. As previously mentioned, the effect MU and overall modulation has on ArcCHECK results are also of interest.

5.2 Conclusions

The planning and delivery of rotational IMRT techniques is on the cusp of both time and complexity. A search for the word 'RapidArc' on PubMed at the commencement of this work produced 10 results, whilst the same search produced 81 results at the time of submission. In this time period the technique has matured to a level where single institution annual data is now published, along with a plethora of planning studies for a wide variety of clinical sites. In a field that is so highly dependent on technology, planning studies of this nature must suffice as a method for comparison, but the scrutiny of phase III clinical trials beckons for not only rotational but static gantry intensity modulated techniques. When compared with traditional intensity modulated techniques, RA has been shown to be dosimetrically comparable, whilst allowing for reductions in both treatment time and MUs . This advantage comes at the cost of an even more complex and novel treatment, extending to the inverse planning process, dose calculation and the delivery and verification of treatment.

To compliment the expanding data set of comparative planning studies a streamlined RA planning strategy - or class solution - has been formulated. This strategy gives detail regarding the initial field set-up, contouring, starting objectives, recommended optimisation user interactions and post-optimisation adjustments. The strategy was then applied to a cohort of 10 previously treated high and intermediate risk prostate patients. The resulting plans were then subject to an inter-comparative planning study with static gantry IMRT, as a justification for the planning strategy itself and not RA techniques in general, as has been previously published. The results of this study were shown to be generally comparable to previously published planning studies, in the sense that target coverage between the two techniques were comparable and RA OAR sparing was slightly improved. Although a direct comparison with other prostate planning studies is limited, it was also concluded that the results were of a directly comparable nature.

The now justified planning study was then applied to an independent but related clinical site, in an effort to both solve a clinical problem and fill a hole in the RA comparative literature. The clinical site in question was treatment of the prostate bed in the post-operative setting. This site is traditionally difficult to treat with conformal therapies, due to the fact that the clinical target volume resides within close proximity of dose limiting normal structures, combined with the techniques inability to produce concave dose distributions and spare said structures. As part of the presented planning comparison it is seen that conformal techniques are unable to treat the target volume without giving unacceptable doses to the rectum, and that consistently adequate sparing was only achieved through a significant compromise in the target volume. Thus, increasing the risk for a geographical miss and potentially reducing the quality of the treatment. This issue was alleviated through the implementation of modified RA planning strategies, whereby the entire patient cohort could be adequately treated with out compromising the target volume or over dosing the rectum. Furthermore, it has been shown that RA techniques give scope for significant dose escalation from 64 to 70 Gy in the majority of patients. In saying this, care still needs to be taken not to over-modulate the plan or have large volumes of the rectum and PTV occupying the same volume of physical space.

The complex nature of RA delivery is mirrored with the associated dose modeling and verification with much still unknown, namely, how well do current calculation algorithms deal with complex, irregular and often small MLC apertures. It was originally hypothesised that this modeling may improve if more appropriate input beam data was provided for the configurations of such algorithms. Namely, beam data that was collected with the MLC defining the field rather than the jaws. This hypothesis has been proven incorrect, with different input data having a negligible effect on the configured algorithm. Consequently it is recommended that convention is not broken and future configuration data be collected with the jaws defining the field edge. The configuration process has been seen to be very sensitive to the beam PDDs that are used as input data and therefore it is recommended that extra care be taken when these measurements are taken. Furthermore, it is recommended that departments with more than one linac have more than one calculation algorithm if their machines are now well matched in energy.

Since the seminal paper by Otto [6] in early 2008, delivering highly modulated radiotherapy treatments in a continuous arc has proven to be a time efficient alternative to static gantry intensity-modulated techniques. In saying this, the technique is still in its early stage of development with many questions still unanswered, including those pertinent to VMAT specifically, and IMRT in general. This thesis has addressed several of these questions, related to inverse planning techniques, dose calculation algorithms and clinical applications.

6. References

1. Thwaites, D.I. and J.B. Tuohy, *Back to the future: the history and development of the clinical linear accelerator.* Phys Med Biol, 2006. **51**(13): p. R343-62.
2. Beckmann, E.C., *CT scanning the early days.* Br J Radiol, 2006. **79**(937): p. 5-8.
3. Brahme, A., *Optimization of stationary and moving beam radiation therapy techniques.* Radiother Oncol, 1988. **12**(2): p. 129-40.
4. Bortfeld, T., *IMRT: a review and preview.* Phys Med Biol, 2006. **51**(13): p. R363-79.
5. Jemal, A., et al., *Cancer statistics, 2009.* CA Cancer J Clin, 2009. **59**(4): p. 225-49.
6. Otto, K., *Volumetric modulated arc therapy: IMRT in a single gantry arc.* Med Phys, 2008. **35**(1): p. 310-7.
7. Perez C. A, B.L.W., Roti J. L, *"Overview" In principals and Practice of Radiation Oncology*. 1998, Lippincott-Raven: Philadelphia, PA. p. 1-78.
8. VanDyk, J., *The Modern Technology of Radiation Oncology. A Compendium for Medical Physicists and Radiation Oncologists*, ed. J. VanDyk. 1999, Madison, Wisconsin: Medical Physics Publishing.
9. Del Regato, J.A., *Claudius Regaud.* Int J Radiat Oncol Biol Phys, 1976. **1**(9-10): p. 993-1001.
10. Meredith, W.J., *40 years of development in radiotherapy.* Phys Med Biol, 1984. **29**(2): p. 115-20.
11. Schaller, R.R., *Moore's law: past, present and future.* Spectrum, IEEE, 1997. **34**(6): p. 52-59.
12. Bentzen, S.M., *Radiation therapy: intensity modulated, image guided, biologically optimized and evidence based.* Radiother Oncol, 2005. **77**(3): p. 227-30.
13. Nutting, C., *Intensity-modulated radiotherapy (IMRT): the most important advance in radiotherapy since the linear accelerator?* Br J Radiol, 2003. **76**(910): p. 673.

14. Censor, Y., M. Altschuler, and W. Powlis, *A computational solution of the inverse problem in radiation-therapy treatment planning.* Applied Mathematics and Computation, 1988. **25**(1): p. 57-87.
15. Webb, S., *Optimisation of conformal radiotherapy dose distributions by simulated annealing.* Phys Med Biol, 1989. **34**(10): p. 1349-70.
16. Bortfeld, T., et al., *Methods of image reconstruction from projections applied to conformation radiotherapy.* Phys Med Biol, 1990. **35**(10): p. 1423-34.
17. Convery, D.J. and M.E. Rosenbloom, *The generation of intensity-modulated fields for conformal radiotherapy by dynamic collimation.* Physics in Medicine and Biology, 1992. **37**(6): p. 1359.
18. Munro, P., *Megavoltage Radiotherapy for treatment verification*, ed. J.V. Dyke. 1999.
19. Bhide, S.A. and C.M. Nutting, *Recent advances in radiotherapy.* BMC Med, 2010. **8**: p. 25.
20. Bortfeld, T., et al., *Realization and verification of three-dimensional conformal radiotherapy with modulated fields.* Int J Radiat Oncol Biol Phys, 1994. **30**(4): p. 899-908.
21. Ling, C.C., et al., *Conformal radiation treatment of prostate cancer using inversely-planned intensity-modulated photon beams produced with dynamic multileaf collimation.* Int J Radiat Oncol Biol Phys, 1996. **35**(4): p. 721-30.
22. Mackie, T.R., et al., *Tomotherapy: a new concept for the delivery of dynamic conformal radiotherapy.* Med Phys, 1993. **20**(6): p. 1709-19.
23. Mackie, T.R., *History of tomotherapy.* Phys Med Biol, 2006. **51**(13): p. R427-53.
24. WHO, *http://www.who.int/mediacentre/factsheets/fs297/en/index.html*. 2004.
25. *Cancer in New Zealand: Trends and Projections*. 2002: Ministry of health.
26. *Cancer in Australia: an overview, 2008*. 2008: Australian Institute of Health and Welfare, Australasian Association of Cancer Registries.
27. McDermid, I., *Cancer incidence projections Australia 2002 to 2011*. 2005: Australian Institute of Health and Welfare
28. Purdy, J., *Intensity-modulated radiotherapy: current status and issues of interest.* Int J Radiat Oncol Biol Phys, 2001. **51**(4): p. 880-914.
29. Hall, E.J., *Intensity-modulated radiation therapy, protons, and the risk of second cancers.* Int J Radiat Oncol Biol Phys, 2006. **65**(1): p. 1-7.

30. Yu, C.X., *Intensity-modulated arc therapy with dynamic multileaf collimation: an alternative to tomotherapy.* Phys Med Biol, 1995. **40**(9): p. 1435-49.
31. Bratengeier, K., *Applications of two-step intensity modulated arc therapy.* Strahlenther Onkol, 2001. **177**(8): p. 394-403.
32. Earl, M.A., et al., *Inverse planning for intensity-modulated arc therapy using direct aperture optimization.* Phys Med Biol, 2003. **48**(8): p. 1075-89.
33. Shepard, D.M., et al., *An arc-sequencing algorithm for intensity modulated arc therapy.* Med Phys, 2007. **34**(2): p. 464-70.
34. Palma, D.A., et al., *New developments in arc radiation therapy: a review.* Cancer Treat Rev, 2010. **36**(5): p. 393-9.
35. Palma, D., et al., *Volumetric modulated arc therapy for delivery of prostate radiotherapy: comparison with intensity-modulated radiotherapy and three-dimensional conformal radiotherapy.* Int J Radiat Oncol Biol Phys, 2008. **72**(4): p. 996-1001.
36. Yoo, S., et al., *Radiotherapy Treatment Plans with RapidArc for Prostate Cancer Involving Seminal Vesicles and Lymph Nodes.* Int J Radiat Oncol Biol Phys, 2009.
37. Wolff, D., et al., *Volumetric modulated arc therapy (VMAT) vs. serial tomotherapy, step-and-shoot IMRT and 3D-conformal RT for treatment of prostate cancer.* Radiother Oncol, 2009. **93**(2): p. 226-33.
38. Weber, D.C., et al., *RapidArc, intensity modulated photon and proton techniques for recurrent prostate cancer in previously irradiated patients: a treatment planning comparison study.* Radiat Oncol, 2009. **4**: p. 34.
39. Vanetti, E., et al., *Volumetric modulated arc radiotherapy for carcinomas of the oro-pharynx, hypo-pharynx and larynx: a treatment planning comparison with fixed field IMRT.* Radiother Oncol, 2009. **92**(1): p. 111-7.
40. Verbakel, W.F., et al., *Volumetric intensity-modulated arc therapy vs. conventional IMRT in head-and-neck cancer: a comparative planning and dosimetric study.* Int J Radiat Oncol Biol Phys, 2009. **74**(1): p. 252-9.
41. Wagner, D., et al., *Radiotherapy of malignant gliomas: comparison of volumetric single arc technique (RapidArc), dynamic intensity-modulated technique and 3D conformal technique.* Radiother Oncol, 2009. **93**(3): p. 593-6.

42. Shaffer, R., et al., *A Comparison of Volumetric Modulated Arc Therapy and Conventional Intensity-Modulated Radiotherapy for Frontal and Temporal High-Grade Gliomas.* Int J Radiat Oncol Biol Phys, 2009.
43. Stieler, F., et al., *A fast radiotherapy paradigm for anal cancer with volumetric modulated arc therapy (VMAT).* Radiat Oncol, 2009. **4**: p. 48.
44. Nicolini, G., et al., *Simultaneous integrated boost radiotherapy for bilateral breast: a treatment planning and dosimetric comparison for volumetric modulated arc and fixed field intensity modulated therapy.* Radiat Oncol, 2009. **4**: p. 27.
45. Cozzi, L., et al., *A treatment planning study comparing volumetric arc modulation with RapidArc and fixed field IMRT for cervix uteri radiotherapy.* Radiother Oncol, 2008. **89**(2): p. 180-91.
46. Lagerwaard, F.J., et al., *Whole-brain radiotherapy with simultaneous integrated boost to multiple brain metastases using volumetric modulated arc therapy.* Int J Radiat Oncol Biol Phys, 2009. **75**(1): p. 253-9.
47. Hsu, F., et al., *Whole Brain Radiotherapy with Hippocampal Avoidance and Simultaneous Integrated Boost for 1-3 Brain Metastases: A Feasibility Study Using Volumetric Modulated Arc Therapy.* Int J Radiat Oncol Biol Phys, 2009.
48. Fogliata, A., et al., *On the performances of Intensity Modulated Protons, RapidArc and Helical Tomotherapy for selected paediatric cases.* Radiat Oncol, 2009. **4**: p. 2.
49. Bedford, J.L. and A.P. Warrington, *Commissioning of volumetric modulated arc therapy (VMAT).* Int J Radiat Oncol Biol Phys, 2009. **73**(2): p. 537-45.
50. Guckenberger, M., et al., *Is a single arc sufficient in volumetric-modulated arc therapy (VMAT) for complex-shaped target volumes?* Radiother Oncol, 2009. **93**(2): p. 259-65.
51. Bortfeld, T. and S. Webb, *Single-Arc IMRT?* Phys Med Biol, 2009. **54**(1): p. N9-20.
52. Otto, K., *Letter to the Editor on 'Single-Arc IMRT?'* Phys Med Biol, 2009. **54**(8): p. L37-41; author reply L43-4.
53. Verbakel, W.F., et al., *Comments on 'Single-Arc IMRT?'* Phys Med Biol, 2009. **54**(8): p. L31-4; author reply L35-6.

54. Zacarias, A.S., M.F. Brown, and M.D. Mills, *Volumetric Modulated Arc Therapy (VMAT) Treatment Planning for Superficial Tumors.* Med Dosim, 2009.
55. Oliver, M., W. Ansbacher, and W.A. Beckham, *Comparing planning time, delivery time and plan quality for IMRT, RapidArc and Tomotherapy.* J Appl Clin Med Phys, 2009. **10**(4): p. 3068.
56. Lagerwaard, F.J., et al., *Volumetric modulated arc radiotherapy for vestibular schwannomas.* Int J Radiat Oncol Biol Phys, 2009. **74**(2): p. 610-5.
57. Bignardi, M., et al., *Critical appraisal of volumetric modulated arc therapy in stereotactic body radiation therapy for metastases to abdominal lymph nodes.* Int J Radiat Oncol Biol Phys, 2009. **75**(5): p. 1570-7.
58. Popescu, C.C., et al., *Volumetric modulated arc therapy improves dosimetry and reduces treatment time compared to conventional intensity-modulated radiotherapy for locoregional radiotherapy of left-sided breast cancer and internal mammary nodes.* Int J Radiat Oncol Biol Phys. **76**(1): p. 287-95.
59. Clark, G.M., et al., *Feasibility of single-isocenter volumetric modulated arc radiosurgery for treatment of multiple brain metastases.* Int J Radiat Oncol Biol Phys. **76**(1): p. 296-302.
60. Popple, R.A., et al., *RapidArc radiation therapy: first year experience at the University of Alabama at Birmingham.* Int J Radiat Oncol Biol Phys, 2010. **77**(3): p. 932-41.
61. Pesce, G.A., et al., *Early clinical experience of radiotherapy of prostate cancer with volumetric modulated arc therapy.* Radiat Oncol, 2010. **5**: p. 54.
62. Mott, J.H., J.E. Livsey, and J.P. Logue, *Development of a simultaneous boost IMRT class solution for a hypofractionated prostate cancer protocol.* Br J Radiol, 2004. **77**(917): p. 377-86.
63. Khoo, V.S. and D.P. Dearnaley, *Question of dose, fractionation and technique: ingredients for testing hypofractionation in prostate cancer--the CHHiP trial.* Clinical oncology (Royal College of Radiologists (Great Britain)), 2008. **20**(1): p. 12-4.
64. Oliver, M., et al., *Analysis of RapidArc optimization strategies using objective function values and dose-volume histograms.* J Appl Clin Med Phys, 2009. **11**(1): p. 3114.

65. Howell, R.M., et al., *Calculation of effective dose from measurements of secondary neutron spectra and scattered photon dose from dynamic MLC IMRT for 6 MV, 15 MV, and 18 MV beam energies.* Med Phys, 2006. **33**(2): p. 360-8.
66. *Eclipse algorithim reference guide*. 2008, Varian medical systems.
67. *Eclipse inverse planning. Administration and physics*. 2008: Varian medical systems.
68. Sidhom, M.A., et al., *Post-prostatectomy radiation therapy: consensus guidelines of the Australian and New Zealand Radiation Oncology Genito-Urinary Group.* Radiother.Oncol., 2008. **88**(1): p. 10-19.
69. Schreibmann, E. and L. Xing, *Feasibility study of beam orientation class-solutions for prostate IMRT.* Med Phys, 2004. **31**(10): p. 2863-70.
70. Feuvret, L., et al., *Conformity index: a review.* Int J Radiat Oncol Biol Phys, 2006. **64**(2): p. 333-42.
71. Niemierko, A., *Reporting and analyzing dose distributions: a concept of equivalent uniform dose.* Med Phys, 1997. **24**(1): p. 103-10.
72. Xu, X.G., B. Bednarz, and H. Paganetti, *A review of dosimetry studies on external-beam radiation treatment with respect to second cancer induction.* Phys Med Biol, 2008. **53**(13): p. R193-241.
73. Thompson, I.M., Jr., et al., *Adjuvant radiotherapy for pathologically advanced prostate cancer: a randomized clinical trial.* JAMA, 2006. **296**(19): p. 2329-2335.
74. Wiegel, T., et al., *Phase III postoperative adjuvant radiotherapy after radical prostatectomy compared with radical prostatectomy alone in pT3 prostate cancer with postoperative undetectable prostate-specific antigen: ARO 96-02/AUO AP 09/95.* J Clin Oncol, 2009. **27**(18): p. 2924-30.
75. Thompson, I.M., et al., *Adjuvant radiotherapy for pathological T3N0M0 prostate cancer significantly reduces risk of metastases and improves survival: long-term followup of a randomized clinical trial.* J.Urol., 2009. **181**(3): p. 956-962.
76. Bolla, M., et al., *Postoperative radiotherapy after radical prostatectomy: a randomised controlled trial (EORTC trial 22911).* Lancet, 2005. **366**(9485): p. 572-578.

77. Stephenson, A.J., et al., *Predicting the outcome of salvage radiation therapy for recurrent prostate cancer after radical prostatectomy.* J Clin Oncol, 2007. **25**(15): p. 2035-41.
78. Hayes, S.B. and A. Pollack, *Parameters for treatment decisions for salvage radiation therapy.* J Clin Oncol, 2005. **23**(32): p. 8204-11.
79. Dearnaley, D.P., et al., - *Escalated-dose versus standard-dose conformal radiotherapy in prostate cancer: first results from the MRC RT01 randomised controlled trial.[see comment]*. - Lancet Oncology, 2007. **8**(6): p. 475-487.
80. Peeters, S.T., et al., - *Dose-response in radiotherapy for localized prostate cancer: results of the Dutch multicenter randomized phase III trial comparing 68 Gy of radiotherapy with 78 Gy.[see comment]*. - Journal of Clinical Oncology, 2006. **24**(13): p. 1990-1996.
81. Pollack, A., et al., - *Prostate cancer radiation dose response: results of the M. D. Anderson phase III randomized trial.[see comment]*. - International Journal of Radiation Oncology, Biology, Physics, 2002. **53**(5): p. 1097-1105.
82. Zietman, A.L., et al., - *Comparison of conventional-dose vs high-dose conformal radiation therapy in clinically localized adenocarcinoma of the prostate: a randomized controlled trial.[see comment]*. - JAMA, 2005. **294**(10): p. 1233-1239.
83. Anscher, M.S., R. Clough, and R. Dodge, *Radiotherapy for a rising prostate-specific antigen after radical prostatectomy: the first 10 years.* Int J Radiat Oncol Biol Phys, 2000. **48**(2): p. 369-75.
84. Cozzarini, C., et al., *Need for high radiation dose (>or=70 gy) in early postoperative irradiation after radical prostatectomy: a single-institution analysis of 334 high-risk, node-negative patients.* Int.J.Radiat.Oncol.Biol.Phys., 2009. **75**(4): p. 966-974.
85. King, C.R. and M.T. Spiotto, *Improved outcomes with higher doses for salvage radiotherapy after prostatectomy.* Int J Radiat Oncol Biol Phys, 2008. **71**(1): p. 23-7.
86. Valicenti, R.K., et al., *Effect of higher radiation dose on biochemical control after radical prostatectomy for PT3N0 prostate cancer.* Int J Radiat Oncol Biol Phys, 1998. **42**(3): p. 501-6.

87. King, C.R. and D.S. Kapp, *Radiotherapy after prostatectomy: is the evidence for dose escalation out there?* Int J Radiat Oncol Biol Phys, 2008. **71**(2): p. 346-50.
88. Kassabian, V.S., et al., *Possible mechanism for seeding of tumor during radical prostatectomy.* J Urol, 1993. **150**(4): p. 1169-71.
89. Sella, T., et al., *Suspected local recurrence after radical prostatectomy: endorectal coil MR imaging.* Radiology, 2004. **231**(2): p. 379-85.
90. Poortmans, P., et al., *Guidelines for target volume definition in post-operative radiotherapy for prostate cancer, on behalf of the EORTC Radiation Oncology Group.* Radiother.Oncol., 2007. **84**(2): p. 121-127.
91. Michalski, J.M., et al., *Development of RTOG consensus guidelines for the definition of the clinical target volume for postoperative conformal radiation therapy for prostate cancer.* Int J Radiat Oncol Biol Phys, 2010. **76**(2): p. 361-8.
92. Wiltshire, K.L., et al., *Anatomic boundaries of the clinical target volume (prostate bed) after radical prostatectomy.* Int J Radiat Oncol Biol Phys, 2007. **69**(4): p. 1090-9.
93. Fiorino, C., et al., *Rectal and bladder motion during conformal radiotherapy after radical prostatectomy.* Radiother Oncol, 2005. **74**(2): p. 187-95.
94. Corletto, D., et al., *Inverse and forward optimization of one- and two-dimensional intensity-modulated radiation therapy-based treatment of concave-shaped planning target volumes: the case of prostate cancer.* Radiother.Oncol., 2003. **66**(2): p. 185-195.
95. De Meerleer, G.O., et al., *Radiotherapy of prostate cancer with or without intensity modulated beams: a planning comparison.* Int.J.Radiat.Oncol.Biol.Phys., 2000. **47**(3): p. 639-648.
96. Damen, E.M., et al., *Planning, computer optimization, and dosimetric verification of a segmented irradiation technique for prostate cancer.* Int.J.Radiat.Oncol.Biol.Phys., 2001. **49**(4): p. 1183-1195.
97. Cahlon, O., M. Hunt, and M.J. Zelefsky, *Intensity-modulated radiation therapy: supportive data for prostate cancer.* Semin Radiat Oncol, 2008. **18**(1): p. 48-57.

98. Zelefsky, M.J., et al., *Long-term outcome of high dose intensity modulated radiation therapy for patients with clinically localized prostate cancer.* J.Urol., 2006. **176**(4 Pt 1): p. 1415-1419.
99. De Meerleer, G., et al., *Intensity-modulated radiotherapy as primary treatment for prostate cancer: acute toxicity in 114 patients.* Int J Radiat Oncol Biol Phys, 2004. **60**(3): p. 777-87.
100. De Meerleer, G.O., et al., *Intensity-modulated radiation therapy for prostate cancer: late morbidity and results on biochemical control.* Radiother Oncol, 2007. **82**(2): p. 160-6.
101. Fonteyne, V., et al., *Late radiotherapy-induced lower intestinal toxicity (RILIT) of intensity-modulated radiotherapy for prostate cancer: the need for adapting toxicity scales and the appearance of the sigmoid colon as co-responsible organ for lower intestinal toxicity.* Radiother Oncol, 2007. **84**(2): p. 156-63.
102. Liauw, S.L., et al., *Biochemical control and toxicity after intensity-modulated radiation therapy for prostate cancer.* Technol Cancer Res Treat, 2009. **8**(3): p. 201-6.
103. Vora, S.A., et al., *Analysis of biochemical control and prognostic factors in patients treated with either low-dose three-dimensional conformal radiation therapy or high-dose intensity-modulated radiotherapy for localized prostate cancer.* Int J Radiat Oncol Biol Phys, 2007. **68**(4): p. 1053-8.
104. De Meerleer, G., et al., *Salvage intensity-modulated radiotherapy for rising PSA after radical prostatectomy.* Radiother.Oncol., 2008. **89**(2): p. 205-213.
105. Ost, P., et al., *Adjuvant high-dose intensity-modulated radiotherapy after radical prostatectomy for prostate cancer: clinical results in 104 patients.* Eur.Urol., 2009. **56**(4): p. 669-675.
106. Sandhu, A., et al., *Prostate bed localization with image-guided approach using on-board imaging: reporting acute toxicity and implications for radiation therapy planning following prostatectomy.* Radiother Oncol, 2008. **88**(1): p. 20-5.
107. Jolly, D., D. Alahakone, and J. Meyer, *A RapidArc planning strategy for prostate with simultaneous integrated boost.* J Appl Clin Med Phys. **12**(1): p. 3320.

108. Burman, C., et al., *Fitting of normal tissue tolerance data to an analytic function.* Int J Radiat Oncol Biol Phys, 1991. **21**(1): p. 123-35.
109. Letourneau, D., et al., *Novel dosimetric phantom for quality assurance of volumetric modulated arc therapy.* Med Phys, 2009. **36**(5): p. 1813-21.
110. Yan, G., et al., *Calibration of a novel four-dimensional diode array.* Med Phys, 2010. **37**(1): p. 108-15.
111. Iftimia, I., et al., *Quality assurance methodology for Varian RapidArc treatment plans.* J Appl Clin Med Phys, 2010. **11**(4): p. 3164.
112. De Meerleer, G., et al., *Salvage intensity-modulated radiotherapy for rising PSA after radical prostatectomy.* Radiother Oncol, 2008. **89**(2): p. 205-13.
113. Nath, S.K., et al., *Toxicity analysis of postoperative image-guided intensity-modulated radiotherapy for prostate cancer.* Int J Radiat Oncol Biol Phys, 2010. **78**(2): p. 435-41.
114. Schiffner, D.C., et al., *Daily electronic portal imaging of implanted gold seed fiducials in patients undergoing radiotherapy after radical prostatectomy.* Int J Radiat Oncol Biol Phys, 2007. **67**(2): p. 610-9.
115. Ulmer, W. and D. Harder, *Applications of a Triple Gaussian Pencil Beam Model for Photon Beam Treatment Planning.* Z. Med. Phys., 1996. **6**: p. 68-74.
116. Ulmer, W. and D. Harder, *A Triple Gaussian Pencil Beam Model for Photon Beam Treatment Planning.* Z. Med. Phys., 1995. **5**: p. 25-30.
117. Storchi, P.R., L.J. van Battum, and E. Woudstra, *Calculation of a pencil beam kernel from measured photon beam data.* Phys Med Biol, 1999. **44**(12): p. 2917-28.
118. Ronde, H.S. and L. Hoffmann, *Validation of Varian's AAA algorithm with focus on lung treatments.* Acta Oncol, 2009. **48**(2): p. 209-15.
119. Gagne, I.M. and S. Zavgorodni, *Evaluation of the analytical anisotropic algorithm in an extreme water-lung interface phantom using Monte Carlo dose calculations.* J Appl Clin Med Phys, 2007. **8**(1): p. 33-46.
120. Rogers, D.W., *Fifty years of Monte Carlo simulations for medical physics.* Phys Med Biol, 2006. **51**(13): p. R287-301.
121. LoSasso, T., C.S. Chui, and C.C. Ling, *Physical and dosimetric aspects of a multileaf collimation system used in the dynamic mode for implementing intensity modulated radiotherapy.* Med Phys, 1998. **25**(10): p. 1919-27.

122. Vial, P., et al., *An experimental investigation into the radiation field offset of a dynamic multileaf collimator.* Phys Med Biol, 2006. **51**(21): p. 5517-38.
123. Gagne, I.M., et al., *A Monte Carlo evaluation of RapidArc dose calculations for oropharynx radiotherapy.* Phys Med Biol, 2008. **53**(24): p. 7167-85.
124. Fogliata, A., et al., *Dosimetric validation of the anisotropic analytical algorithm for photon dose calculation: fundamental characterization in water.* Phys Med Biol, 2006. **51**(6): p. 1421-38.
125. Van Esch, A., et al., *Testing of the analytical anisotropic algorithm for photon dose calculation.* Med Phys, 2006. **33**(11): p. 4130-48.
126. Bragg, C.M. and J. Conway, *Dosimetric verification of the anisotropic analytical algorithm for radiotherapy treatment planning.* Radiother Oncol, 2006. **81**(3): p. 315-23.
127. Gay, H.A. and A. Niemierko, *A free program for calculating EUD-based NTCP and TCP in external beam radiotherapy.* Phys Med, 2007. **23**(3-4): p. 115-25.
128. Wang, J.Z. and X.A. Li, *Evaluation of external beam radiotherapy and brachytherapy for localized prostate cancer using equivalent uniform dose.* Med Phys, 2003. **30**(1): p. 34-40.
129. Levegrun, S., et al., *Risk group dependence of dose-response for biopsy outcome after three-dimensional conformal radiation therapy of prostate cancer.* Radiother Oncol, 2002. **63**(1): p. 11-26.
130. Wu, Q., et al., *Optimization of intensity-modulated radiotherapy plans based on the equivalent uniform dose.* Int J Radiat Oncol Biol Phys, 2002. **52**(1): p. 224-35.
131. Ezzell, G.A., et al., *IMRT commissioning: multiple institution planning and dosimetry comparisons, a report from AAPM Task Group 119.* Med Phys, 2009. **36**(11): p. 5359-73.
132. Podgorsak, E.B., *Radiation oncology physics: A handbook for teachers and students*. 2005, Vienna: IAEA. 373.
133. Aspradakis, M.M., et al., *IPEM report number 103; Small Field MV Photon Dosimetry* 2010.
134. Vassiliev, O.N., et al., *Validation of a new grid-based Boltzmann equation solver for dose calculation in radiotherapy with photon beams.* Phys Med Biol. **55**(3): p. 581-98.

Appendices

A1 Author Statements

Unless acknowledged or referenced, the manuscript as presented is the work of the author and is submitted as partial fulfillment of the masters degree in medical physics at the University of Canterbury, New Zealand.

This work has been financially supported by the Capital and Coast District Health Board.

The author has no conflicts of interest.

A2 Author Publications

A RapidArc planning strategy for prostate with simultaneous integrated boost

David Jolly, Dineli Alahakone and Juergen Meyer

Journal of applied clinical medical physics

Volume 12, issue 1, 2011

A class solution for RapidArc prostate planning with simultaneous integrated boost (presentation)

David Jolly, Dineli Alahakone, Juergen Meyer and John Violet.

EPSM-ABEC 2010

Melbourne, Australia, December 2010

AAA Q&A: What are the differences in algorithms configured with either the jaws or MLCs? (presentation)

David Jolly, Dineli Alahakone and Juergen Meyer.

EPSM-ABEC 2010

Melbourne, Australia, December 2010